Calhoun: The NPS Institutional Archive

DSpace Repository

Theses and Dissertations | 1. Thesis and Dissertation Collection, all items

2012-09

The Comparison of Hydrotreated Vegetable Oils With respect to Petroleum Derived Fuels and the Effects of Transient Plasma Ignition in a Compression-Ignition Engine

Carr, M. Aaron

Monterey, California. Naval Postgraduate School

http://hdl.handle.net/10945/17333

Downloaded from NPS Archive: Calhoun

http://www.nps.edu/library

Calhoun is the Naval Postgraduate School's public access digital repository for research materials and institutional publications created by the NPS community. Calhoun is named for Professor of Mathematics Guy K. Calhoun, NPS's first appointed -- and published -- scholarly author.

Dudley Knox Library / Naval Postgraduate School
411 Dyer Road / 1 University Circle
Monterey, California USA 93943

NAVAL POSTGRADUATE SCHOOL

MONTEREY, CALIFORNIA

THESIS

THE COMPARISON OF HYDROTREATED VEGETABLE OILS WITH RESPECT TO PETROLEUM DERIVED FUELS AND THE EFFECTS OF TRANSIENT PLASMA IGNITION IN A COMPRESSION-IGNITION ENGINE

by

M. Aaron Carr

September 2012

Thesis Co-Advisors: Knox Millsaps
Jim Cowart

Approved for public release; distribution is unlimited

THIS PAGE INTENTIONALLY LEFT BLANK

REPORT DOCUMENTATION PAGE			Form Approved OMB No. 0704-0188
Public reporting burden for this collection of information is estimated to average 1 hour per response, including the time for reviewing instruction, searching existing data sources, gathering and maintaining the data needed, and completing and reviewing the collection of information. Send comments regarding this burden estimate or any other aspect of this collection of information, including suggestions for reducing this burden, to Washington headquarters Services, Directorate for Information Operations and Reports, 1215 Jefferson Davis Highway, Suite 1204, Arlington, VA 22202-4302, and to the Office of Management and Budget, Paperwork Reduction Project (0704-0188) Washington DC 20503.			
1. AGENCY USE ONLY ***(Leave blank)***	**2. REPORT DATE** September 2012	**3. REPORT TYPE AND DATES COVERED** Master's Thesis	
4. TITLE AND SUBTITLE The Comparison of Hydrotreated Vegetable Oils With respect to Petroleum Derived Fuels and the Effects of Transient Plasma Ignition in a Compression-Ignition Engine		**5. FUNDING NUMBERS**	
6. AUTHOR(S) M. Aaron Carr			
7. PERFORMING ORGANIZATION NAME(S) AND ADDRESS(ES) Naval Postgraduate School Monterey, CA 93943-5000		**8. PERFORMING ORGANIZATION REPORT NUMBER**	
9. SPONSORING /MONITORING AGENCY NAME(S) AND ADDRESS(ES) Office of Naval Research 875 N. Randolph Street, Suite 1425 Arlington, Va. 22203		**10. SPONSORING/MONITORING AGENCY REPORT NUMBER**	
11. SUPPLEMENTARY NOTES The views expressed in this thesis are those of the author and do not reflect the official policy or position of the Department of Defense or the U.S. Government. IRB Protocol Number __N/A____			
12a. DISTRIBUTION / AVAILABILITY STATEMENT Approved for public release; distribution unlimited		**12b. DISTRIBUTION CODE**	
13. ABSTRACT (maximum 200 words) This thesis presents the results of an experimental study of the combustion characteristics of algae and camelina derived biofuels as well as the effects of Transient Plasma Ignition in a Compression-Ignition Engine. Testing was conducted for Hydrotreated Renewable Diesel, algae, and benchmarked against F-76 and Diesel #2 fuels as well as Hydrotreated Renewable Jet, camelina, benchmarked against JP-5 across a matrix of constant engine speeds and engine loads in a Detroit Diesel 3-53 legacy engine. A heat release rate analysis and a cycle analysis were performed at each matrix point. The algae and camelina fuels averaged 1.4 Crank Angle Degrees earlier ignition, 2 Crank Angle Degrees longer burn duration, 2.25 atmospheres decrease in Peak Pressure, 1.4 Crank Angle Degrees delay in Angle of Peak Pressure, 0.5% increase in Indicated Mean Effective Pressure, and 6% decrease in Break Specific Fuel Consumption than their petroleum counterpart. A comparison between Diesel #2 at idle was performed between Transient Plasma Ignition Assisted Compression-Ignition and conventional Compression-Ignition. Transient Plasma Ignition averaged a Crank Angle Degree earlier start of combustion, faster pressure rise, but lower Peak Pressures than Compression-Ignition. However, due to failure of the plasma electrode it was not ascertained if this phenomenon is repeatable.			
14. SUBJECT TERMS Reciprocating Machinery, Piston Engine, Diesel Engine, Compression Ignition, Biofuels, Algae, Camelina, Hydrotreated Renewable Diesel (HRD), Hydrotreated Renewable Jet (HRJ), Hydrotreated Vegetable Oils (HVO), Transient Plasma Ignition (TPI)			**15. NUMBER OF PAGES** 117
			16. PRICE CODE
17. SECURITY CLASSIFICATION OF REPORT Unclassified	**18. SECURITY CLASSIFICATION OF THIS PAGE** Unclassified	**19. SECURITY CLASSIFICATION OF ABSTRACT** Unclassified	**20. LIMITATION OF ABSTRACT** UU

NSN 7540-01-280-5500 Standard Form 298 (Rev. 2-89)
Prescribed by ANSI Std. 239-18

THIS PAGE INTENTIONALLY LEFT BLANK

Approved for public release; distribution is unlimited

THE COMPARISON OF HYDROTREATED VEGETABLE OILS WITH RESPECT TO PETROLEUM DERIVED FUELS AND THE EFFECTS OF TRANSIENT PLASMA IGNITION IN A COMPRESSION-IGNITION ENGINE

M. Aaron Carr
Ensign, United States Navy
B.S., United States Naval Academy, 2011

Submitted in partial fulfillment of the
requirements for the degree of

MASTER OF SCIENCE IN MECHANICAL ENGINEERING

from the

NAVAL POSTGRADUATE SCHOOL
September 2012

Author: M. Aaron Carr

Approved by: Knox Millsaps
Thesis Co-Advisor

Jim Cowart
Thesis Co-Advisor
Associate Professor, United States Naval Academy

Knox Millsaps
Chair, Department of Mechanical and Aerospace Engineering

THIS PAGE INTENTIONALLY LEFT BLANK

ABSTRACT

This thesis presents the results of an experimental study of the combustion characteristics of algae and camelina derived biofuels as well as the effects of Transient Plasma Ignition in a Compression-Ignition Engine. Testing was conducted for Hydrotreated Renewable Diesel, algae, and benchmarked against F-76 and Diesel #2 fuels as well as Hydrotreated Renewable Jet, camelina, benchmarked against JP-5 across a matrix of constant engine speeds and engine loads in a Detroit Diesel 3-53 legacy engine. A heat release rate analysis and a cycle analysis were performed at each matrix point. The algae and camelina fuels averaged 1.4 Crank Angle Degrees earlier ignition, 2 Crank Angle Degrees longer burn duration, 2.25 atmospheres decrease in Peak Pressure, 1.4 Crank Angle Degrees delay in Angle of Peak Pressure, 0.5% increase in Indicated Mean Effective Pressure, and 6% decrease in Break Specific Fuel Consumption than their petroleum counterpart. A comparison between Diesel #2 at idle was performed between Transient Plasma Ignition Assisted Compression-Ignition and conventional Compression-Ignition. Transient Plasma Ignition averaged a Crank Angle Degree earlier start of combustion, faster pressure rise, but lower Peak Pressures than Compression-Ignition. However, due to failure of the plasma electrode it was not ascertained if this phenomenon is repeatable.

THIS PAGE INTENTIONALLY LEFT BLANK

TABLE OF CONTENTS

THIS PAGE INTENTIONALLY LEFT BLANK

LIST OF FIGURES

LIST OF TABLES

THIS PAGE INTENTIONALLY LEFT BLANK

LIST OF ACRONYMS AND ABBREVIATIONS

Abbreviation	Acronym	Units
AC	Alternating Current	
AFR	Air-to-Fuel Ratio	[1]
AOP	Angle of Peak Pressure	degrees
ATDC	After Top Dead Center	degrees
A_w	Surface Area of Combustion Chamber	m^2
B	Bore	m
BDC	Bottom Dead Center	
BDR	Burn Duration	degrees
BMEPd	Break Mean Effective Pressure differential	PSI or Bar
BSFC	Brake Specific Fuel Consumption	lbs/hp-hr or kg/W-s
BTDC	Before Top Dead Center	degrees
CAD	Crank Angle Degrees	degrees
CAD10	Location of 10% Mass Fraction Burned	degrees
CAD90	Location of 90% Mass Fraction Burned	degrees
CFM	Cubic Feet per Minute	ft^3/min
CG	Guided Missile Cruiser	
C_h	Coefficient of the Heat Transfer Coefficient	[1]
CI	Compression Ignition	
CO	Carbon Monoxide	
CO_2	Carbon Dioxide	
COTS	Commercial off the Shelf	
C_p	Specific Heat Capacity at Constant Pressure	J/kg-K
CR	Compression Ratio	[1]
ConRod	Connecting Rod Length	m
C_v	Specific Heat Capacity at Constant Volume	J/kg-K
D	Displacement	in^3 or m^3
DDG	Guided Missile Destroyer	

$dP/d\theta$	Change in Pressure as a Function of CAD	Pa/degree
$dQ_w/d\theta$	Heat Transfer Rate Through the Wall	J/degree
$dV/d\theta$	Change in Volume as a Function of CAD	m^3/degree
dW/dt	Change in Weight as a Function of Time	lbs/s or kg/s
E_{fuel}	Energy Content per Combustion	J
FAME	Fatty Acid Methyl Ester	
FMEP	Friction Mean Effective Pressure	PSI or Bar
FT	Fischer-Tropsch	
h	Heat Transfer Coefficient	J/m^2-K-min
H*	Hydrogen Radical	
H_2	Diatomic Hydrogen	
HC	Hydrocarbon	
HMMWV	High Mobility Multi-purpose Vehicle	
HP	Horsepower	550 ft-lbs/s
HRD	Hydrotreated Renewable Diesel Fuel	
HRJ	Hydrotreated Renewable Jet Fuel	
HRR	Heat Release Rate	
HVO	Hydrotreated Vegetable Oils	
IGD	Ignition Delay	degrees
IMEP	Indicated Mean Effective Pressure	PSI or Bar
JP-5	U.S. Navy designation for Carrier-Based Jet Fuel	
LHV	Lower Heating Value	MJ/kg
$\dot{m}_{air}$	Mass Flow Rate – Air	kg/s
$\dot{m}_{fuel}$	Mass Flow Rate – Fuel	kg/s
$m_{\text{fuel of combustion}}$	Mass Charge of Fuel per Combustion	kg
M	Charged Cylinder Mass	kg
NATO	North Atlantic Treaty Organization	
NPS	Naval Postgraduate School	
NO_x	Nitrous Oxides	
OH*	Hydroxide Radical	

ONR	Office of Naval Research	
P	Pressure	Pa, Bar, or PSI
$P_{cylinder}$	Cylinder Pressure	Pa, Bar, or PSI
phase	Encoder – BDC Offset	degrees
P_i	Instantaneous Global Cylinder Pressure	Pa
PP	Peak Pressure	PSI or Bar
PPR	Pulses per Revolution	
PSIa	Pounds per Square Inch Absolute	lbs/in^2
PSIg	Pounds Per Square Inch Gauge	lbs/in^2
R_g	Specific Gas Constant	$kg\text{-}m^2/s^2\text{-}K$
RPM	Rotations per Minute	
S	Stroke	m
SI	International System of Units	
SOC	Start of Combustion	degrees
SOI	Start of Injection	degrees
S_p	Mean Piston Speed	m/s
TDC	Top Dead Center	
T_i	Instantaneous Global Cylinder Temperature	K
Torque	Torque	ft-lbs
TPI	Transient Plasma Ignition	
TTL	Transistor-Transistor Logic	
T_w	Wall Temperature	K
U_{gas}	Internal Energy of the Cylinder's Gas	J
USC	University of Southern California	
$\dot{V}_{air}$	Volumetric Flow Rate – Air	CFM
V	Volume	m^3
$V_{cylinder\ head}$	Cylinder Head Volume	m^3
VE	Volumetric Efficiency	[1]
V_{signal}	Charge Amp Voltage	V
y_{piston}	Piston Position from Crankshaft Axis	m

γ	Ratio of Specific Heats	[1]
θ_{CAD}	Crankshaft Position – Degrees	degrees
θ_{rad}	Crankshaft Position – Radians	
λ	Lambda, Ratio of AFRs	[1]
ρ_{air}	Density of Air	kg/m^3

ACKNOWLEDGMENTS

The author would like to thank the technical expertise of Mr. Douglas Seivwright, Lab Technician, Department of Mechanical Engineering, of the Naval Postgraduate School (NPS), as well as the installation support from Andrew Cunningham, NPS intern. The frequency based LabVIEW codes and instrumentation consulting were provided by the United States Naval Academy from Dr. Patrick Caton, and Dr. Jim Cowart. CDR Matthew A. Carr, Permanent Military Professor of the Mechanical Engineering Department at the United States Naval Academy, provided valuable editorial assistance in reading the drafts of this thesis. All plasma related equipment and on site expertise were provided by the University of Southern California (USC) by Dr. Martin Gunderson, Dr. Andy Kuthi, and supporting graduate students. All model making and machine shop support was provided by John Mobley and other machine shop technicians. Finally, the author would like to thank the Office of Naval Research for their financial support, Dr. Sharon Beermann-Curtin, Program Manager, and Dr. Richard Carlin, (SES).

THIS PAGE INTENTIONALLY LEFT BLANK

I. INTRODUCTION

A. NAVAL FUEL INITIATIVES

1. Energy Economy and Operational Risks

During the next several decades, the quantity and accessibility of petroleum-based fuels is expected to diminish, thereby forcing a global shift towards alternate fuels. The United States achieved peak oil production in 1971 and is currently importing 60% of its oil needs as reported by the U.S. Energy Information Administration [1]. Obtaining crude oil will become more expensive and riskier. Simple economics predicts the rise in fuel prices, and fuel companies will have to drill in more challenging places to obtain oil as the more accessible reserves of this precious resource are exhausted. The 2010 Deepwater Horizon oil spill incident is a recent example of the higher risks imposed by drilling for oil in challenging environments. Furthermore, international geopolitical instability affecting oil resources could limit the United States' economy and Navy's operational capabilities. The United States Navy Energy, Environment, and Climate Change Website [2] best summarizes the energy situation for the Department of Defense: "Energy security is critical to mission success[,]… energy efficiency is critical to mission effectiveness[,]… and [energy] sustainability is critical to preservation of mission capability." These combinations of factors highlight the urgent need for developing non-petroleum derived fuels for economic stability and military capabilities.

2. Future Naval Fuels Program

The United States Navy is heavily dependent upon petroleum-derived fuels. With the exception of nuclear-powered aircraft carriers and submarines, all ships, aircraft, amphibious and land-based vehicles require liquid fuel for propulsion. Even nuclear-powered ships and submarines require liquid fuel for their backup generators. Furthermore, guided missile cruisers (CGs) and guided missile destroyers (DDGs) refuel typically every four-to-five days during normal operations as reported by Bryan [3]. Underway replenishments are inherently dangerous and very demanding on a ship's

crew, while refueling in foreign ports may take place in unstable regions of the world, e.g., USS Cole bombing at Aden, Yemen in 2000.

The Navy currently uses JP-5 for aircraft and (North Atlantic Treaty Organization) NATO F-76 for shipboard and motor vehicle fuels. These fuels are compatible with seawater compensation for ballast and have a high flash point (e.g. 140° Fahrenheit) to meet shipboard safety standards. Alternative fuels must be compatible with current fuels and demonstrate similar attributes: tolerance to contact with seawater under shipboard storage tank compensation, high flash points, long-term storage stability, resistance to bio-contamination, and no negative impact to refueling logistics.

The Future Naval Fuels Program under the Office of Naval Research (ONR) is sponsoring a testing regiment covering a variety of alternate fuels in order to characterize their combustion performance for current and projected future gas turbines and Diesel engines utilized by the Navy and Fleet Marine Force. Ultimately, the U.S. Navy aims to understand the effects of varying feedstock and processing with respect to engine life, reliability, and operations, as well as develop a certification program to validate candidate fuels for U.S. Naval use. The research program is investigating fuel combustion dynamics, flame stability, emissions, material compatibility, and long term stability for storage as well as attempting to validate current mathematical and physical combustion models. The final deliverable of the program is to design a synthetic fuel capable of higher specific heat content that could increase the operational capabilities of the United States Navy as reported by the ONR [4].

3. Great Green Fleet

From 1907 to 1909, the United States sent 16 battleships, together with multiple smaller warships and support vessels, known as the “Great White Fleet” around the world to display the United States’ sea power and to spread goodwill. These ships were all powered by coal. Now, more than a century later, the Department of the Navy plans to sail a carrier battle group being called the “Great Green Fleet” around the world in 2016. This fleet will serve as a validation of the work of the ONR and serve as a proof of concept of maritime energy sustainability. On April 22, 2010, the Navy flew an F/A-18

Super Hornet on a 50/50 blend of camelina-derived fuel and JP-5 in a craft nicknamed the "Green Hornet" as reported by Wright [5].

4. Diesel Engines in the Navy

The Navy and Fleet Marine Force use a variety of Diesel engines for primary propulsion and electrical energy generation. They can range from several hundred to several thousand horsepower. Most numerous and laboratory testable are small legacy engines such as the AM General High Mobility Multi-purpose Vehicle (HMMWV) engine and the Detroit Diesel 3-53 engine. For logistical reasons, sometimes these engines can and are run on JP-5 jet fuel, which is composed of slightly shorter hydrocarbon (HC) chains than typical Diesel fuels. These CI engines serve as a practical test bed for both jet and Diesel fuels.

B. ALTERNATIVE DIESEL FUELS

1. Cetane Number

Like an octane rating that the consumer can select at the filling station gas pump, Diesel fuel is rated by a cetane number. Both are scales of a fuel's tendency to auto-ignite. However, each scale was developed so that higher numbers represent a higher quality of fuel for their intended use. It is generally beneficial to have high resistance of auto-ignition in a spark ignition engine, where ignition is controlled by spark timing. On the other hand, it is generally beneficial to have a low resistance to auto-ignition in a Diesel engine, where ignition is controlled by injector timing. In essence, the two scales are opposites, while they both measure auto-ignition tendencies.

Gasoline engines are rated for a certain octane level, based on their compression ratios, cylinder geometry, and cylinder materials. Number 2 Diesel fuel is regulated by ASTM D975 Diesel fuel standards with a minimum cetane number of 40 with a nominal range of 42-45. All legacy U.S. Navy Diesel engines have been designed to run on fuels with approximately the same cetane number. Legacy engines are very flexible and can accommodate a wide range of cetane numbers. Lower cetane fuels tend to have more mixing time before ignition, but because of their increased mixing, burn more rapidly

than higher cetane fuels. The end result is that peak pressure occurs at about the same crank position for a large range of cetane numbers.

2. Types of Alternative Fuels

As previously reported by Carr, Caton, et al. [6]: "Biodiesel" is Diesel fuel created from plant-based oils, animal fats, and more recently, algae-derived oils. Biodiesel has gained popularity in North America over the past decade, but the ester content of Fatty Acid Methyl Ester (FAME) fuel creates both cold weather and water-based operational issues. The Fischer-Tropsch (FT) process produces liquid fuels from "syngas," a mixture of hydrogen (H_2) and carbon monoxide (CO). Coal-rich Germany made significant use of the FT process to create liquid fuels during World War II. FT fuels have also seen renewed interest in the past decade, although the production and use of these fuels generates a large amount of carbon dioxide (CO_2), which is a "greenhouse gas." Hydro-treated Renewable Diesel (HRD) fuels are a newer addition to the world of alternative Diesel fuels. Like biodiesel, these alternative fuels can utilize a range of renewable feed stocks, such as vegetable oils. However, unlike biodiesel, these alternatives generally contain only paraffinic HCs, with no esters or bound oxygen as reported by Bruno and Baibourine [7]. This makes HRD a potential drop-in replacement for petroleum Diesel fuel.

The U.S. Navy is looking into hydro-treated algae oil as a Diesel fuel replacement, as well as hydro-treated camelina oil (mustard seed, "*Camelina sativa*") as a Hydro-treated Renewable Jet (HRJ) fuel replacement. These Hydro-treated Vegetable Oils (HVO), both HRD and HRJ, are not the ester-based biodiesel of recent years, but rather pure HC fuels with no molecularly bound oxygen.

3. Conventional Fuel Constituents

Conventional petroleum HC-based fuels for Diesel engines can be characterized as mixtures of five different HC classes: straight-chain (normal) alkanes, branched (iso) alkanes, cyclic alkanes, aromatics, and alkene HCs. Diesel fuel has been shown to have approximately equal amounts of straight-chain alkanes, aromatics, and cyclic alkanes with a minority fraction of branched alkane species as reported by Challen and Baranescu

[8]. Jet fuel has been shown to contain over 50% straight and branched alkanes, with another 25% of the fuel coming from cyclic alkanes (mono-, di- and tri-). The final minority fraction (up to 25%) was shown to be an aromatic species as reported by Edwards [9].

4. Differences Between Alternative and Conventional Fuels

The molecular structure and makeup of newer alternative fuels differ in important ways from conventional petroleum-based HC Diesel fuels. FT fuels are principally comprised of normal and branched alkanes. Both of these HC fuel structures have lower density than aromatic compounds, and thus FT fuels have lower densities overall when compared with conventional petroleum Diesel and jet fuels. The lack of sulfur and aromatic components often causes FT synthetic fuels to be characterized as "cleaner" due to the absence of these two important precursors of particulate matter (soot).

Alternative Diesel and jet engine fuels produced from hydro-treating renewable sources have begun to receive attention in recent years as reported by Kuronen, Mikkonen, et al. [10]. These fuels are also principally composed of normal and branched paraffins. HRD fuels, produced from hydro-treating renewable biological oils, including algae, typically have a similar molecular structure to FT fuels as reported by Aatola, Larmi, et al. [11]. The absence of aromatics and cyclo-alkanes causes FT and HRD fuels to have a higher cetane number than petroleum-based Diesel fuels as reported by Kitano, Sakata, et al. [12].

While the lack of aromatic content may help reduce precursors for soot formation, these aromatic species also will have an important effect on the physical mixing process, the chemistry leading to ignition, and even the lubricating properties of the fuel, which affect piston ring and fuel pump durability. Other concerns exist as well, such as the interaction of elastomeric seals without aromatic species in the fuel. For these reasons, some addition of aromatic species into an HRD mixture is likely to enhance fuel system component durability as reported by Moses [13]. Understanding the effects of these aromatic species on the physical process of air and fuel mixing, and the chemical processes leading to ignition, are important in order to ensure compatibility with legacy

and future Diesel engines. Introducing up to 50% aromatics in the fuel does little to the combustion characteristics in a legacy engine. This number far surpasses the lubricity needs of any engine as reported by Carr [6].

C. IGNITION METHODS

1. Compression Ignition

The Diesel Cycle operates by injecting a metered amount of fuel which is then ignited by the high temperatures of the cylinder gas created by the compression stroke. First order analysis of the ideal Diesel cycle assumes constant pressure combustion (whereas the ideal Otto cycle is represented as constant volume combustion). The compression ratio (CR) of Diesel engines is typically far higher than gasoline engines, and therefore the cylinder's gas is much greater in pressure and temperature at the end of compression. Assuming constant specific heat ratios:

$$p = p_0 \times CR^{\gamma} \tag{1}$$

$$T = T_0 \times CR^{1-\gamma} \tag{2}$$

For example the Detroit Diesel 3-53: assume p_0 is 17 pounds per square inch absolute (PSIa) (from induction at one atmosphere and a small pressure boost from the supercharger); T_0 is 70° Fahrenheit (530° Rankine); the actual CR is 17.4:1; and the ratio of specific heats (γ) is 1.4, the in-cylinder pressure will be approximately 930 PSIa at 1,200° Fahrenheit, which is well above the auto-ignition temperature of any of the fuels tested.

Breaking down HCs is an exothermic reaction. Stoichiometric combustion of paraffinic HCs in oxygen produces water and carbon dioxide. However, each fuel is made up of numerous constituents and each type of fuel molecule takes numerous complex steps from reactant to product. Simply put, HCs tend to sequentially loose one or two carbon structures per step of the chemical reaction. The mechanism by which the fuel breaks down is the physical collision of molecular radicals.

The primary radical of combustion is the hydroxide radical (OH*), created by hydrogen radicals at higher temperatures and the decomposition of hydro-peroxides at moderate temperatures. These radicals originate from non-aromatic HC combustion. Incidentally, aromatic structures are low in cetane number because they neutralize the OH* radical. High temperature cylinder gasses in the Diesel Cycle initiate H* production. After exothermic breakdown at the initiation point(s) of combustion, even more radicals are present. Combustion and radical formation form a positive feedback loop until the consumption of all reactants. Pressures and temperatures increase above that of the motoring trace, and the power stroke is performed.

2. Transient Plasma-Assisted Ignition

TPI-assisted CI offers the promise of increased performance and thermodynamic efficiency above that of a standard CI engine. The use of non-equilibrium, highly transient, plasmas generates electrons throughout the volume of the cylinder. These electrons introduce more radicals and other electrically excited molecules throughout the cylinder's volume than a purely thermal based combustion. Radical formation occurs through electron impact dissociation, excitation, and ionization of the cylinder's air as reported by Cathey, Tang, et al. [14]. Transient plasma is introduced by a high electrical field associated with and through a device very similar to a spark plug. While it may sound blasphemous to use a spark plug in a Diesel engine, it is the electron-plasma source for the current experiment. Instead of allowing the electron gap to ionize the air (observable by a visible spark), the electron field is cycled at very high frequencies, on the order of nanoseconds, to introduce "streamers" of electrons. These electron streamers would become a visible spark if the device were always on, hence the word transient. This configuration creates a low temperature plasma that augments the combustion's radical creation mechanism of molecular impact dissociation. In theory, with more radicals present in the cylinder, the fuel should burn more rapidly and more thoroughly.

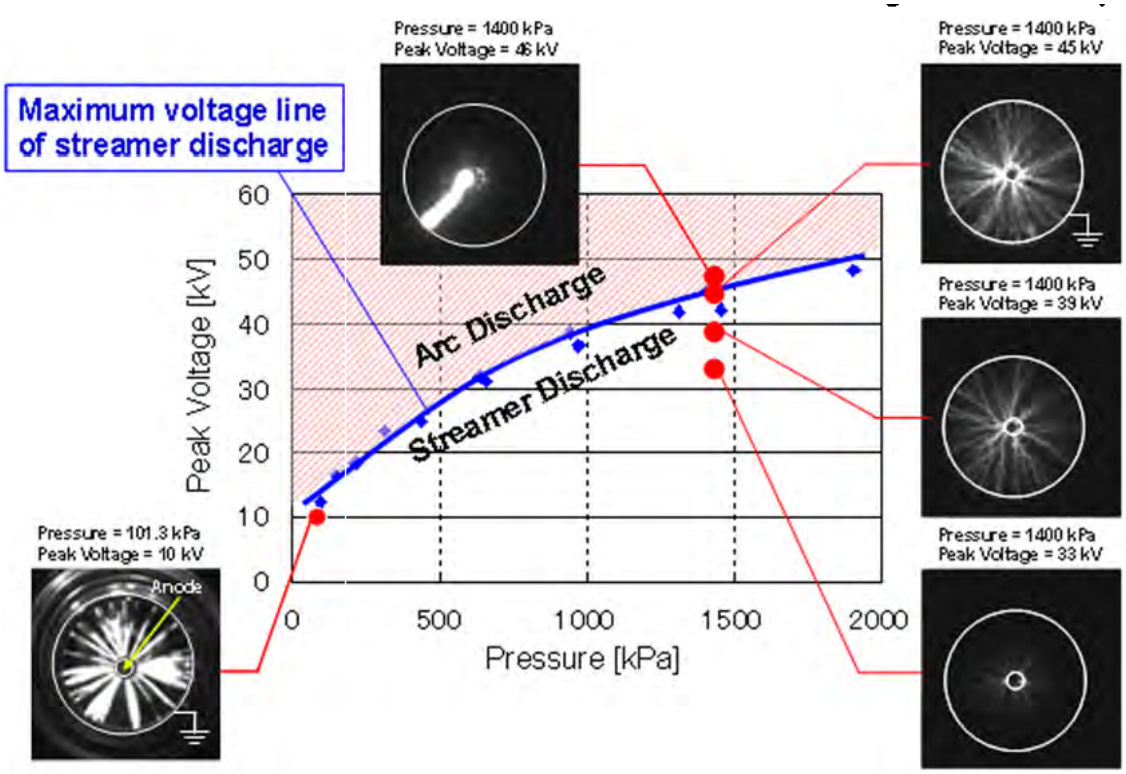

Figure 1. Peak Voltage of Streamer Discharge as a Function of Pressure by Shiraishi, Urushihara, et al. [15]

This technology has been applied to a gasoline engine with significant and positive results. In a study between Nissan and USC, TPI produced significantly faster flame propagation speeds, demonstrated by a 20 percent increase in peak pressures over conventional spark gap ignition, 13–17 percent reduction in ignition delay, and a decrease in burn duration which becomes more prominent at leaner air-fuel mixtures as shown by Cathey [14].

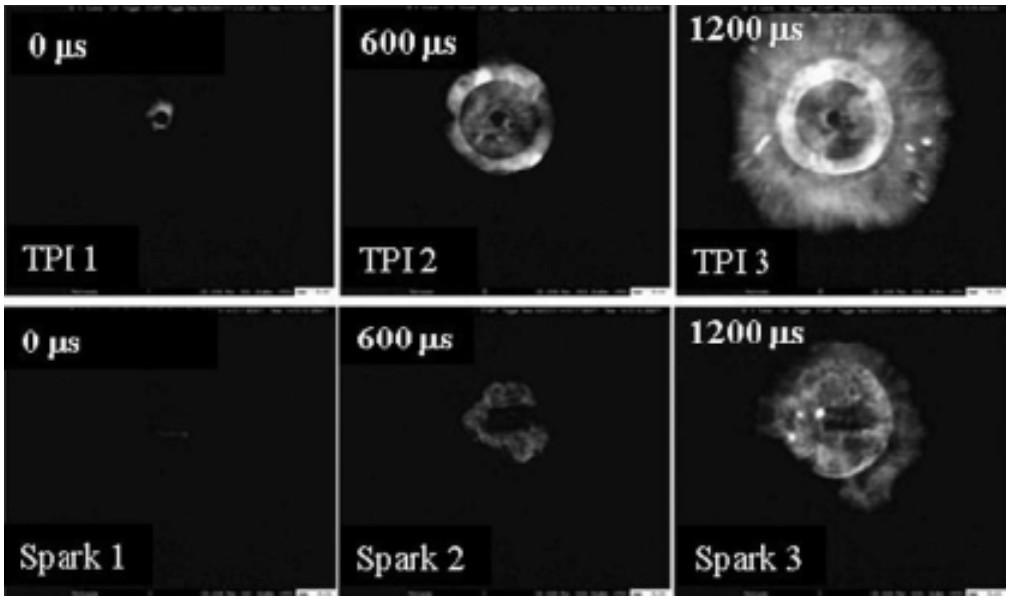

Figure 2. Spark Ignition and Transient Plasma Ignition in a Otto Cycle Engine by Cathey [14]

While the physical mechanism of fuel delivery for combustion differs greatly between Otto and Diesel cycles, the chemical mechanism for combustion remains the same. In theory, there should be a less, but still noticeable effect of TPI in a CI engine compared to an Otto Cycle engine. Transient plasma may decrease the fuel's ignition delay and thereby increase the apparent cetane rating of the fuel, decrease the burn duration and thereby increase the efficiency and break specific fuel consumption (BSFC) of the engine, or reduce harmful emissions such as NO_x and CO.

D. RESEARCH OBJECTIVES

1. Observe the relative combustion characteristic differences between HRD Algae - F-76, HRD Algae - Diesel #2, and HRJ Camelina - JP-5 by Pressure – Volume cycle analyses and HRR analyses.
2. Observe noticeable effects of low temperature plasmas in a combustion event by comparing Pressure – CAD and Pressure - Volume diagrams with conventional CI.
3. Update the Naval Postgraduate School's Diesel engine facility to support future fuel studies.

THIS PAGE INTENTIONALLY LEFT BLANK

II. EXPERIMENTAL SETUP AND EQUIPMENT

A. THE THREE-CYLINDER TWO-STOKE DIESEL ENGINE

The Diesel engine utilized for this experiment is a Detroit Diesel 3-cylinder 53 series engine, shown in Fig. 3 below. This engine was used in an U.S. Army amphibious 1-1/4 Ton Cargo Truck called the "Gamma Goat" as reported by Armstrong [16]. It is a two-stroke engine with a Roots™ positive displacement air intake blower, four exhaust valves per cylinder, and a sequential exhaust manifold. It, conveniently, has glow plug ports for warming up the cylinders when operating in cold environments. Also shown in Table 1 are the characteristics of the engine.

Figure 3. Detroit Diesel 3-53 Test Engine (Orange) and Dynamometer (Blue)

Table 1. Engine Characteristics

Model	5033-5001
Number of Cylinders	3
Bore and Stroke	3.875 x 4.5 inches
Cylinder Displacement	53 cubic inches
Engine Displacement	159 cubic inches
Compression Ratio	21.0:1
Engine Type	Inline 3 Cylinder – 2 Cycle
Maximum Power Output	92 BHP @ 2,800 RPM
Peak Torque	198 foot-pounds @ 1,500 RPM
Brake Mean Effective Pressure	83 psi

B. THE DYNAMOMETER

The engine is instrumented with a SuperFlow™ SF-901 dynamometer suite. The suite includes an engine stand, water turbine power absorber, fuel system, water cooling system, and control console. The power absorber is the blue object in the near field of Fig. 3. Various sensors send signals to the control system, which is comprised of a Motorola 6809 microprocessor, 12-bit multiplexed analog-to-digital converter, 15 channel programmable counter, 32K programmable ROM, eight K battery-backed RAM, and 256-byte non-volatile calibration RAM. The suite receives a tachometer signal from a magnetic pick-up on a 60 tooth gear; torque from a load cell with a strain gauge bridge on the water turbine; fuel consumption from two FloScan™ turbine flow transducers; airflow from a four inch diameter turbine with thermistor to adjust to standard temperatures and pressures; exhaust temperatures from K-type thermocouples that are ungrounded; oil pressure; manifold pressure; and barometric pressure. The SuperFlow™ bench calculates horsepower, airflow, fuel flow, air-to-fuel ratio, break specific fuel consumption, and break specific air consumption.

Notably, there is not a lot of academic confidence with the fuel flow turbines. Therefore, while the SuperFlow™ SF-901 multiplexes between lots of instruments, this research is only interested in the engine torque and mass airflow data obtained from the

SuperFlow™ suite. A gravimetric fuel system was designed and constructed, and a lambda (λ) sensor was mounted in the exhaust stream to measure air-to-fuel ratios (AFR), in order to obtain a more accurate and precise measurement of fuel consumption. More details of the fuel system are explained below. The SF-901 also provides servo control of the water turbine valve to increase engine load as well as throttle control to manipulate engine speed.

Figure 4. SuperFlow™ SF-901 Bench and Data Acquisition Computer

C. FUEL MEASUREMENTS

1. Gravimetric Fuel System

This experiment requires precise fuel mass flow rate measurements. Furthermore, due to the variety of fuels tested and their expense, a system that has the ability to drain and flush rapidly was essential in order to minimize cross-contamination of the fuels and well as minimize the time between fuel swaps. Lastly, the engine's mechanical fuel injection system has a recirculation feature that had to be maintained for proper fuel

pump and injection operation. Consequently, a fuel system was designed and constructed that provided these attributes.

A rectangular tank (Appendix A) is suspended as a point load from a load cell which sends a signal to a LabVIEW™ virtual instrument (Appendix B) via a pair of National Instruments data acquisition cards with break out boards. The load cell is a Futek 25-lb S Beam Load Cell with 0.05% nonlinearity and a 0.01" deflection. The hardware and setup of the LabVIEW™ data acquisition system are explained in the cycle analyzer section below. Bursts of 20,000 data samples are averaged every 0.3 seconds to create an average weight hung by the load cell. Finally, 100 averaged data packets are plotted using a method of least squares to find the derivative of the fuel's weight with respect to time. This measurement with respect to shaft power yields very accurate BSFC values.

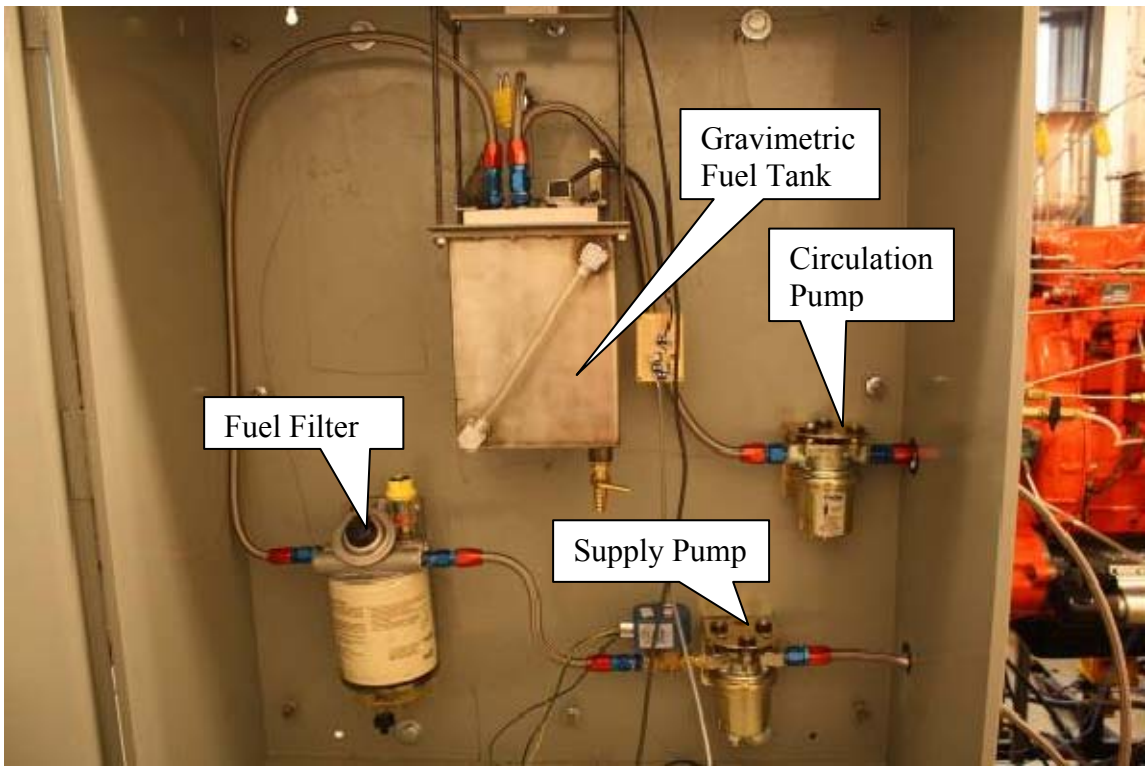

Figure 5. Gravimetric Tank, Intermittent Supply Pump, Fuel Filter, and Continuous Circulation Pump

The whole gravimetric system has been equipped with Jiffy-Tite™ quick-disconnect fittings to isolate the system, allow for easy fuel changes, and simplify

flushing of the system. The Racor fuel filter and gravimetric fuel tank are equipped with drain cocks to remove leftover fuel and simplify fuel flushing. Finally, a check valve was placed before the system to prevent any backflow and contamination into the alternate fuels supplied from a "jerry jug." Fuel flushes involve draining the whole system of the original fuel, refilling and circulating the system with the new fuel including a good rinse of the jerry jug, a secondary draining of the system, dumping out the jerry jug, filling up the system again with the new fuel, and finally running the engine and collecting data.

In addition to the load cell, the gravimetric system is instrumented with a K-type thermocouple and fuel float. The thermocouple is present for overheated fuel temperature warnings as well as enthalpy addition for a planned, future and more complex heat release rate (HRR) analysis than what was performed in this report. The fuel float is a potentiometer and has an attached excitation device. This device is necessary since the LabVIEW^{TM} and National Instruments data acquisition system can only sample voltages. A pair of relay circuits and a 12 volt Alternating Current (AC) powered power supply controls the two fuel pumps from the control room. The logic for this system was implemented and controlled using LabVIEW^{TM}-based logic to control the two electric fuel pumps.

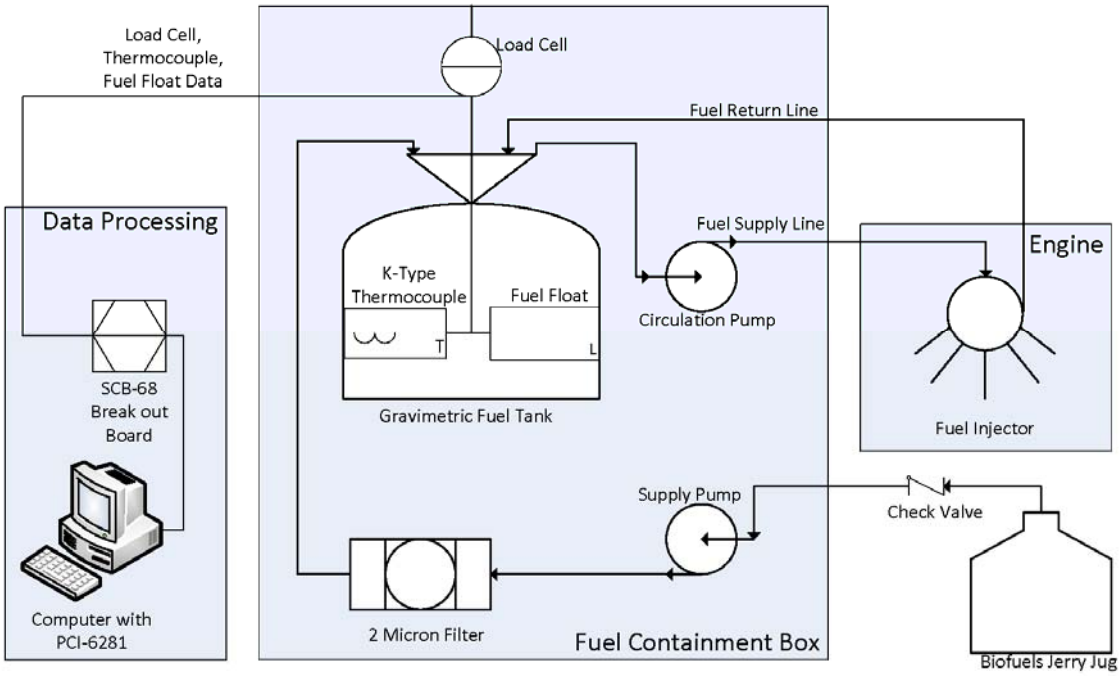

Figure 6. Gravimetric Fuel System Schematic

2. Oxygen Sensor Measurement

An oxygen sensor was installed to measure the AFR of the exhaust. This sensor is placed next to cylinder number three in the box manifold. With an accurate AFR and a known airflow, fuel flow is calculated, and ultimately BSFC. The oxygen sensor's BSFC is used to validate the gravimetric system's BSFC, and serves only as a complement to the gravimetric system.

Figure 7. Sequential Exhaust Box Manifold with Oxygen Sensor and three K Type Thermocouples for Exhaust Temperatures

D. FUELS

The ONR, Code 33, Division 332, provided NPS with four 55-gallon drums of fuel. Conventional fuels provided are the fleet standard Diesel and jet fuels, pure NATO F-76 and pure JP-5, respectively. Alternative fuels provided are pure HVO algae Diesel (HRD) and pure HVO camelina (HRJ). These fuels have been safely stored in a locked containment enclosure. A hand pump was purchased for safe fuel transfer into the alternate fuels jerry jug, which was then used as the source of fuel to the gravimetric fuel measurement apparatus, described above.

Table 2. ONR Supplied Fuels

Fuel Type	Fuel Standard (MIL-DTL)	Barrel #	Requisition #	Flash Point
JP-5	5624U	12017-04389-000	1311C718	>140°F
HRJ Camelina	5624U	12017-04390-000		
F-76	16884L	12017-04382-000		
HRD Algae	16884L	12017-04365-000		

Figure 8. ONR Test Fuels with Pump and Jerry Jug on Containment Palate

Table 3. Heating Values and Cetane Numbers of Tested Fuels

Fuel	Diesel #2	F-76*	JP-5[+]	HVO Algae*	HVO Camelina[+]
LHV (MJ/kg)	42.6	43.2	43.2	43.9	43.9
Cetane #	43	43	46	77	66

*[+]Table values as reported by Caton, Williams, et al. [17] and Hamilton, Williams et al. [18], respectively.

E. CYCLE ANALYSIS

The cycle analysis software and sensor hardware provide the thermodynamic analysis used to measure a fuel's combustive performance. A HRR analysis shows the relative differences between petroleum-based fuels and biofuels, as well as the effects of plasma-aided ignition in a combustion event. The hardware that makes up the system is a crankshaft position sensor, an in-cylinder pressure sensor, as well as the LabVIEW™ data acquisition system that collects hardware timed and frequency based readings (Appendix C) of the position and pressure sensors.

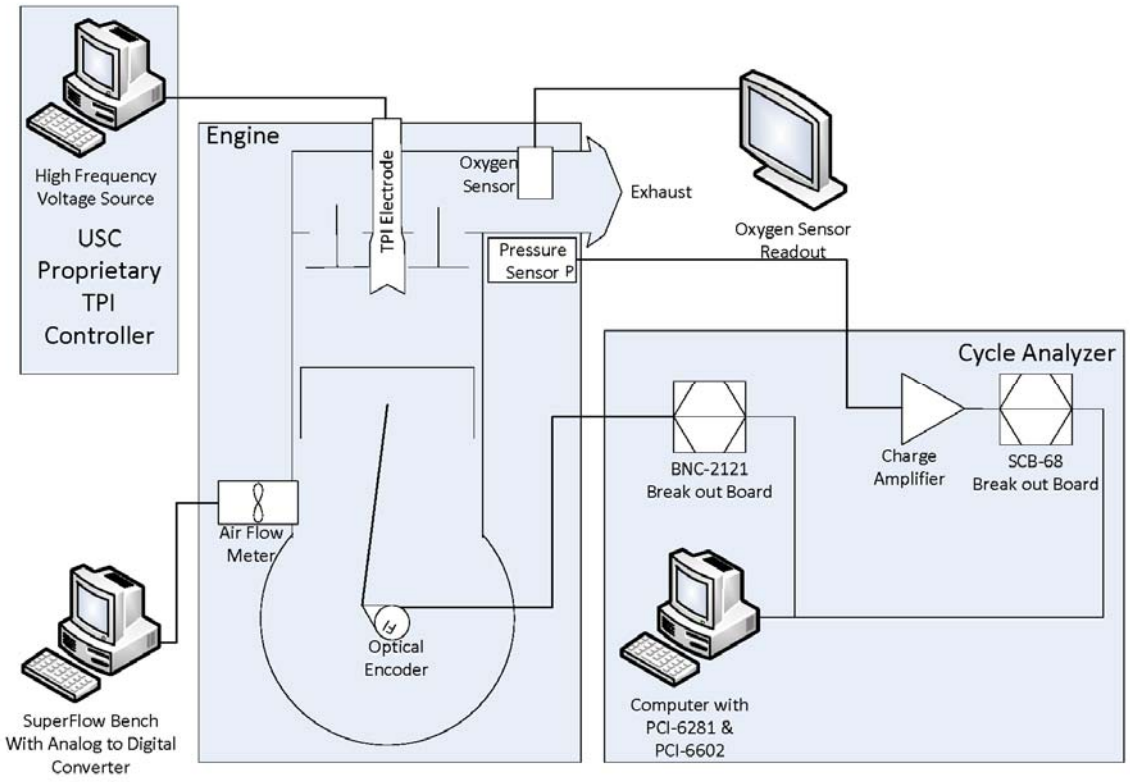

Figure 9. Cycle Analyzer, Oxygen Sensor, SuperFlow™ Measurements, and Transient Plasma Ignition Electrode and Controller

1. Crankshaft Position Sensor

Crankshaft position is necessary for obtaining cylinder gas volume for a Pressure-Volume "indicator" plot from the Pressure - Crank Angle Degree (CAD) data obtained by the LabVIEW™ data acquisition system. Volume is calculated from engine connecting rod, crankshaft, cylinder, and cylinder head geometry at each crankshaft position. Cylinder volume is necessary for calculating indicated mean effective pressures (IMEP), as well as calculating the HRR of the fuel.

A BEIsensors™ 720-tooth glass disk quadrature optical encoder is mounted in a custom aluminum housing (Appendix D) and coupled to the crankshaft via a flexible shaft coupling. It was determined that the original aluminum housing was overheating the optical encoder and causing premature failure of the encoder. Therefore, the existing design was modified to include a water passage about the mount to absorb the heat being

conducted from the engine to the encoder. The encoder produces a five-volt transistor-transistor logic (TTL) signal on two signal outputs, and two more complements signals, that are offset by a half pulse width - quadrature encoding. A 5th output signal is used to reset the encoder each revolution. The encoder is connected to a National Instruments PCI-6602 card via a BNC-2121 break out board.

Figure 10. Encoder and Encoder Mount with Integrated Water Jacket

The encoder was in-phase with the one-pulse-per-revolution at the first cylinder's bottom dead center (BDC). Physically measuring top dead center (TDC) or BDC can be quite difficult as the piston velocity approaches zero at these locations; the piston does not change much in displacement a couple CAD before or after TDC/BDC due to its sinusoidal movement. Therefore, it is recommended to phase the encoder with respect to in cylinder pressure maximums rather than physical measurements via a motoring trace by rotating the engine without fuel injection.

2. In-Cylinder Pressure Sensor

The engine was previously instrumented with Kistler™ in-cylinder pressure transducers in each of the three cylinders' glow plug ports. Since the engine is started from room temperature, the glow plugs are conveniently unnecessary. One of the three pressure sensors had failed, and a second was becoming unreliable after long engine runs. Therefore, the pressure sensors needed to be replaced. Furthermore, cylinder number 1 needed to be instrumented with a smaller sensor than the Kistler model in an auxiliary port machined in the cylinder head to open up the glow plug port for the TPI electrode.

A pair of PCB™ piezoelectric fast acting pressure transducers, model #41918, was donated for testing and validation of a new line of sensors that PCB™ is intending to market. Their signal was compared to the Kistler™ pressure transducers of cylinders number two and three and deemed just as good, if not better than, the Kistlers. These sensors are used in conjunction with a Kistler 5010 charge amplifier and connected to a National Instruments PCI-6281 card via an SCB-68 break out board.

3. LabVIEW™ and National Instruments Hardware

The PCI-6281 and the PCI-6602 circuit boards are connected via a RTSE cable that synchronizes the hardware with respect to the LabVIEW™ data acquisition clock. The PCI-6281 has eight differential analog input channels with an 18-bit single analog-to-digital converter that multiplexes between voltage signals from negative ten volts to ten volts, and it can sample up to 625,000 analog samples per second. It also has a pair of analog outputs and 24 bi-directional digital channels. The PCI-6281 collects data from the three cylinders, collects data from the gravimetric fuel system, and controls the pumps of the fuel system, thereby processing many signals. Some of the analog channels are referenced to ground, sampled in the multiplexing sequence, with their channel's data thrown out in order to minimize "ghosting" effects of one signal influencing another signal. The PCI-6602 collects data from the optical encoder. It has eight up and down 32-bit five V TTL counters.

The signals from the PCI-6281 and the PCI-6602 can be collected by either frequency timed sampling or phase locked sampling. LabVIEW™ codes were developed

for both methods, with phase locked the preferred method of data collection. For phase locked sampling, samples are collected at every 0.5 CAD and processed via a LabVIEW™ 10.0.1 code. The optical encoder signal is adjusted to have the motoring trace peak pressure at -0.5 degrees before TDC. Due to the compression of gasses in the cylinder, the compressed gasses are hotter than the cylinder wall and heat is transferred to the engine block. As such, PP occurs before TDC by 0.5 to 0.75 CADs as reported by Tunestal [19]. Cylinder wall temperature is assumed to be constant at 450° Fahrenheit as reported by Heywood [20]. This is a fair approximation due to the relative heat capacities of the engine block to the cylinder's charged mass. CADs are converted to volume from the engines' CR, connecting rod length, bore diameter, and stroke dimensions. The pressure signal is referenced to a known baseline pressure, and scaled by the specifications supplied with the piezoelectric pressure sensor. Fifty rotations of Pressure - CAD were collected and post-processed via a Matlab™ script (Appendix E) to find peak pressure (PP), angle of peak (AOP), and IMEP from the averaged 50 samples comprising the Pressure-CAD data points.

Ultimately, the Pressure-Volume plot is exported to an excel spreadsheet for a HRR analysis to calculate burn duration (BDR) and ignition delay (IGD) as performed by Goering [21]. A HRR analysis is a controlled-mass first law analysis of the compression and combustion events. It accounts for the energy of the fuel injection into the cylinder, *PdV* work done on the piston, heat transfer from and to the cylinder wall, and the thermal energy exiting the cylinder in the exhaust at each data point on the Pressure – Volume plot. The analysis produces a HRR of the fuel that can ultimately be used to calculate how much of the fuel has been burned per measured CAD. This analysis tool is very useful for determining how quickly the fuel is igniting and how long it is burning, and therefore is a valuable analysis tool for comparing the relative differences of fuels and the effects of biofuels or TPI in steady state conditions.

F. TRANSIENT PLASMA IGNITION

1. Transient Plasma Ignition Source

In order to create a plasma arc for the plasma combustion portion of this experiment, a high voltage short pulse generator is wired into a custom made electrode that is designed specifically for the NPS Detroit Diesel 3-53 engine. This device is similar in construction to a spark plug. A high voltage source is switched on and off by a pseudospark switch, amplified by a pulse transformer, and driven across the electrodes. The electrode has a much larger gap between cathode and anode, and both the cathode and anode have a much greater surface areas, than a common spark plug in order to obtain a larger and more desirable plasma discharge volume. The thickness of the insulator was also increased in order to withstand the higher voltages driven across the electrode. The device produces approximately 80 ns pulses as reported by Shiraishi [15]. The device was constructed and installed by USC personnel.

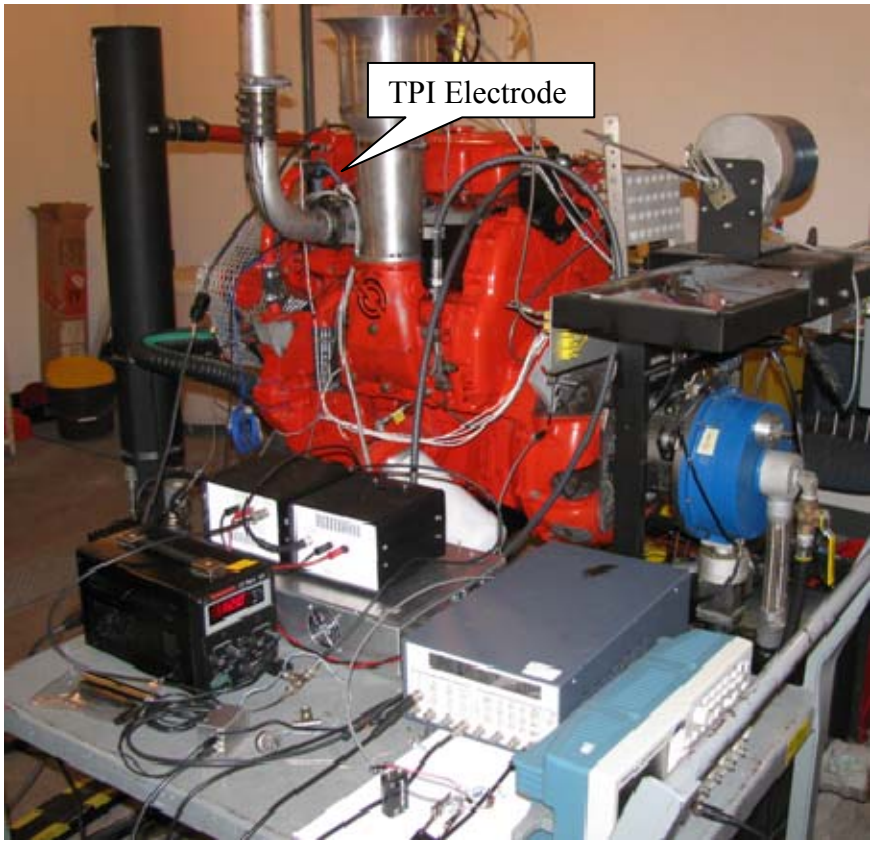

Figure 11. TPI Cart with USC Equipment

2. Modifying the Cylinder Head

The electrode is placed into the glow plug port of cylinder number one. Again, the engine was initially setup with three pressure sensors individually fastened to each of the three cylinder's glow plug ports. Since the transient plasma source's electrode is occupying the existing pressure sensor's location of cylinder number one, a small hole was drilled from the side of the head to obtain a pressure signal. An intersecting hole was drilled from the combustion chamber's cylinder face of the head. The Detroit Diesel 3-53 cylinder head is a complex labyrinth of exhaust, fuel, and water passages. Blueprints of the cylinder head are proprietary information and were not available from Detroit Diesel. Therefore, an exemplar head was used to practice and validate the machine work before cutting metal on the operational head.

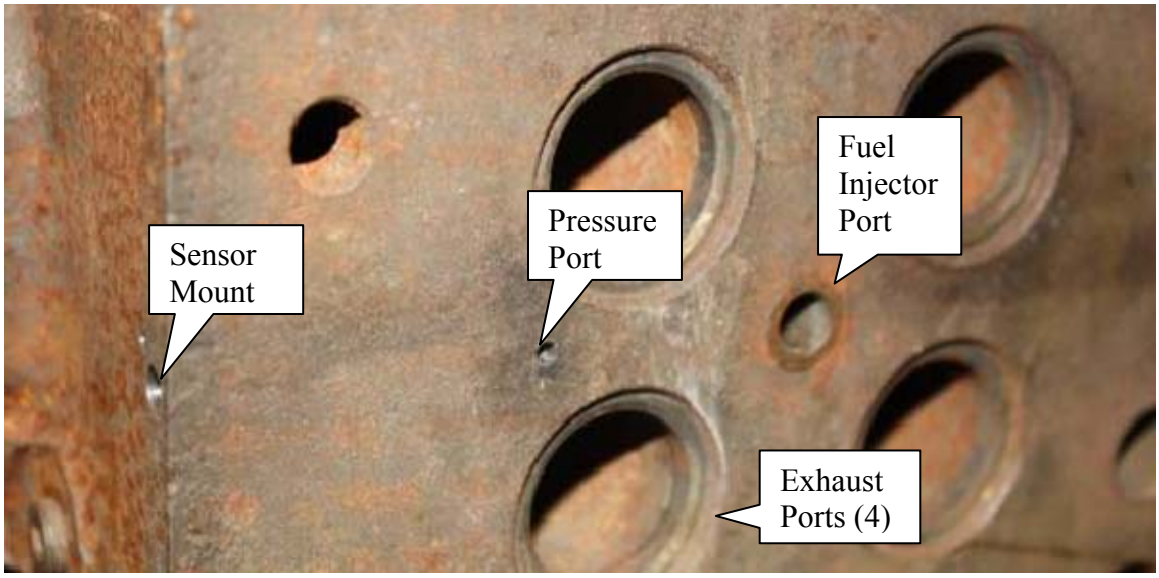

Figure 12. Cylinder Head Machine Work on Exemplar Cylinder Head

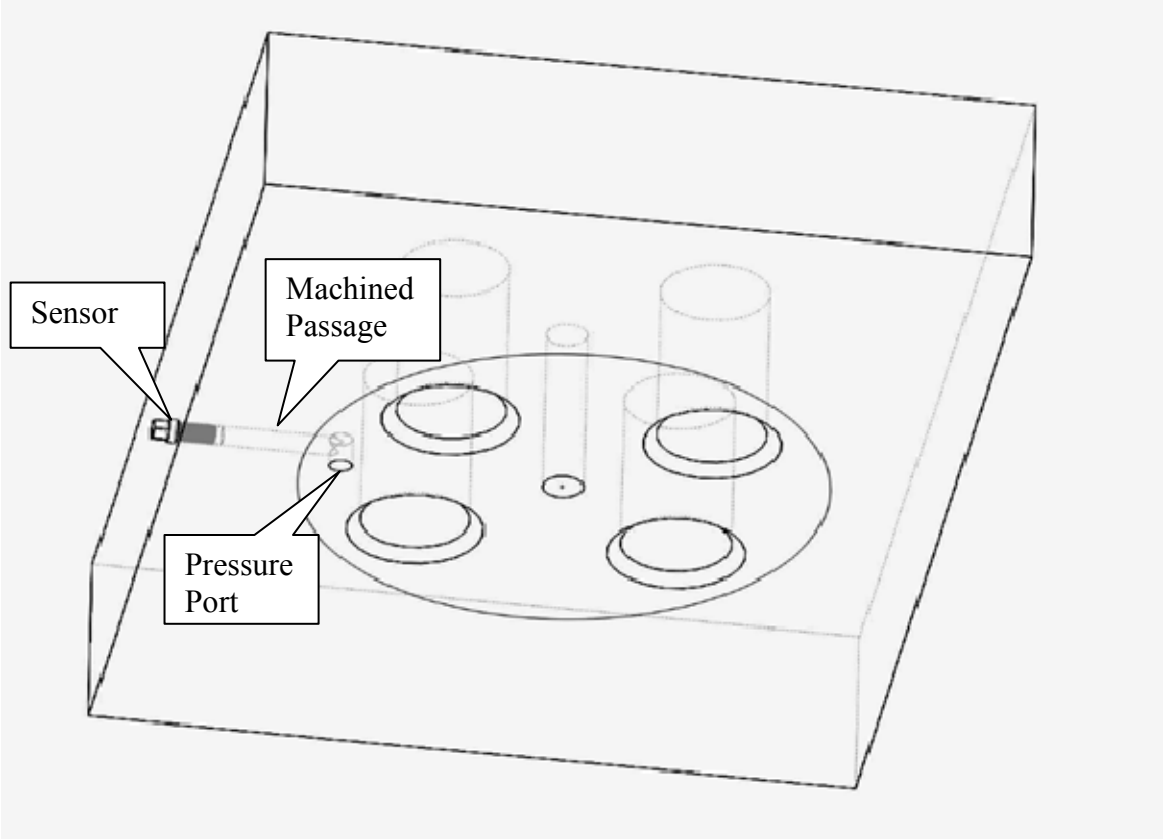

Figure 13. SolidWorks™ Schematic of Pressure Port Machine Work

III. DATA COLLECTION AND GOVERNING EQUATIONS

A. FUEL TEST REGIMENT

1. Biofuels

The five fuels listed in Table 2 are each tested at three different speeds followed by three different loads: 1,000 rotations per minute (RPM) 50% load, 1,300 RPM 50% load, 1,600 RPM 50% load, another 1,300 RPM 50%, 1,300 RPM 75%, and 1,300 RPM 100%. Maximum load was measured at 120 ft-lbs of torque.

Table 4. Fuel Test Matrix Data Collection Order

RPM\Torque (ft-lbs)	60 (50%)	90 (75%)	120 (100%)
1,600	3	-	-
1,300	2 / 4	5	6
1,000	1	-	-

Relative comparisons are made between each of the fuels with regard to BMEP, Pressure – CAD, Pressure – Volume, PP, AOP, IMEP, BSFC, HRR, and Mass Fraction Fuel Burned – CAD relationships.

Table 5. Fuel Comparison Matrix

HVO Fuel	Petroleum Comparison
HRD Algae	Diesel #2
HRD Algae	NATO F-76
HRJ Camelina	NATO JP-5

2. Transient Plasma Ignition

TPI at 600 RPM no load was compared against regular CI at 600 RPM no load.

B. SUPERFLOW CALCULATIONS

The dynamometer measures torque that is created from the resistance of the water turbine as well as the shaft speed. Horsepower is a derived power measurement with the following torque and speed relationship:

$$horsepower = \frac{torque\,(ft \cdot lbs) \times RPM}{5,252} \tag{3}$$

BMEP is a metric for comparing similar engine types. It is also useful for calculating transmission losses throughout the powertrain. It is the mean pressure that if supplied on the piston from TDC to BDC of the power stroke would produce the measured shaft torque.

$$BMEP(psi) = \frac{75.4 \times torque\,(ft \cdot lbs)}{displacement\,(in^3)} = \frac{75.4 \times torque\,(ft \cdot lbs)}{159.2\,(in^3)} \tag{4}$$

The SuperFlow™ system is also responsible for reporting the mass airflow element volumetric flow rate. The volumetric airflow rate, when coupled with a λ sensor, or oxygen sensor, is useful for calculating the fluids' mass flow rate, but first airflow rate must be converted from volume to mass:

$$\dot{V}_{air}\left(\frac{m^3}{s}\right) = \dot{V}_{air}\left(\frac{ft^3}{min}\right) \times \left(\frac{0.3048\,m}{ft}\right)^3 \times \left(\frac{60\,s}{min}\right) \tag{5}$$

$$\rho_{air}\left(\frac{kg}{m^3}\right) = \frac{P}{R_g T_{atm}} = \frac{101325\,(Pa)}{287.058\left(\frac{kg \cdot m^2}{s^2 \cdot K}\right) \times T_{atm}(K)} \tag{6}$$

$$\dot{m}_{air}\left(\frac{kg}{s}\right) = \dot{V}_{air}\left(\frac{m^3}{s}\right) \times \rho_{air}\left(\frac{kg}{m^3}\right) \tag{7}$$

C. FUEL SYSTEM CALCULATIONS

1. Gravimetric Break Specific Fuel Consumption

The gravimetric system simply reports the change in the loaded fuel's weight with respect to time. It is convenient to convert to the International System (SI) of units:

$$\dot{m}_{fuel}\left(\frac{kg}{s}\right)=\frac{dW}{dt}\left(\frac{lbs}{s}\right)\times\left(\frac{1\,kg}{2.20462\,lbs}\right) \tag{8}$$

2. Oxygen Sensor Break Specific Fuel Consumption

A λ sensor reports the actual AFR to that of a stoichiometric AFR where there is no leftover oxygen. As such, these devices are often referred to as oxygen sensors. The AFR ratio for standard Diesel fuel is 14.5 kg air to every kg fuel. Leaner mixtures will produce a λ reading greater than one, whereas rich mixtures will be less than one. Diesel engines always run lean, where maximum power is produced at λ approximately 1.3, and they idle at much leaner values as reported by Challen [8]:

$$\lambda=\frac{AFR}{AFR_{Stoich}}=\frac{AFR}{14.5} \tag{9}$$

From a known mass flow rate of air as measured from the SuperFlow™ instrumentation, fuel flow rate can be calculated to augment the gravimetric system's data:

$$AFR=\frac{kg\ Air}{kg\ Fuel}=\frac{\dot{m}_{air}}{\dot{m}_{fuel}}\left(\frac{kg/s}{kg/s}\right) \tag{10}$$

BSFC is a measure of the amount of fuel consumed per horsepower. It is an efficiency metric with lower values being ideal:

$$BSFC\left(\frac{lbs}{hp\cdot hr}\right)=\frac{\dot{m}_{fuel}\left(\frac{lbs}{s}\right)}{horsepower}\times\left(\frac{3,600\,s}{hr}\right) \tag{11}$$

Or in SI notation:

$$BSFC\left(\frac{g}{W\cdot hr}\right)=\frac{\dot{m}_{fuel}\left(\frac{kg}{s}\right)}{horsepower}\times\left(\frac{1\,hp}{745.7\,W}\right)\times\left(\frac{3,600\,s}{hr}\right)\times\left(\frac{1,000\,g}{kg}\right) \tag{12}$$

BMEP differential (BMEPd) is a measure of the break horsepower and mass airflow and is useful for determining volumetric efficiency (VE):

$$BMEP_d=\frac{hp}{\dot{V}_m} \tag{13}$$

A more useful derivation with SI units is as follows:

$$BMEP_d\,(psi)=\frac{\rho_{atm}}{AFR\times BSFC\left(\frac{kg}{W\cdot s}\right)}\times\left(\frac{14.7\,psi}{101325\,Pa}\right) \tag{14}$$

A comparison of BMEP and $BMEP_d$ is particularly useful for determining assumptions with the HRR analysis. A VE greater than unity implies that all the exhaust gasses are being expelled in a two cycle engine and/or the supercharger is compressing air inside the cylinder above one atmosphere absolute pressure:

$$VE=\frac{BMEP}{BMEP_d} \tag{15}$$

3. Fuels

While a piston engine is always acting like a pump bringing in fresh air and exhausting waste gases, it is necessary to account for the mass of the fuel inside the cylinder per combustion event in order to account for the energy entering the closed system for a First Law of Thermodynamics' energy balance. This is accounted for using the Lower Heating Value (LHV) since water exits the engine in a vaporous state:

$$m_{fuel\ of\ combustion}\,(kg)=\frac{\dot{m}_{fuel}\left(\frac{kg}{s}\right)}{RPM}\times\left(\frac{60\,s}{min}\right)\times\left(\frac{Rotation}{3\,Combustion\ Events}\right) \tag{16}$$

$$E_{fuel}(J) = m_{fuel\ of\ combustion}\left(kg\right) \times LHV_{fuel}\left(\frac{J}{kg}\right) \tag{17}$$

D. CYCLE ANALYZER

1. Pressure Calculation

Raw data from the pressure sensor is scaled by a programmable charge amplifier from the sensor's specifications as well as the desired output scaling. The scaling on the amplifier is 200 psi per volt, or 13.605 bar per volt. The pressure signal needs to be zeroed, scaled, and added to the known pressure at BDC. It is assumed the pressure sensor is at one atmosphere at BDC:

$$P_{cylinder} = \left(200\ or\ 13.605\frac{MU}{V}\right)(V_{Signal} - V_{Signal\ BDC}) + P_{BDC} \tag{18}$$

2. Volume from Crank Angle Degrees

The crankshaft position sensor is positioned with zero at approximately BDC. While this can be determined mechanically, it is expensive and takes a lot of time to remove and replace the cylinder head. Previous attempts at locating TDC were deemed too great in error such that TDC had to be determined from PP during a motoring trace. It can be corrected by shifting the phase of the reported CAD:

$$\theta_{rad} = \frac{\pi(\theta_{CAD} + phase)}{180} \tag{19}$$

The following is the piston position equation given engine geometry, stroke (S) and connecting rod length ($ConRod$), as well as crank angle (θ):

$$y_{piston} = \left(\frac{S}{2}\right)\cos(\theta_{rad}) + \sqrt{ConRod^2 - \left(\frac{S}{2}\right)^2 \sin^2(\theta_{rad})} \tag{20}$$

The combustion chamber's volume as a function of piston position:

$$V = \left(y_{piston} - y_{piston}(TDC)\right) \times \left(\frac{B^2}{4}\right) + V_{Cylinder\ Head} \tag{21}$$

3. Angle of Peak, Peak Pressure, Indicated Mean Effective Pressure

AOP and PP were found by reviewing the Pressure-CAD plots. The Indicated Mean Effective Pressure (IMEP) is the actual average pressure exerted on the piston:

$$IMEP = \frac{\int_{0}^{360} PdV}{V(BDC) - V(TDC)} \tag{22}$$

A comparison of IMEP and BMEP helps discern frictional losses from the piston skirts, journal bearings, and crankshaft seals; and power consuming portions of the stroke (exhaust and intake); and cycle-related components (supercharger/blower, valves and fuel injectors); and engine-driven auxiliaries, such as the oil pump, and fuel pump. All of these power consuming components and open system portions of the engine cycle are accounted for in the friction mean effective pressure (FMEP) term:

$$FMEP = IMEP - BMEP \tag{23}$$

4. Heat Release Rate Analysis

The HRR analysis accounts for finite changes in pressure and volume in the combustion chamber to monitor the amount of chemical energy released to the cylinder at each measured position of the crankshaft via the instantaneous HRR equation:

$$\frac{dQ}{d\theta} = \frac{V\frac{dP}{d\theta} + \gamma P\frac{dV}{d\theta}}{\gamma - 1} - \frac{dQ_w}{d\theta} \tag{24}$$

The analysis is a First Law Analysis accounting for the energy content of the fuel, the heat released into the combustion chamber by the fuel, and the energy exiting in the exhaust:

$$0 = E_{fuel} + \int_{90_{BTDC}}^{85_{ATDC}} \frac{dQ}{d\theta} d\theta + U_{gas}(TDC + 85) \tag{25}$$

The system was assumed to be a closed system from 90° before TDC (BTDC) to 85° after TDC (ATDC) as indicated in supplied engine literature in Figure 14. There is a ring of ports at the bottom of each cylinder that serve as the intake. Four exhaust valves open

and close per cylinder via camshaft and rocker arms. Fuel injection is also timed via the camshaft. The exhaust valves open before and close after the intake ports. Notably, the fuel injection overlaps with exhaust valve opening makes an accounting of fuel energy in the closed-system, HRR analysis, difficult. A timing diagram is included below with 0° marking TDC as reported by Hudson [22]:

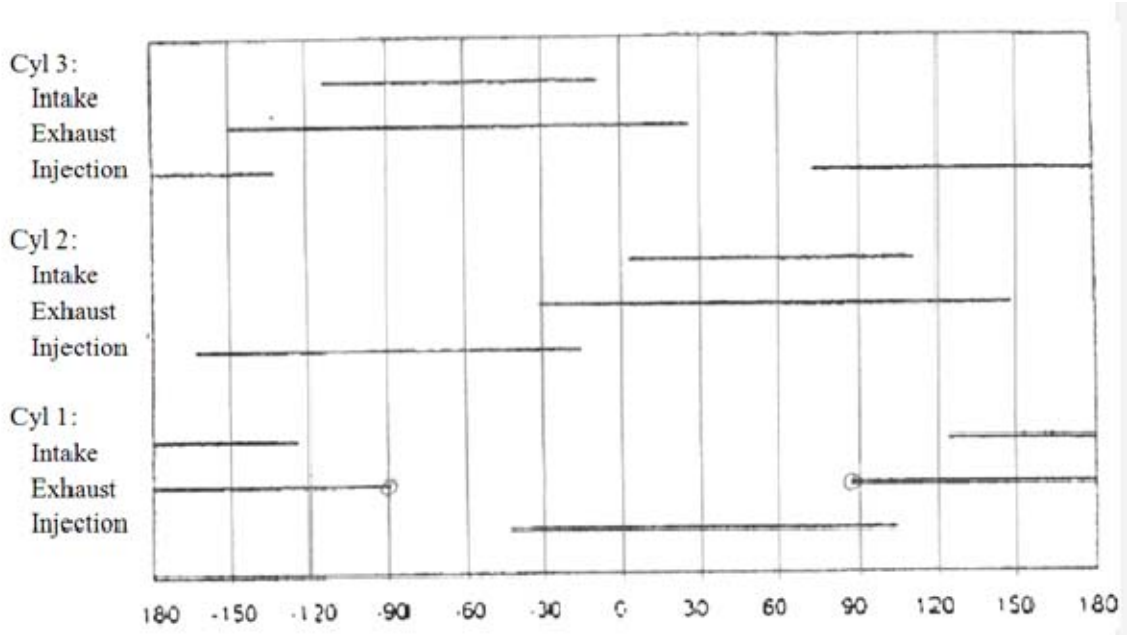

Figure 14. Intake Port, Exhaust Valve, and Injector Timing Diagram

The instantaneous HRR accounts for heat losses to the wall. Therefore, it is necessary to apply a heat transfer equation to the analysis:

$$\frac{dQ_w}{d\theta} = \frac{hA_w\left(T_w - T_i\right)}{RPM} \tag{26}$$

Where:

$$h = C_h S_p^{1/3} (P_i T_i)^{1/2} \tag{27}$$

$$A_w = 2\left(\frac{B^2}{4}\right) + \pi B\left(y_{piston} - y_{piston}(TDC)\right) \tag{28}$$

Measuring T_w is not a trivial task, but is academically accepted to be approximately 450 degrees Kelvin. S_p is the mean piston speed and is a function of stroke (S) and crankshaft speed:

$$S_p = \frac{(S)RPM}{30} \tag{29}$$

Solving for C_h in the heat transfer coefficient equation, h, is an iterative approach where the sum of the energy of the fuel, heat released from the cylinder gases, and the internal energy of the exhaust is driven to zero. There can be a huge engine-to-engine variation for this coefficient and it also changes depending on the engine load case.

To solve for the global temperature, it is necessary to flag a point along the combustion process where the pressure, volume, and temperature is known in order to solve for the charged mass inside the engine. This was done at 90° from BTDC, which is when the exhaust port closes for this engine:

$$M = \frac{P(90_{BTDC})V(90_{BTDC})}{T(90_{BTDC})R_g} \tag{30}$$

Every point from exhaust valve close, compression, combustion, up to exhaust valve open, the charged mass is assumed constant and all other variables are known except global temperature:

$$T_i = \frac{P_i V_i}{MR_g} \tag{31}$$

The changes in pressure and volume with respect to position have the following relationships:

$$\frac{dP}{d\theta}\left(\frac{Pa}{0.5\,CAD}\right) = \frac{-P_{i+2} + 8P_{i+1} - 8P_{i-1} + P_{i-2}}{12} \tag{32}$$

$$\frac{dV}{d\theta}\left(\frac{M^3}{0.5\,CAD}\right) = \frac{-V_{i+2} + 8V_{i+1} - 8V_{i-1} + V_{i-2}}{12} \tag{33}$$

The ratio of specific heats changes with temperature with the following relationships and is necessary for calculating the instantaneous HRR as reported by Goering [21]:

$$\gamma = \left(1 - \frac{R_g}{C_p}\right)^{-1} \tag{34}$$

$$\frac{R_g}{C_p} = \frac{1}{3.0447 + 1.3380E^{-}3T_i - 4.8825E^{-}7T^2{}_i + 8.5547E^{-}11T_i^3 - 5.7013E^{-}15T^4{}_i} \tag{35}$$

Finishing up the First Law energy balance, the exhaust has the following internal energy at 85° ATDC when the exhaust valve opens:

$$U_{gas} = M(kg)C_v\left(\frac{J}{kg \cdot K}\right)T(K) \tag{36}$$

Monitoring the instantaneous HRR throughout combustion reports the percent of fuel burned per CAD:

$$Fuel\ Mass\ Fraction\ Burned\ (x) = \frac{\int_{90_{BTDC}}^{x} \frac{dQ}{d\theta}d\theta}{\int_{90_{BTDC}}^{85_{ATDC}} \frac{dQ}{d\theta}d\theta} \tag{37}$$

SOI is defined to occur at ten percent of the fuel's mass fraction burned and BDR lasts from ten percent of the fuel's mass fraction burned to 90% mass fraction burned.

THIS PAGE INTENTIONALLY LEFT BLANK

IV. RESULTS

A. RELATIVE PERFORMANCE DIFFERENCES BETWEEN HYDROTREATED VEGETABLE OILS AND PETROLEUM FUELS

1. Motoring Trace Phase Correction

The engine was cycled without fuel entering the cylinder at 400 RPM. Peak pressure occurred 6.5 degrees ATDC. All measurements were corrected by moving the signal back 7 degrees.

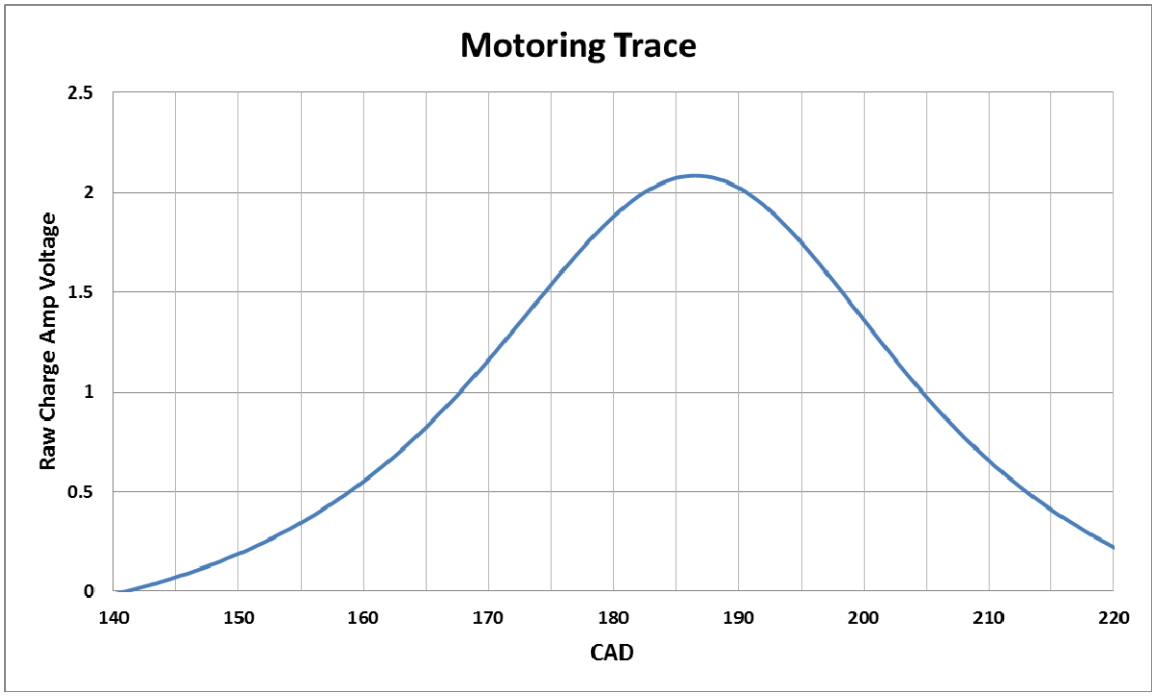

Figure 15. Motoring Trace

2. Gravimetric Fuel System Example

The slope of all gravimetric data was calculated in a Matlab™ script (Appendix E) via a least squares method. One slope has been included as an example of the data collected:

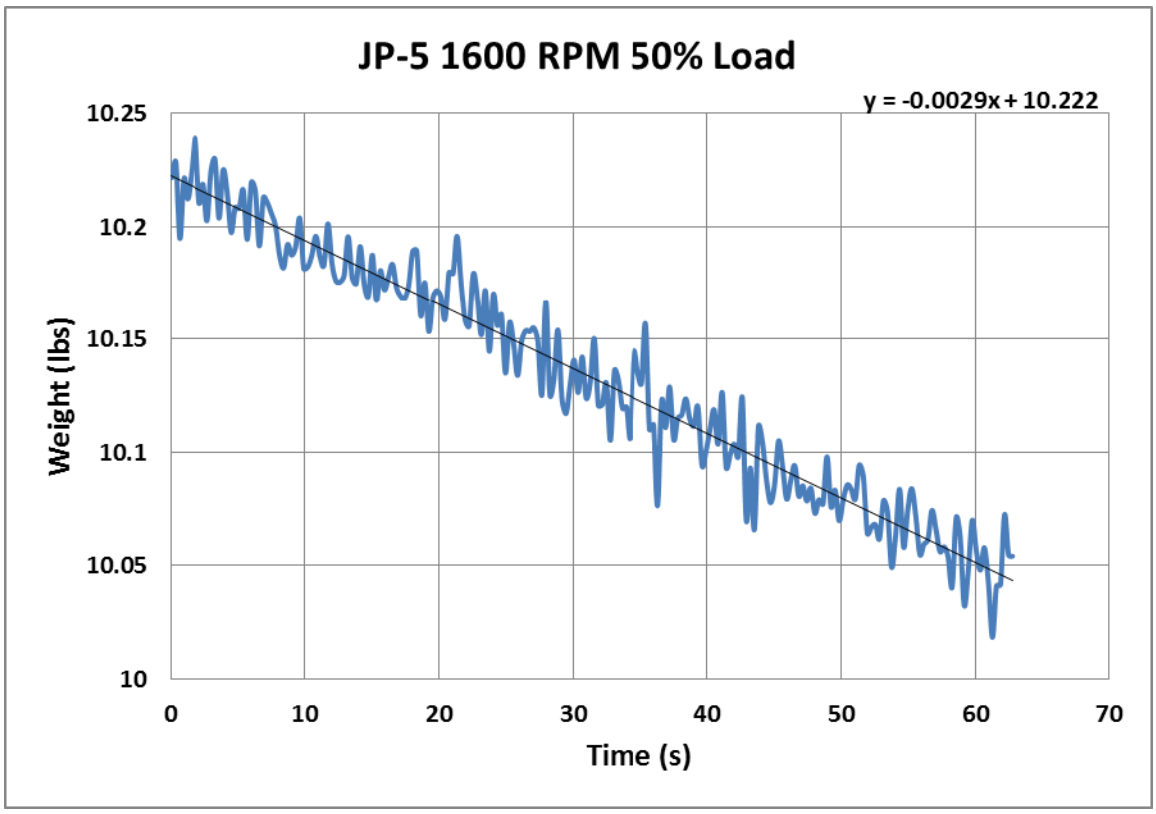

Figure 16. *dW/dt* Least Squares Linear Regression

3. Pressure – CAD & Pressure – Volume Plots

The following plots are an example of the HRD Algae's performance over the tested load speed matrix. After a boxcar filter is applied, PP, AOP, and IMEP are determined. This pressure trace data is then used in a HRR analysis. All Pressure – CAD and Pressure – Volume data is included in Appendix F.

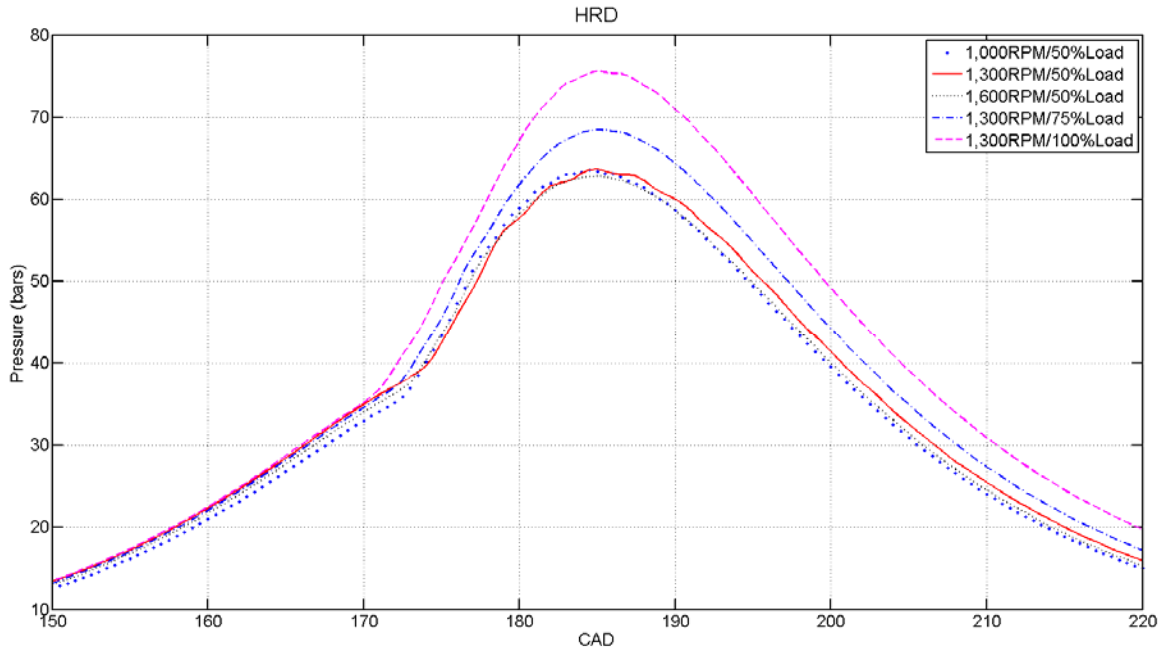

Figure 17. Pressure – CAD Plots of HRD Algae

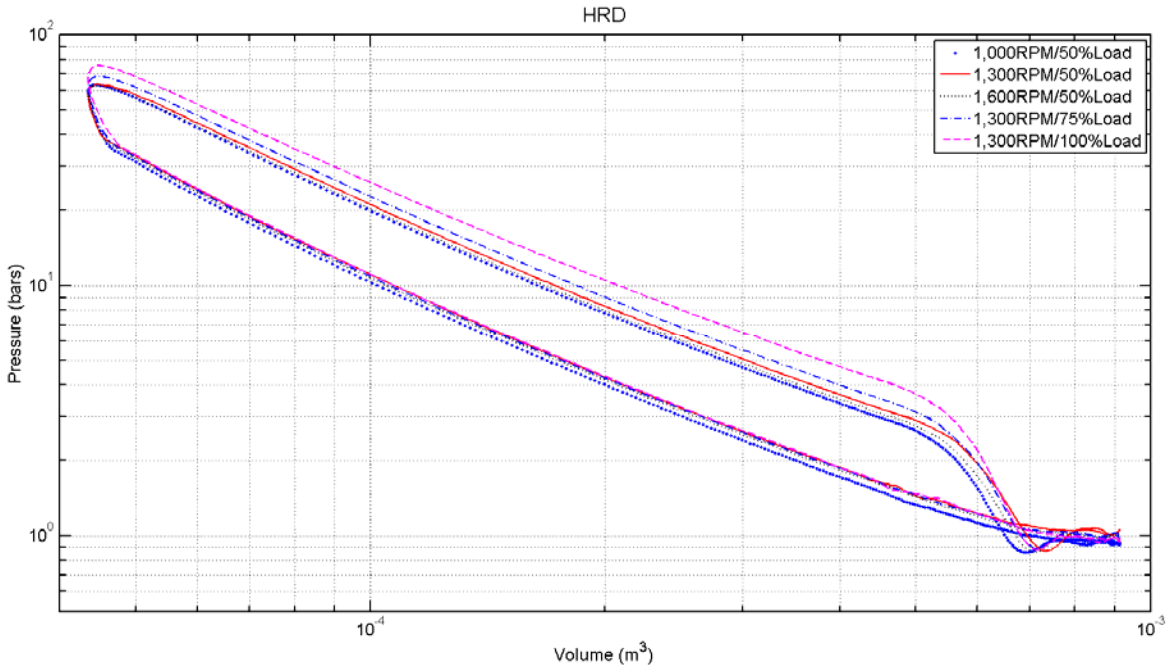

Figure 18. Pressure – Volume Plots of HRD Algae

4. Heat Release Rate

SOI was assumed at 135 CAD by the engine timing diagram. A HRR plot and a mass fraction burn plot have been included as an example to demonstrate the calculation of CAD10 and CAD90 mass fraction burned points. These plots noticeably differ from typical common rail diesel engine HRR plots because the mechanical unit injectors are injecting from 45° BTDC to 105° ATDC, a much longer injection:

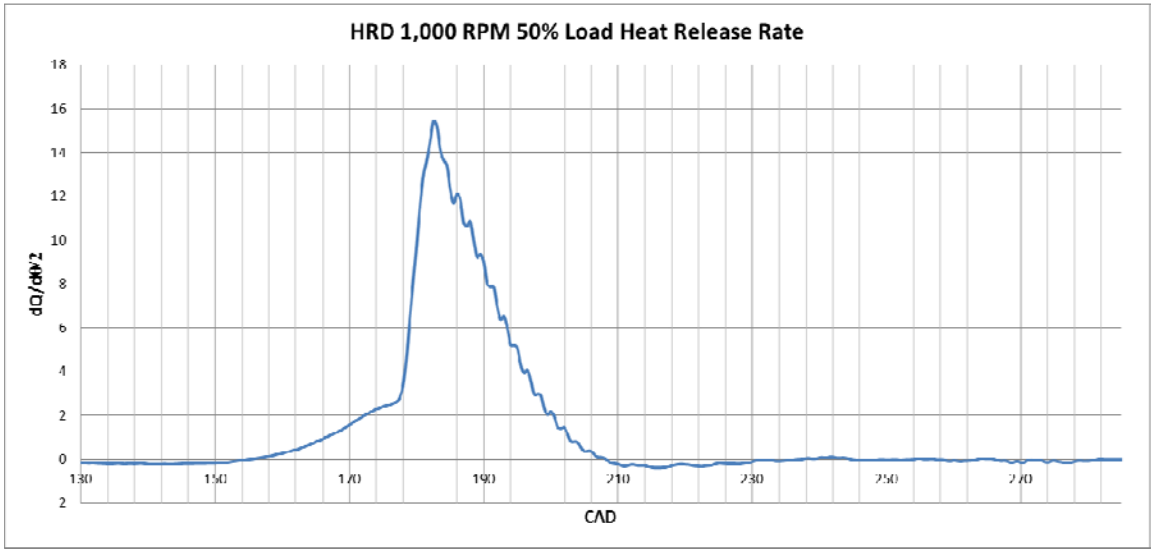

Figure 19. Heat Release Rate Example

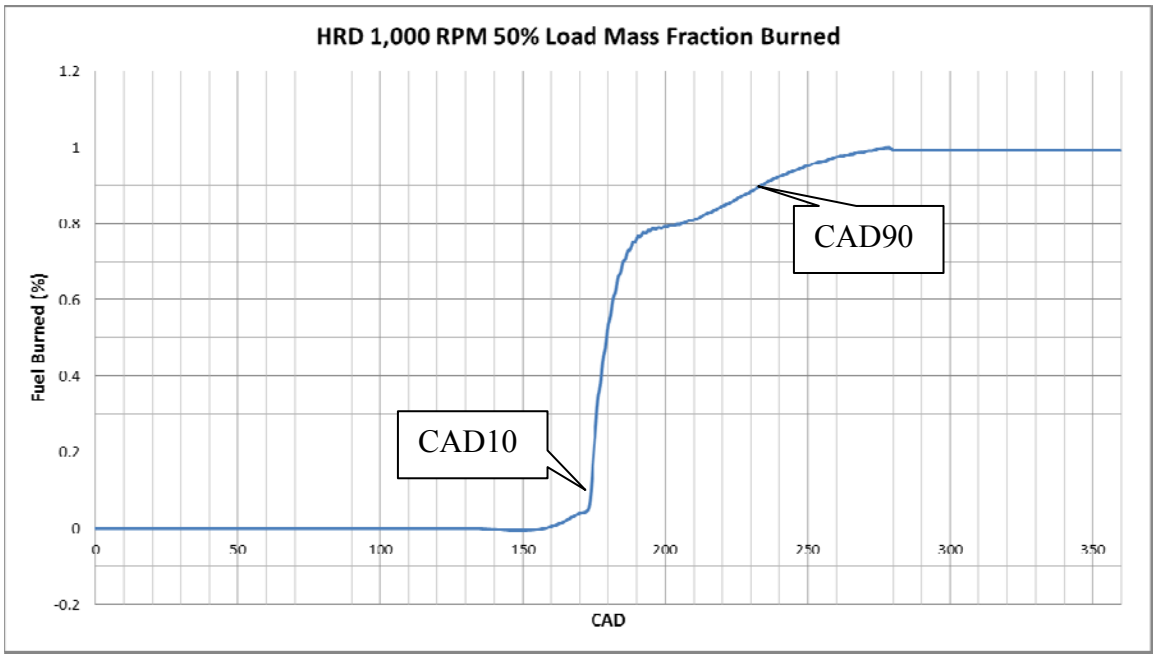

Figure 20. Mass Fraction Burned per CAD

5. HRD Algae vs. Diesel #2

RPM	**1000**	**1300**	**1600**	**1300**	**1300**	**1300**
Torque (ft*lbs)	**60**	**60**	**60**	**60**	**90**	**120**
HRD/D2 BSFC	0.914	0.962	0.769	1.044	0.912	0.874
HRD-D2 PP (Bar)	-0.527	-2.299	-2.465	-2.353	-0.259	-0.065
HRD-D2 AOP (CAD)	2.5	3.0	1.0	-1.0	1.0	1.0
HRD-D2 IMEP (Bar)	0.095	0.041	0.017	0.017	0.007	-0.102
HRD-D2 FMEP (Bar)	0.211	0.029	0.042	0.011	-0.096	-0.041
HRD-D2 IGD (CAD)	-1.5	-1.5	-1.0	-1.0	-1.5	-1.0
HRD-D2 BDR (CAD)	1.5	2.0	2.5	1.0	2.0	1.5

Figure 21. Comparison of HRD Algae and Diesel #2

HRD was on average 9% more efficient in BSFC, 1.3 bars lower in PP, 1.25 CADs delayed in AOP, 0.013 bars higher in IMEP, ignited 1.25 CADs earlier, and burned 1.75 CADs longer than Diesel #2.

6. HRD Algae vs. NATO F-76

RPM	**1000**	**1300**	**1600**	**1300**	**1300**	**1300**
Torque (ft*lbs)	**60**	**60**	**60**	**60**	**90**	**120**
HRD/D2 BSFC	-	-	1.074	0.862	1.003	0.924
HRD-D2 PP (Bar)	-	-2.630	-3.229	-4.702	-1.100	-0.633
HRD-D2 AOP (CAD)	-	3.0	0.5	1.0	2.0	-1.0
HRD-D2 IMEP (Bar)	-	0.073	0.078	-0.036	0.033	-0.052
HRD-D2 FMEP (Bar)	-	0.089	0.126	-0.049	-0.086	0.006
HRD-D2 IGD (CAD)	-	-1.5	-1.5	-1.5	-1.5	-1.0
HRD-D2 BDR (CAD)	-	1.5	1.5	3.0	1.0	1.5

Figure 22. Comparison of HRD Algae and NATO F-76

HRD was on average 3% more efficient in BSFC, 2.5 bars lower in PP, 1.1 CADs delayed in AOP, 0.019 bars higher in IMEP, ignited 1.4 CADs earlier, and burned 1.7 CADs longer than F-76.

7. HRJ Camelina vs. NATO JP-5

RPM	1000	1300	1600	1300	1300	1300
Torque (ft*lbs)	60	60	60	60	90	120
HRD/D2 BSFC	0.786	1.091	0.830	0.922	0.831	1.088
HRD-D2 PP (Bar)	-4.725	-4.490	-	-4.125	0.289	-2.037
HRD-D2 AOP (CAD)	2.0	1.0	-	3.0	0.0	1.5
HRD-D2 IMEP (Bar)	-0.071	-0.105	-	-0.088	0.136	-0.001
HRD-D2 FMEP (Bar)	-0.177	-0.111	-	-0.088	0.004	0.096
HRD-D2 IGD (CAD)	-1.5	-1.5	-	-1.5	-2.0	-1.0
HRD-D2 BDR (CAD)	2.0	2.5	-	3.5	3.5	3.0

Figure 23. Comparison of HRJ Camelina and NATO JP-5

HRJ was on average 6% more efficient in BSFC, 3.0 bars lower in PP, 1.5 CADs later in AOP, 0.026 bars higher in IMEP, ignited 1.5 CADs earlier, and burned 2.9 CADs longer than JP-5.

B. RELATIVE PERFORMANCE DIFFERENCES BETWEEN COMPRESSION IGNITION AND PLASMA ASSISTED IGNITION

The following Pressure – CAD and Pressure - Volume plots were obtained via a 20 kHz frequency based sample rate. It is the average of 100 combustion samples. The encoder was not operational for this measurement, so certain features of the curve have been flagged with known CADs of more current data. The two points selected were the combustion point of inflection found to be at three degrees BTDC and exhaust valve opening at 105° ATDC. Crankshaft speed was assumed to be constant. TDC is 180°. A nine point moving boxcar filter was used to cancel out noise:

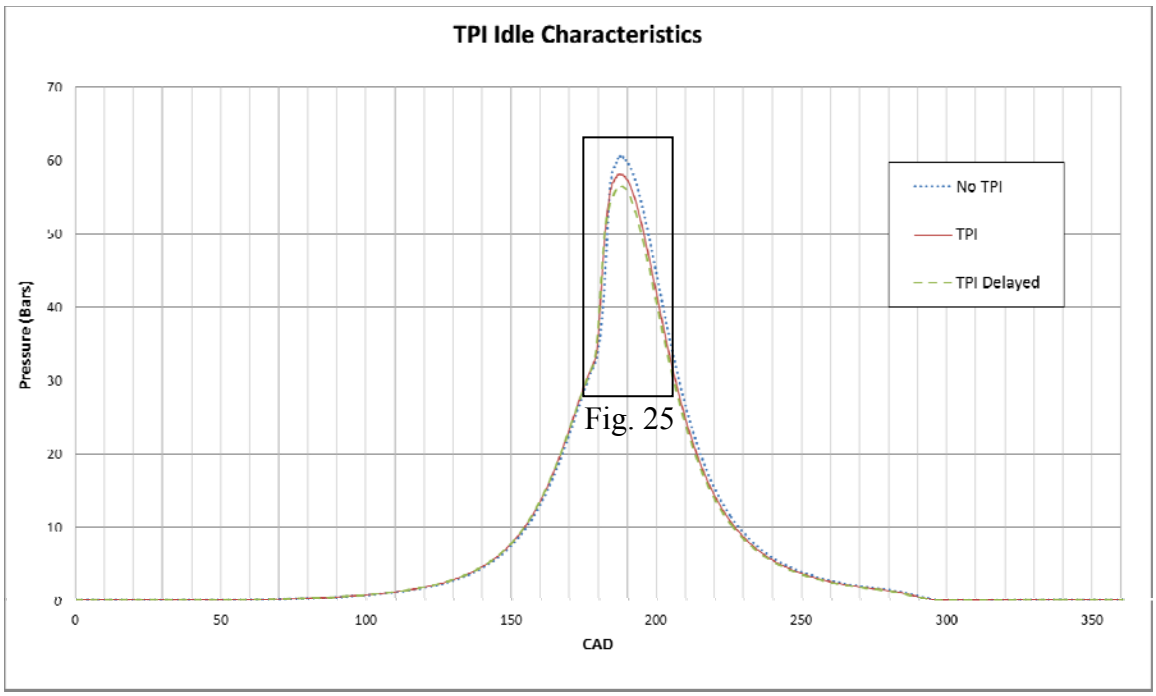

Figure 24. Pressure – CAD Plot of TPI vs. CI

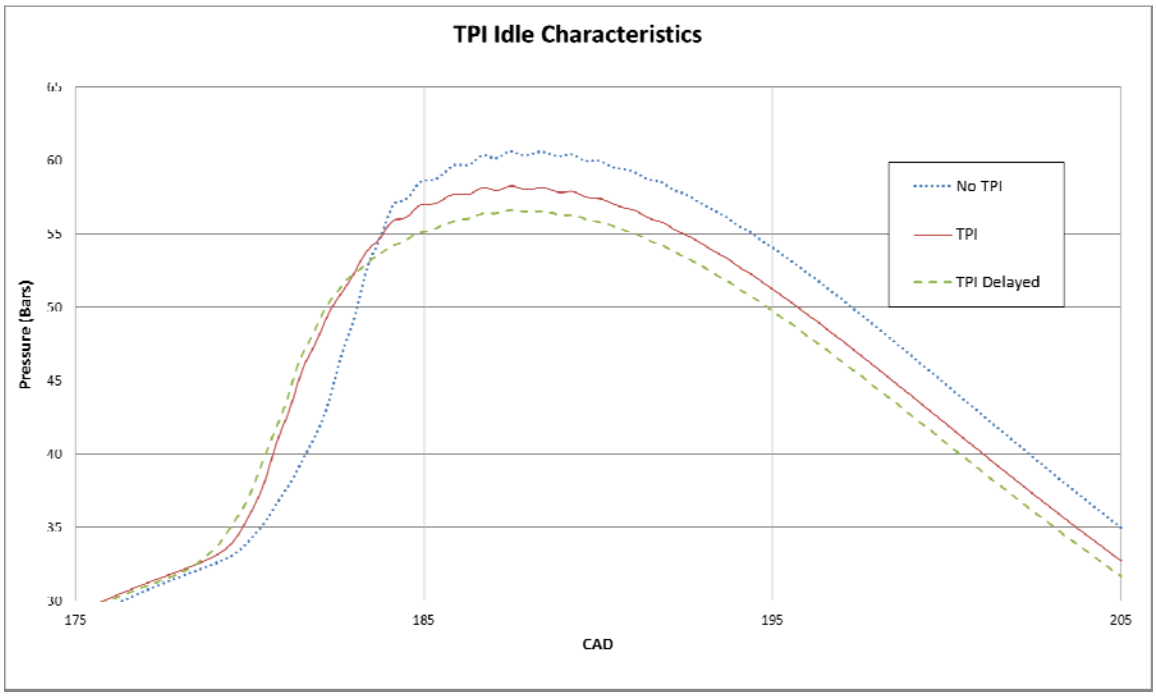

Figure 25. Zoomed in View of Pressure – CAD Plot of TPI vs. CI

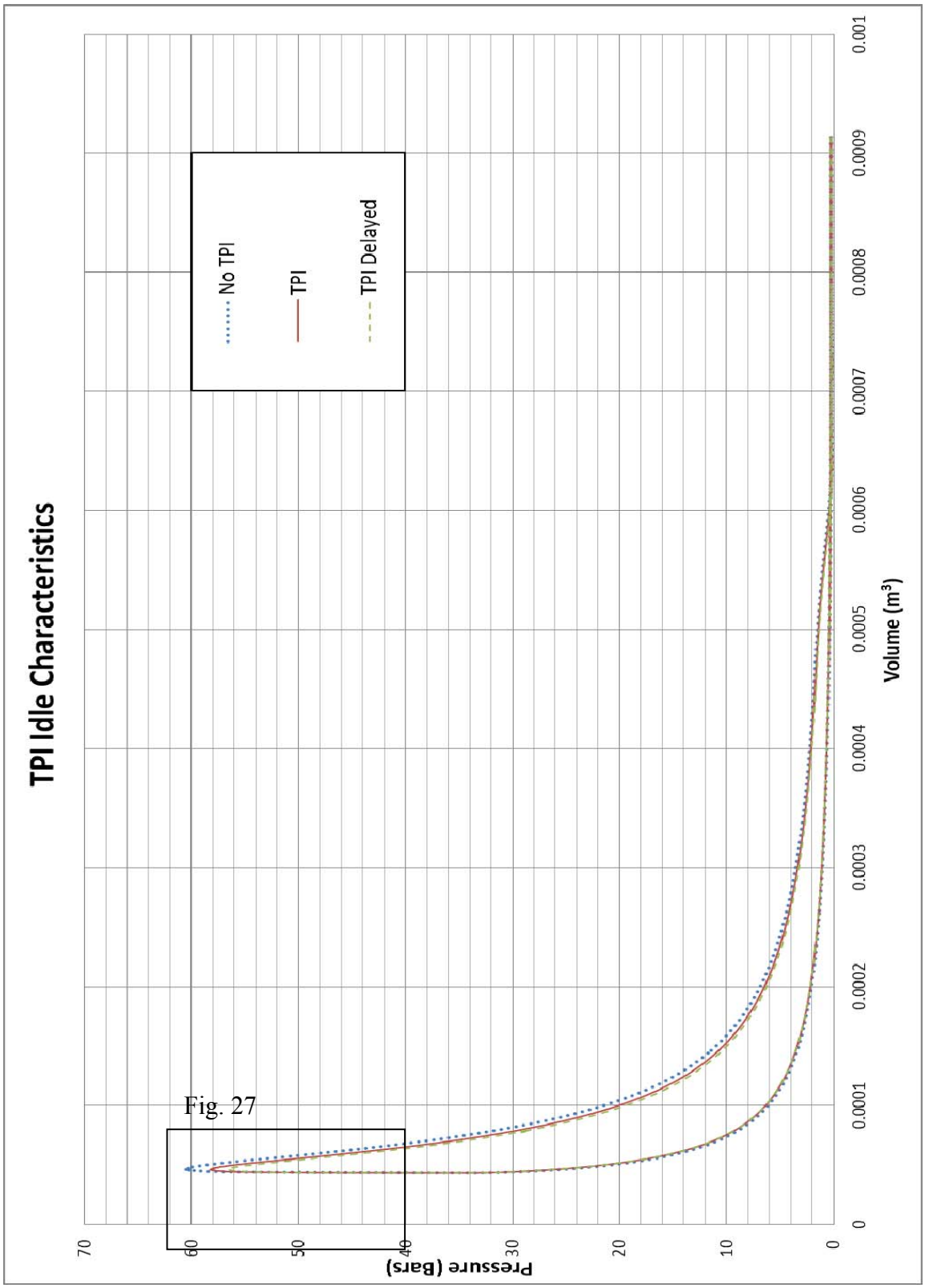

Fig. 27

Figure 26. Pressure – Volume Plot of TPI vs. CI

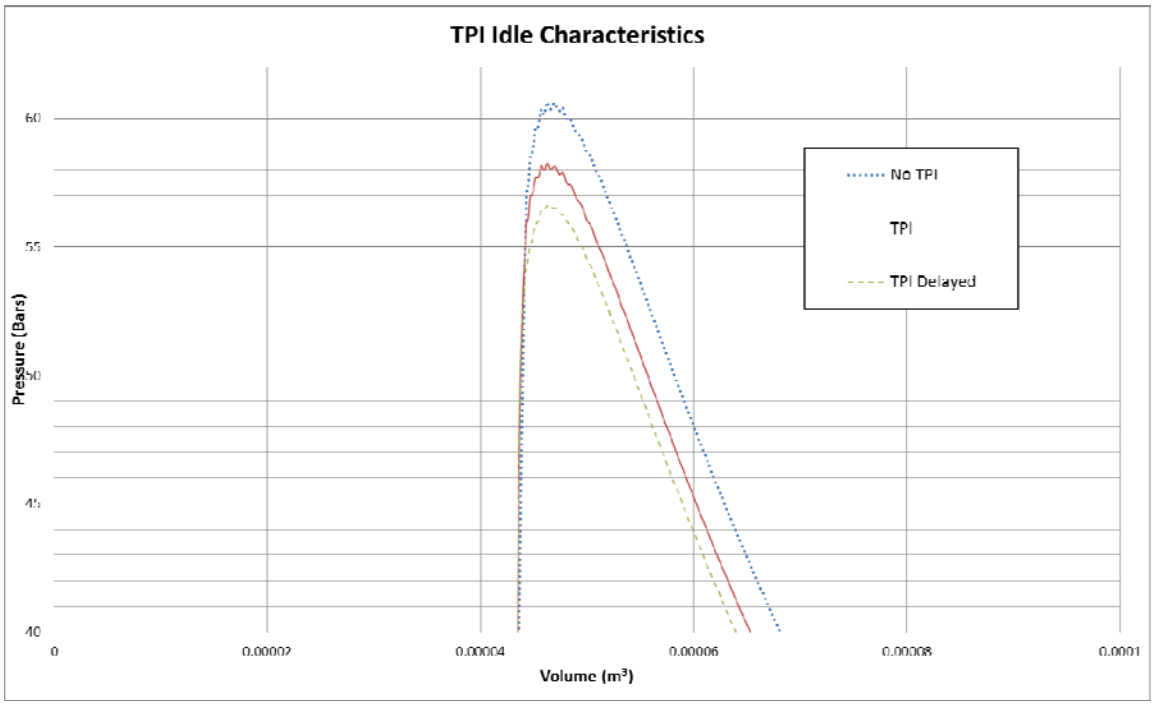

Figure 27. Zoomed in View of Pressure – Volume Plot of TPI vs. CI

Very little TPI data was collected before all three of the USC electrodes failed. There appears to be earlier combustion, but lower peak pressures with TPI. Due to the error of the data collection and data processing, (no encoder), there is no noticeable effect of TPI at this time of experimentation. Moreover, the progressive failure of two of the three electrodes makes it hard to discriminate between the effects of TPI and the effects of a weakening electrode. The no TPI condition was tested first, followed by TPI, followed by TPI with a 199 ms delay.

Electrode failure occurred at approximately one hour of engine runtime each when the alumina isolator either cracked or exploded out of the cylinder. It was believed that the electrodes failed due to a fatigue failure; cycling stresses were exerted on the electrode via engine shaking with the electrode wire hanging from the electrode. The electrode design had been tested on a previous date for approximately 15 minutes at all engine speeds and engine loads. The electrodes all failed at idle where the effective pressures are far less than at load.

Figure 28. Three Failed Electrodes

An alumina electrode was assessed to be too weak for this engine and future designs of the electrode will be made of porcelain. While the limited data collected does not show any benefit in the PV diagram, there are still many more variables that went unexplored in the experiment: the engine never left idle and the TPI was triggered around start of combustion.

THIS PAGE INTENTIONALLY LEFT BLANK

V. SUMMARY AND CONCLUSIONS

A. SUMMARY

The HVO biofuels had on average 1.4 CADs earlier ignition, 2 CADs longer burn duration, 2.25 bars decrease in PP, 1.25 CAD delay in AOP, a 0.5% increase in IMEP, and a 6% improvement in BSFC than their petroleum counterpart.

Table 6. Average Properties of Fuel Comparisons

RPM	HRD/D2	HRD/F-76	HRJ/JP-5
~Δ Cetane #	**34**	**34**	**20**
BSFC Ratio	0.91	0.97	0.93
Δ PP (Bar)	-1.33	-2.46	-3.02
Δ AOP (CAD)	1.25	1.10	1.50
Δ IMEP (Bar)	0.013	0.019	0.026
Δ IGD (CAD)	-1.25	-1.40	-1.5
Δ BDR (CAD)	1.75	1.70	2.9

TPI produced a 1 CAD earlier start of ignition, a faster initial pressure rise following start of ignition, but a 7% drop in PP. IMEP decreased for the TPI condition. A HRR analysis was unable to be performed due to the missing encoder signal.

B. CONCLUSIONS

1. Biofuels

By definition, higher cetane fuels ignite more easily. Earlier ignition limits the fuels' mixing time, and therefore increases the burn duration of the fuel. The HRR

analyses and the cycle analyses of the biofuels tested are both characteristic of higher cetane fuels due to relatively earlier ignition and longer burn durations. High cetane fuels are good for the Detroit Diesel 3-53 because PP is earlier that ideal for standard Diesel #2. By injecting high cetane biofuels in the engine, ignition occurs later and more gradually, burns longer, and pressures drop off later than their petroleum based counterparts. This benefit is directly indicated by the increase in IMEP and indirectly indicated by the decrease in BSFC.

The second generation biofuel tested, HRD Algae and HRJ Camelina, ran in the engine with very similar combustion characteristics to Diesel #2, F-76, and JP-5 respectively. The data collected for this report as well as other legacy engine research by Cowart, Carr, et al. [23] indicates that both fuels are a suitable *combustion* alternative for legacy engines. Entirely unexplored is this research is the effects of lubricity on the fuel system; the long-term material effects on legacy engines should be examined and evaluated before switching to biofuels.

2. Transient Plasma Ignition

Current Pressure – CAD plots of TPI indicate an earlier start of ignition but lower PP than conventional CI. This earlier combustion and lower PP trend is characteristic of the high cetane biofuels evaluated in this thesis. It appears that TPI is increasing the apparent cetane number of the fuel. While there is not a great deal of confidence in the data due to the missing encoder signal, the eventual failure of the electrode, and an absence of any repeated experimental data, TPI appears to improve the ignitability of the fuel.

3. Engine Upgrades

The NPS' Detroit Diesel 3-53 engine facility was successfully upgraded to accept alternate fuels, now has the capability to do HRR analyses, and has a much more precise method for measuring fuel consumption with the gravimetric fuel measurement system.

APPENDIX A. GRAVIMETRIC FUEL CONTAINER DESIGN

The gravimetric fuel bucket was machined and manufactured by Advantage Products in Monterey, California. It consisted of (7) Parts: bucket, bucket clamp, mounting block, mounting block clamp, left bracket, right bracket, and point load hangar. Notably, there is a gap between the mounting block and the fuel bucket. A rubber dam was installed in this gap to prevent fuel contamination and fuel spills. Also, not shown are four pieces of all-thread that connect the H-shaped point load hangar to the fuel bucket.

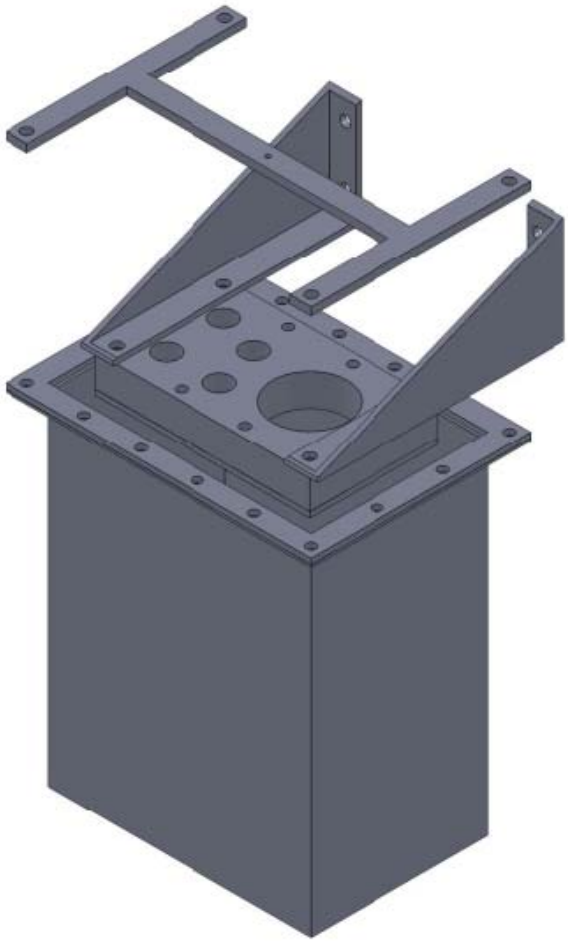

Figure 29. Isometric CAD Graphic of Gravimetric Fuel Measurement System Assembly

The fuel bucket was made out of 16 gauge stainless steel and can contain 192 in^3 of fuel. Given the engine power output, this bucket can hold approximately five minutes of fuel which was deemed enough time to test one fuel on an engine load – engine speed matrix. A diagonal sight glass was installed on the bucket and a fuel tank potentiometer was installed to report tank height to the control room during dynamometer runs. A drain cock was installed in the bottom to allow for easy flushing between fuels. The circumferential holes are made to clamp a rubber dam.

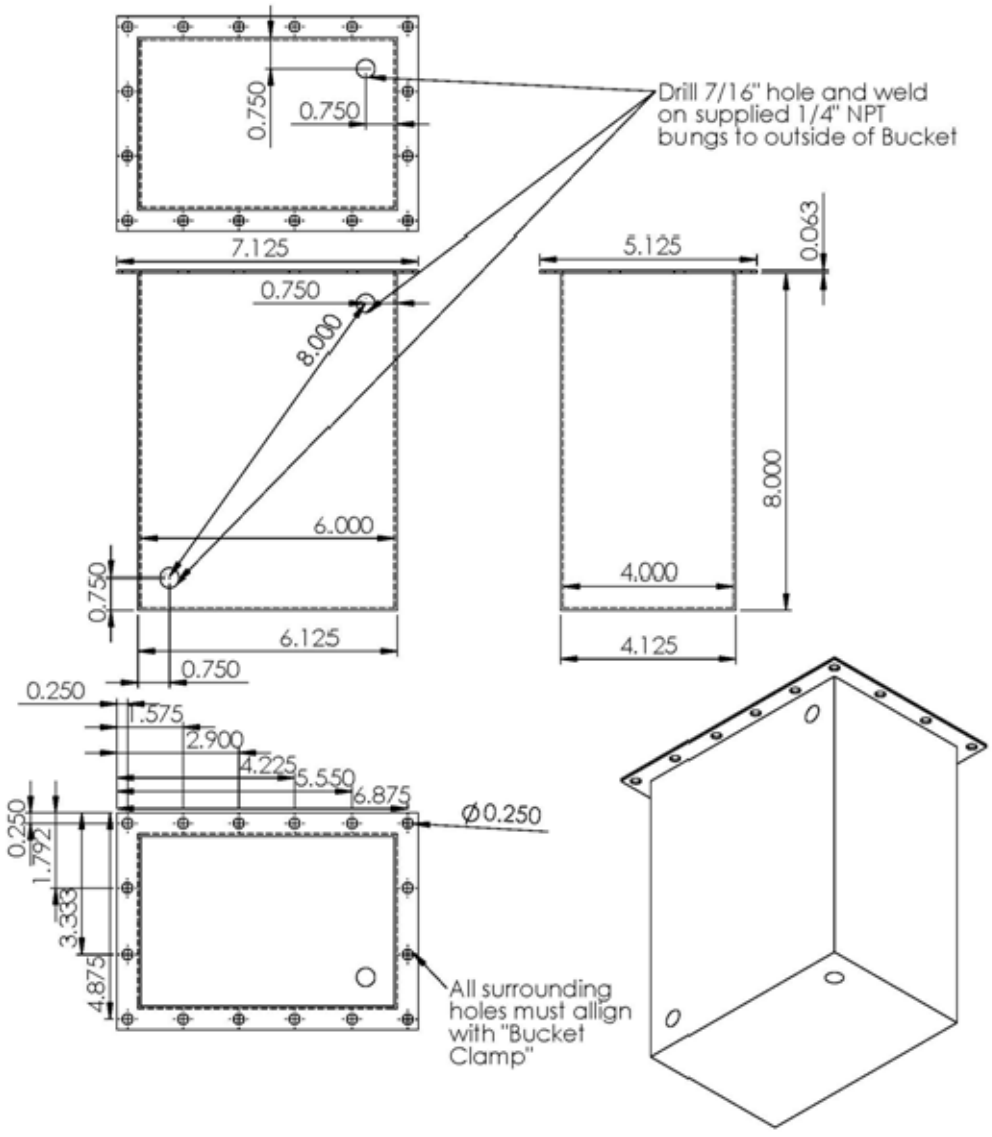

Figure 30. Engineering Drawing of Fuel Bucket

The mounting bracket was made with five holes to mount sensors and route fuel. Like the fuel bucket, the circumferential holes are made to clamp a rubber dam between the mounting bracket and the fuel bucket. It is important that no sensors are hanging against the load cell via the bucket as their weights would contribute to the fuel weight readings. Therefore plumbing is routed to the mounting block. Of the five holes, one is the fuel supply, another is the return, and one is the pickup, the fourth a breather hole that vents through an air filter, and the biggest hole is for a marine fuel tank float.

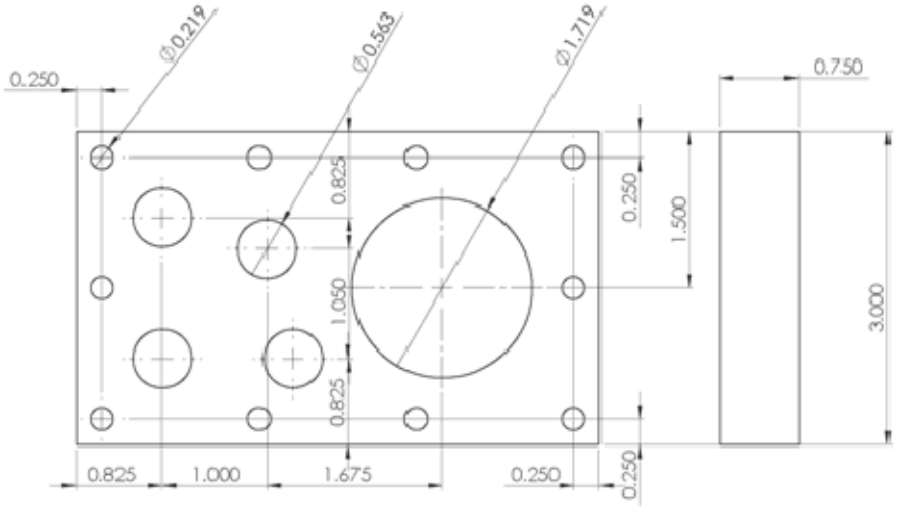

Figure 31. Engineering Drawing of Mounting Bracket

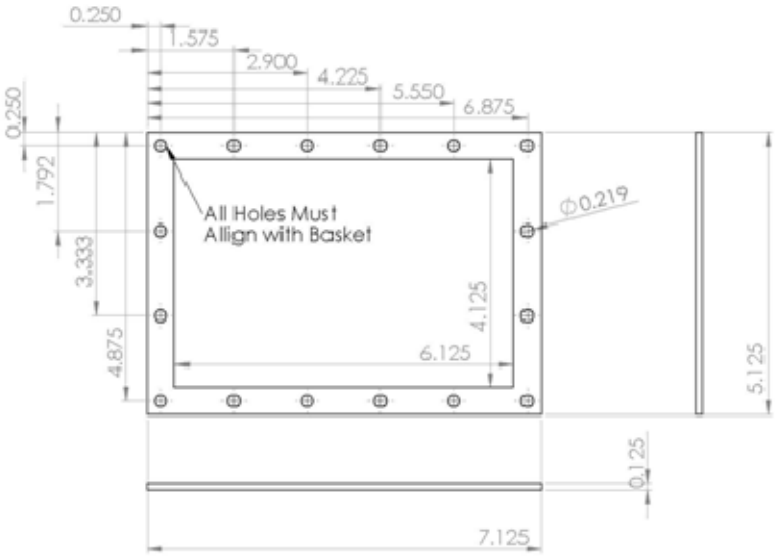

Figure 32. Engineering Drawing of Clamp Bucket

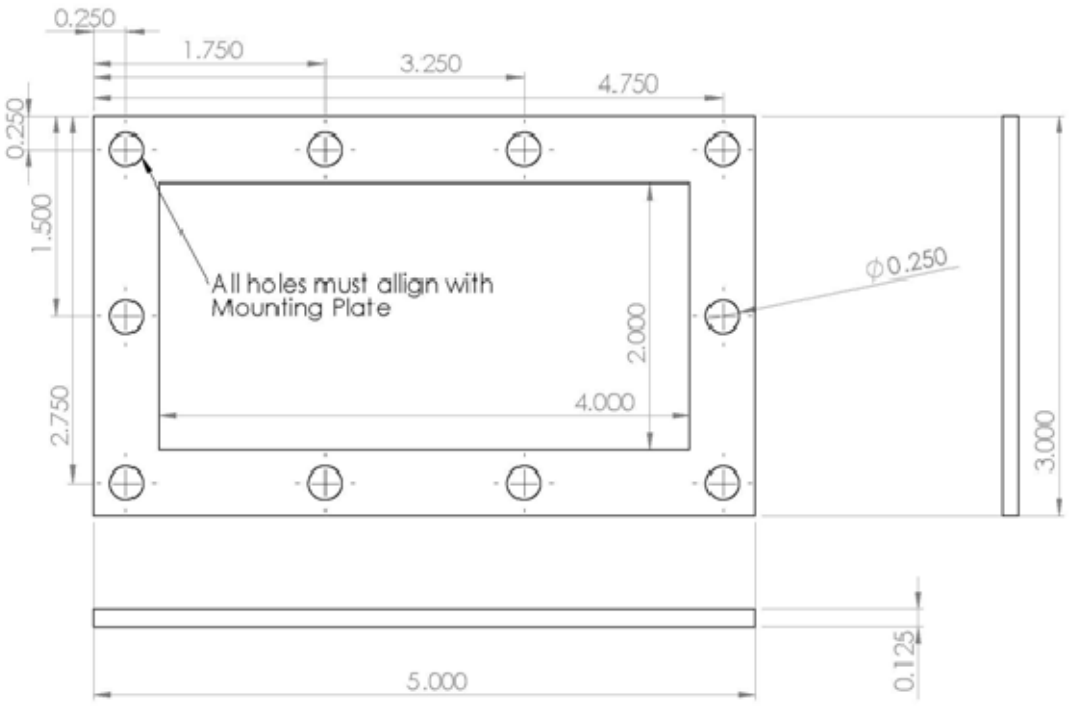

Figure 33. Engineering Drawing of Mounting Plate Clamp

The two brackets and the point load hangar were not necessary to include in this report. They are simply a way to mount the mounting bracket to the fuel cabinet and suspend the bucket and contained fuel from the load cell.

APPENDIX B. LABVIEW FUEL SYSTEM CONTROL

LabVIEW™ is a graphics user interfaced based code. As such, it has a front panel that the user can control a system, as well as observe, collect, and save data. It is driven by a wiring diagram that is also graphical. Wiring diagrams can and are nested in the following documentation.

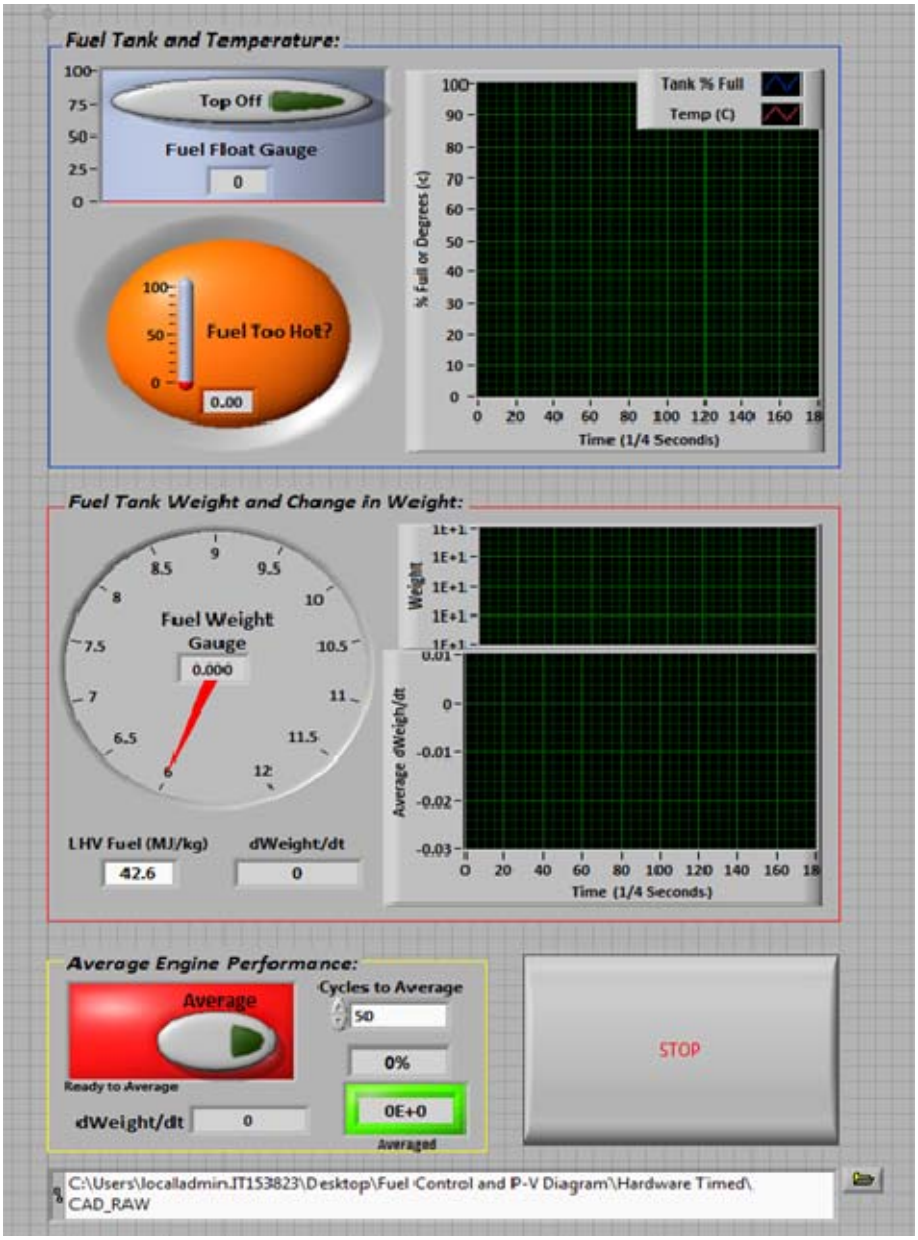

Figure 34. Front Panel of Fuel Measurement System

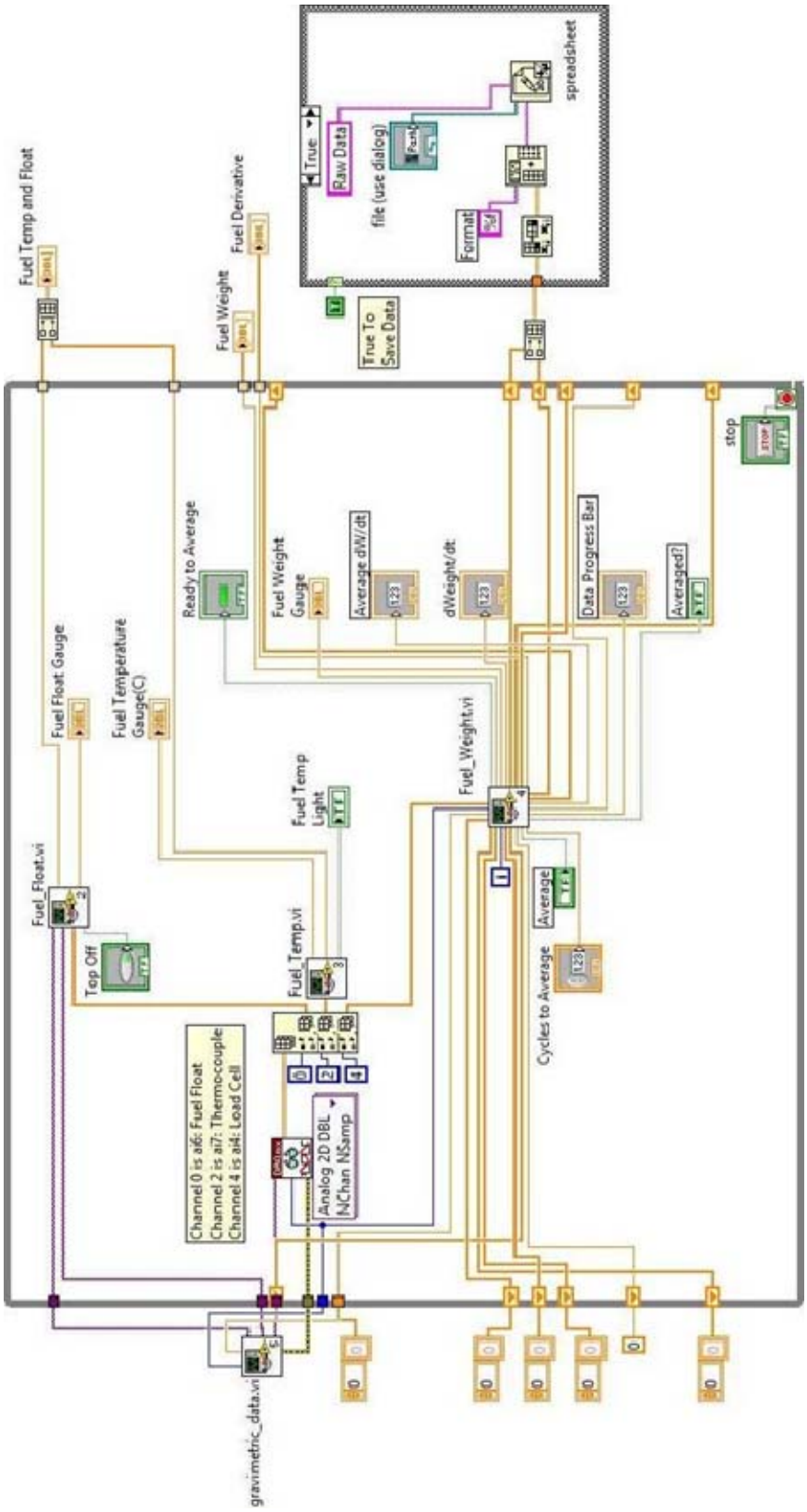

Figure 35. Wiring Diagram of Measurements System

The system collects data from three different sensors listed from top to bottom of Figure 25: Fuel Float Readings, Thermocouple Measurements, and a Load Cell. It also has the control logic necessary to refill the gravimetric fuel bucket when the tank gets low. Ghost channels were observed and thrown out to minimize cross talk effects associated with high frequency multiplexing. A digital five volt channel was created to drive the fuel float excitation device.

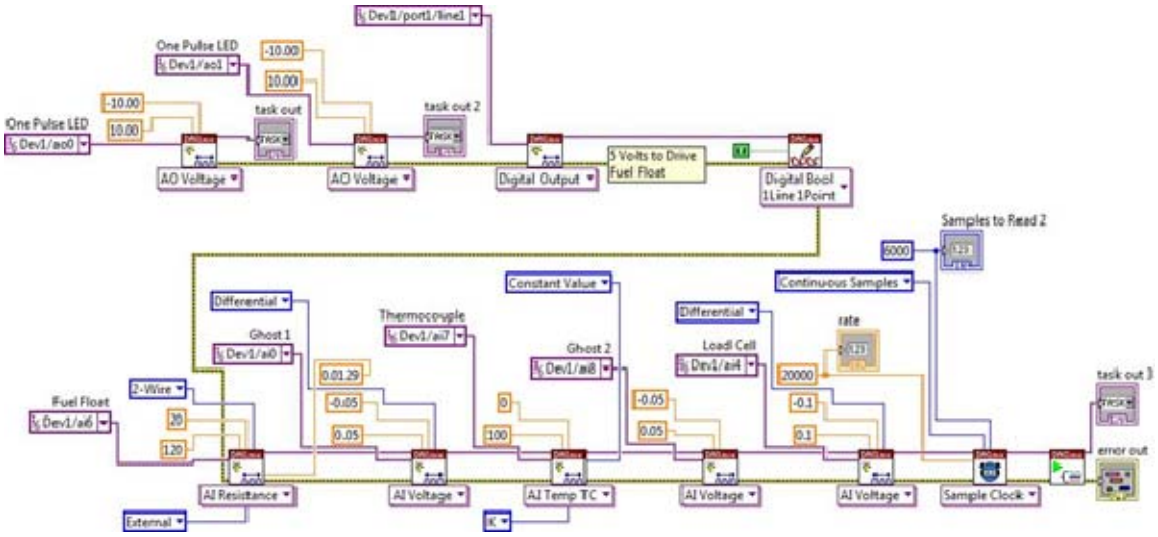

Figure 36. Gravimetric_data.vi

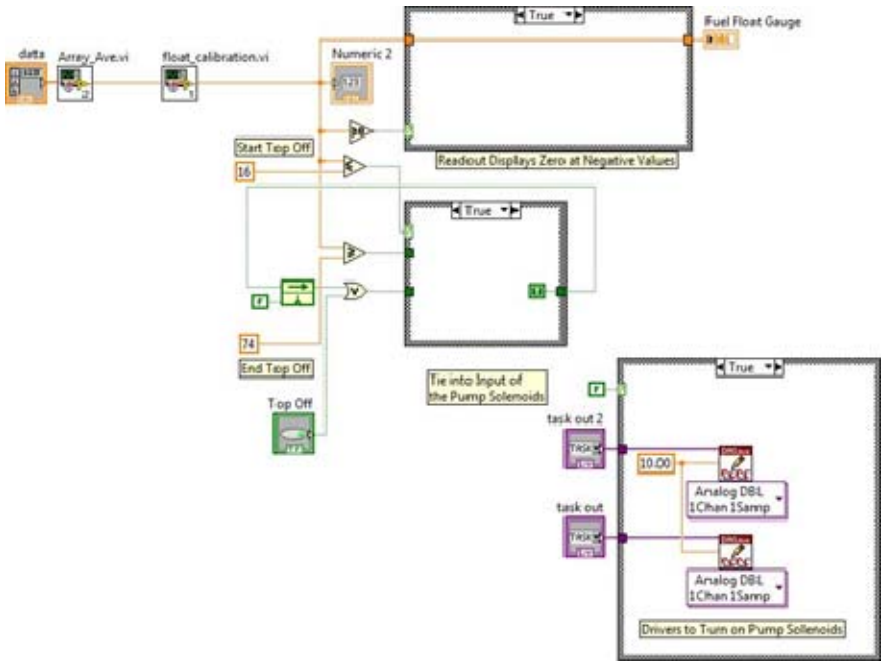

Figure 37. Fuel_Float.vi

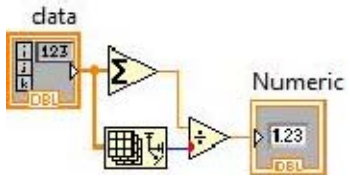

Figure 38. Array_Ave.vi

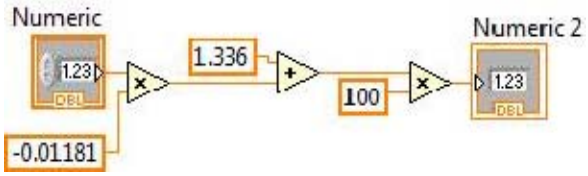

Figure 39. float_calibration.vi

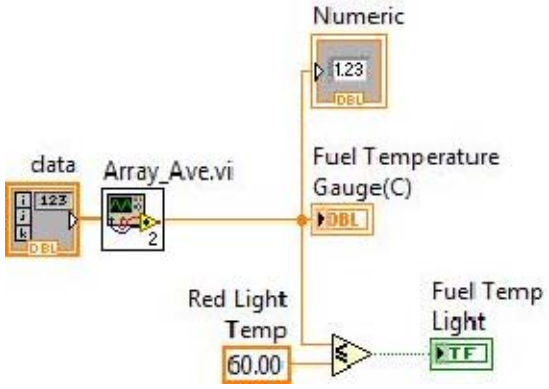

Figure 40. Fuel_Temp.vi

The Fuel_Weight.vi is responsible for processing the load cell readings and is the heart of system. After filtering, averaging, and scaling, a set number of data points are collected before collecting data. After start of data collection a least squares slope is used to calculate the derivative of fuel consumption. Each additional data point replaces the oldest data point and the slope is updated to give a rapid fuel consumption measurement. The weight array is ultimately exported to Matlab™ (Appendix E) for a linear regression analysis.

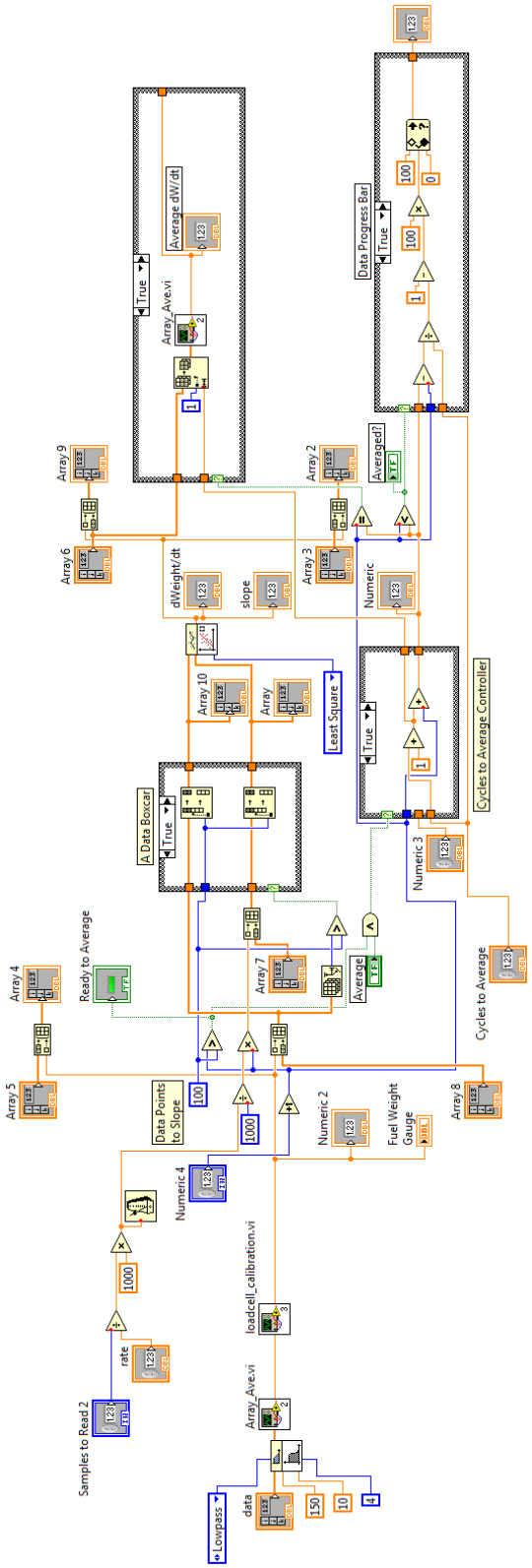

Figure 41. Fuel_Weight.vi

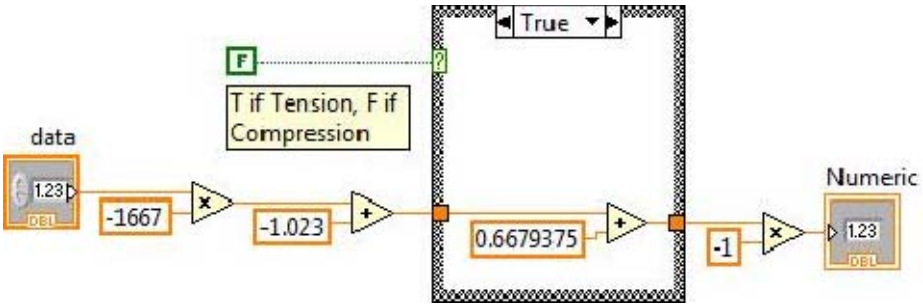

Figure 42. loadcell_calibration.vi

APPENDIX C. LABVIEW CYCLE ANALYZER

1. FREQUENCY MEASUREMENT

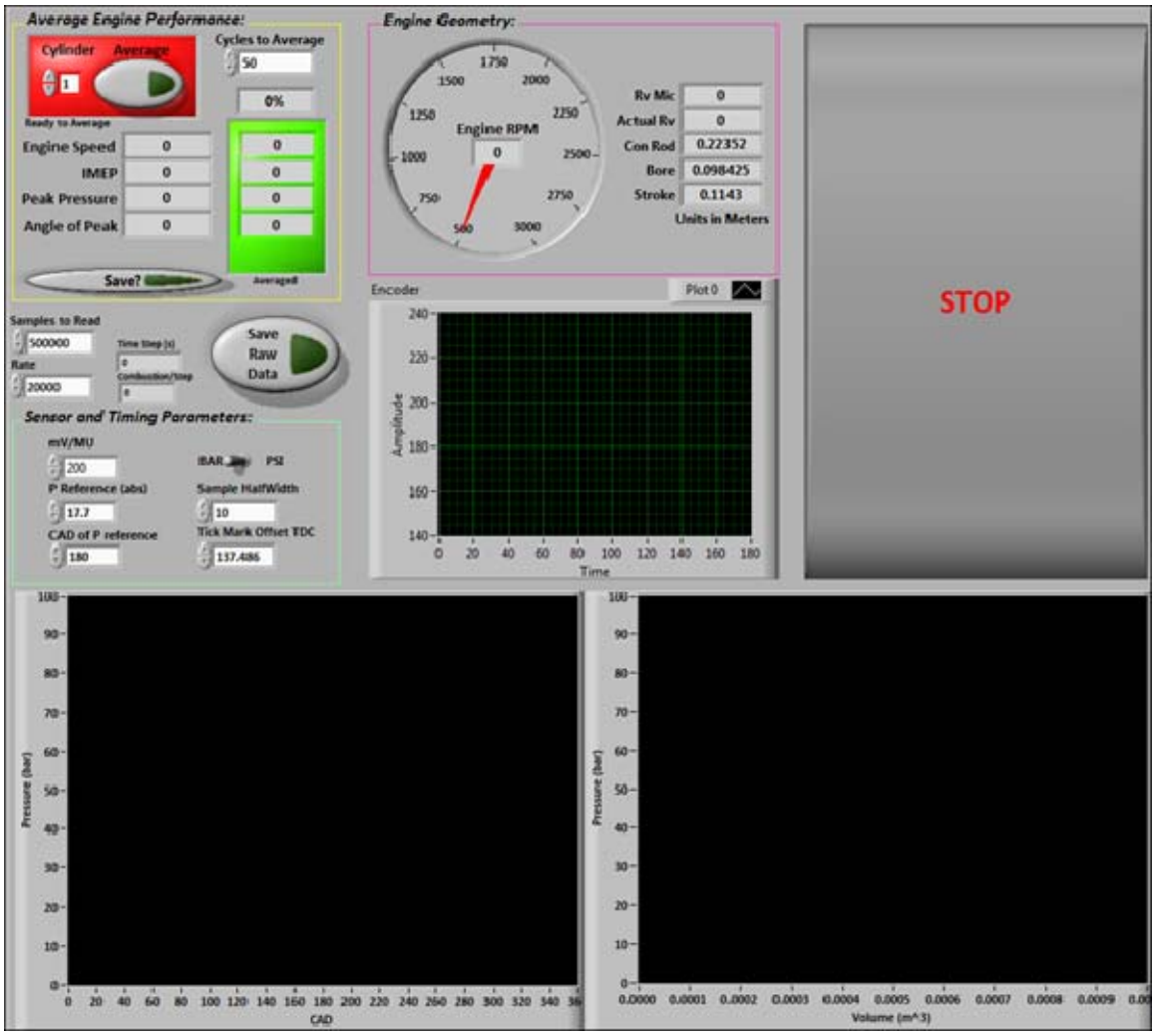

Figure 43. Front Panel of Frequency Measurement (Frequency.vi)

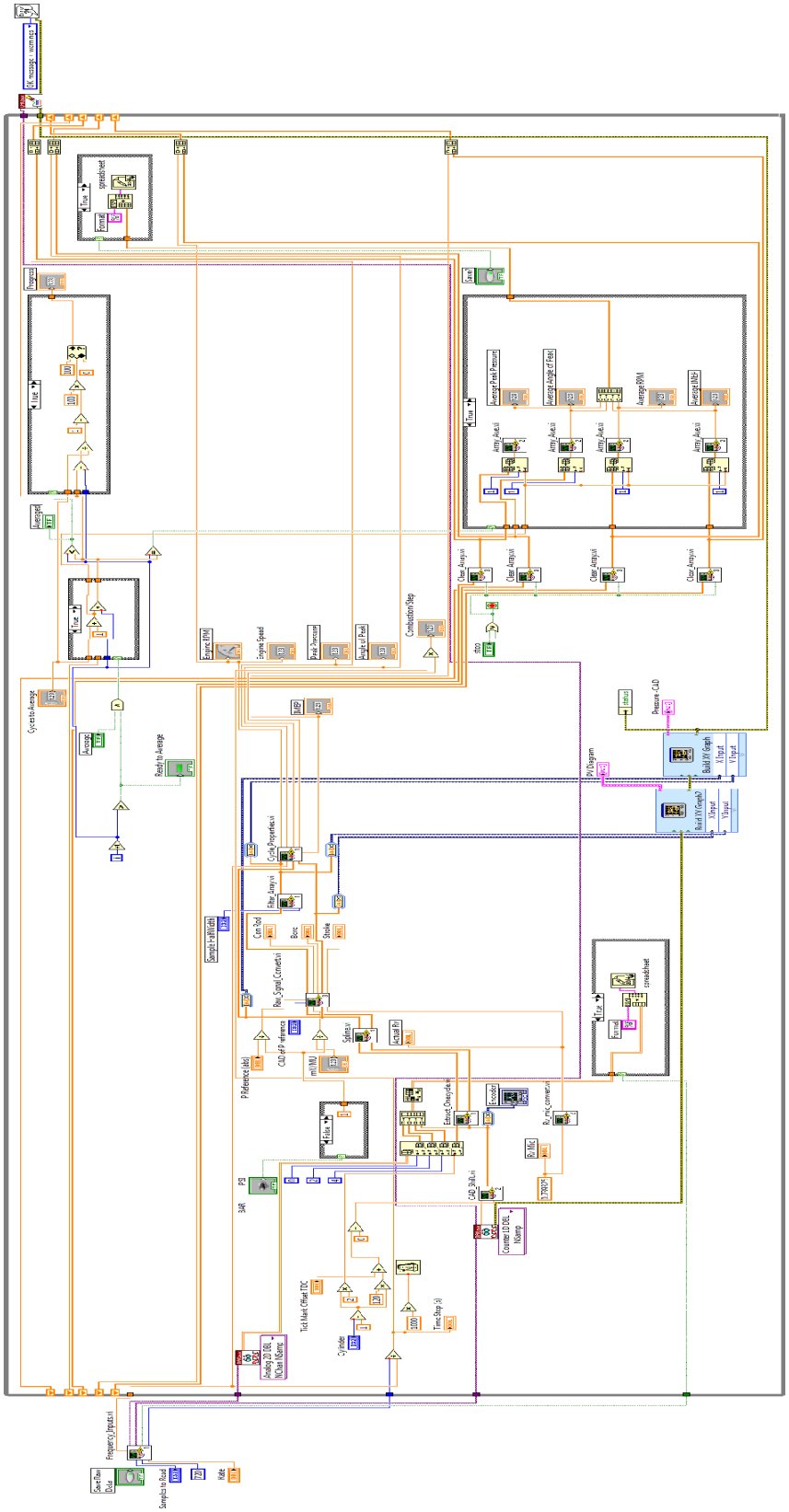

Figure 44. Frequency.vi

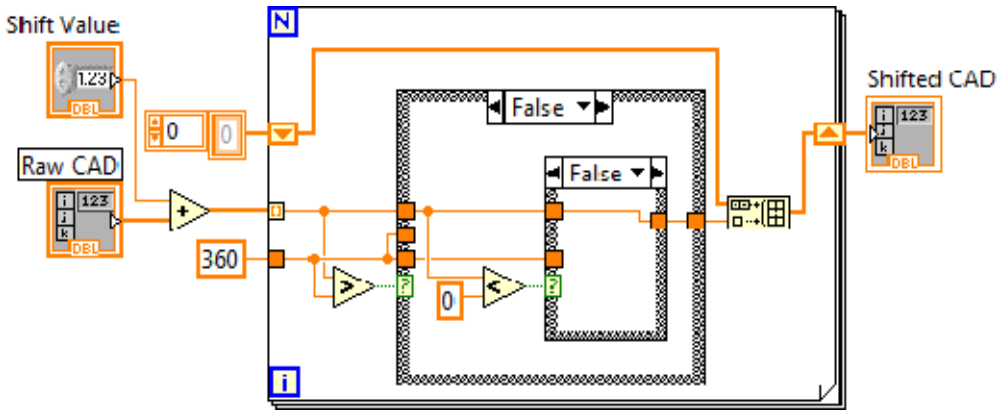

Figure 45. CAD_Shift.vi

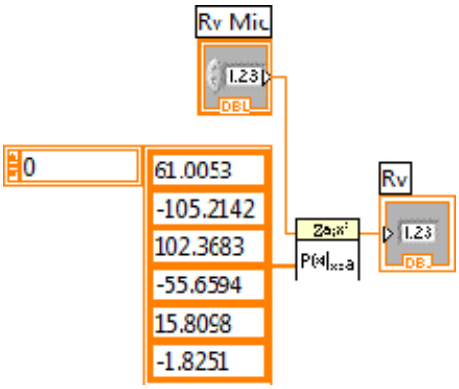

Figure 46. Rv_mic_convert.vi

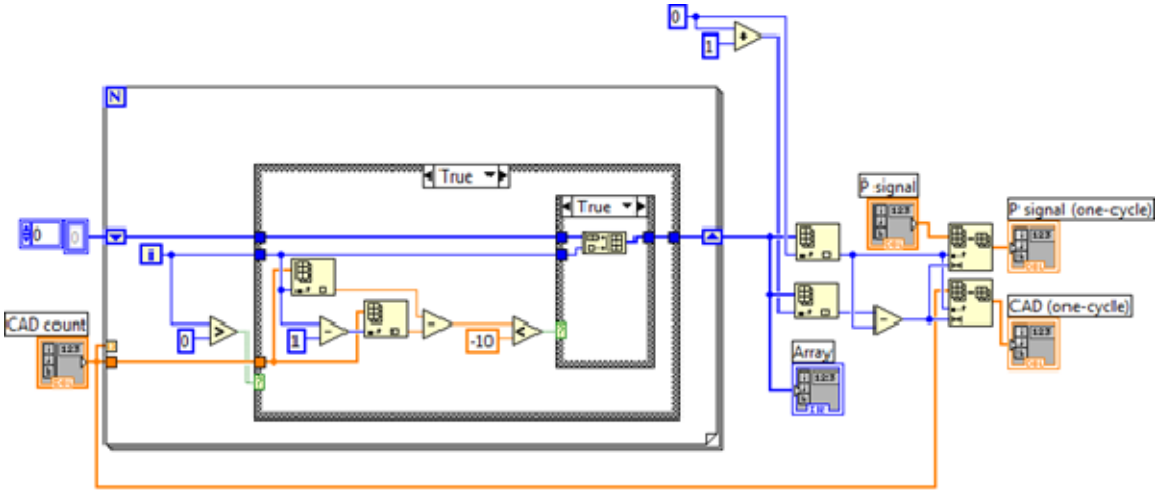

Figure 47. Extract_Onecycle.vi

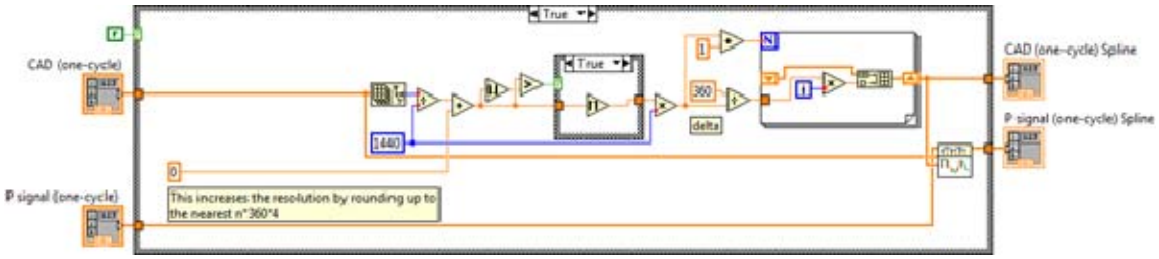

Figure 48. Spline.vi

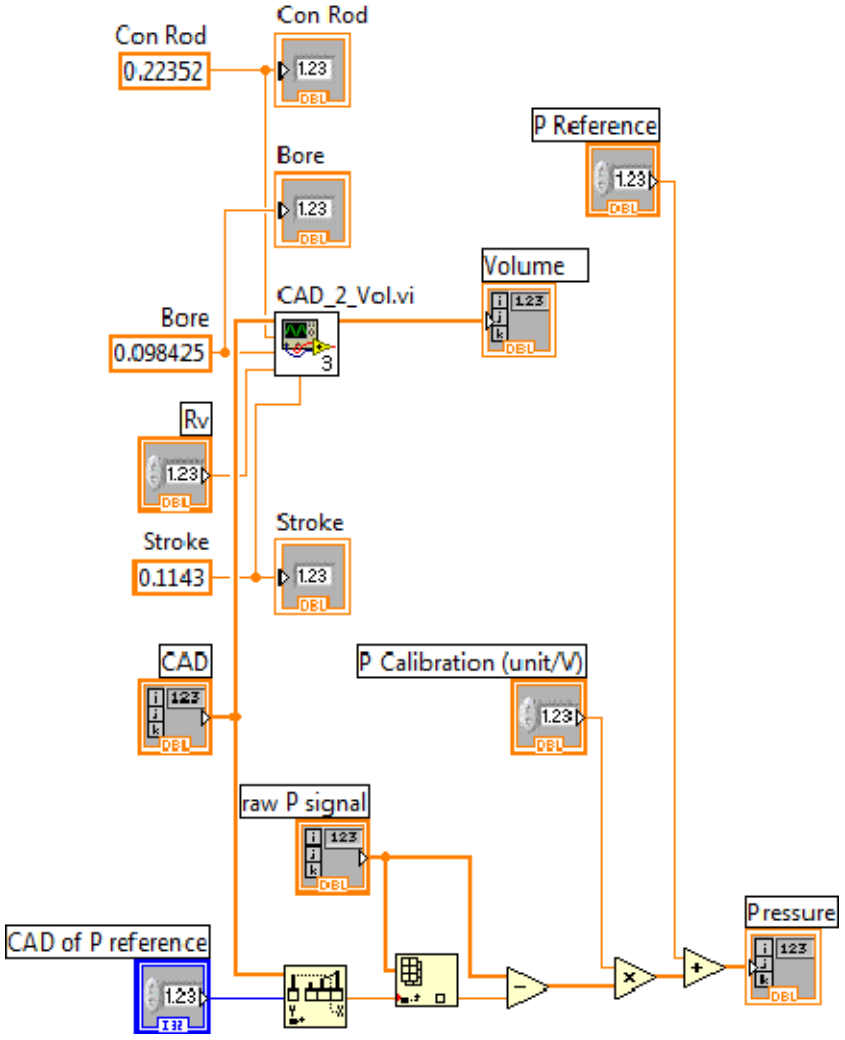

Figure 49. Raw_Signal_Convert.vi

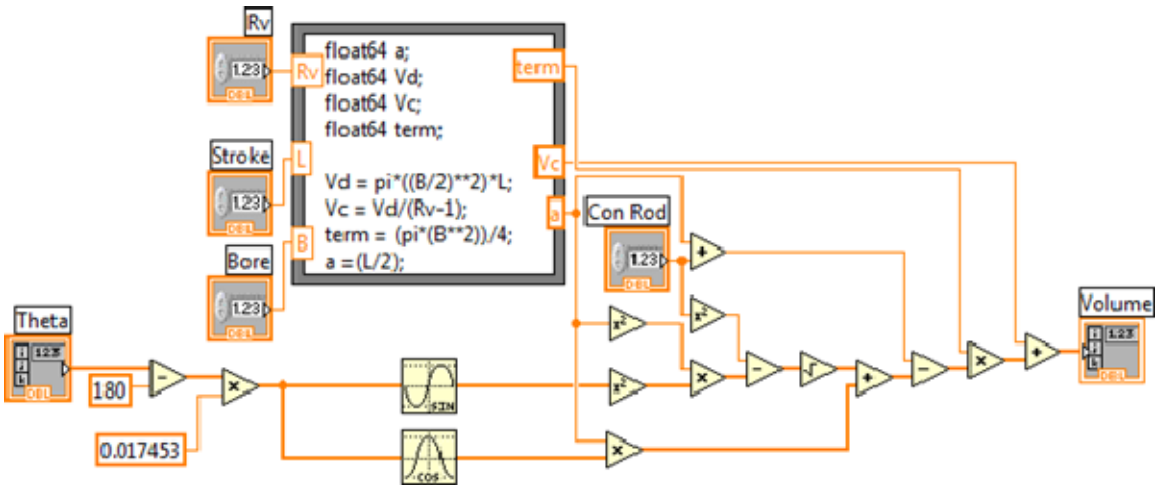

Figure 50. CAD_2_Vol.vi

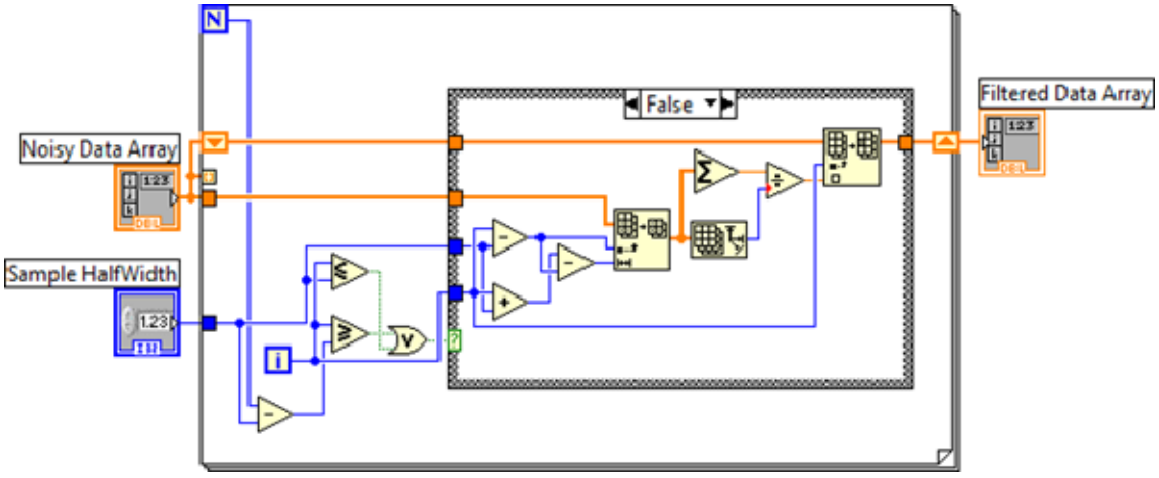

Figure 51. Filter_Array.vi

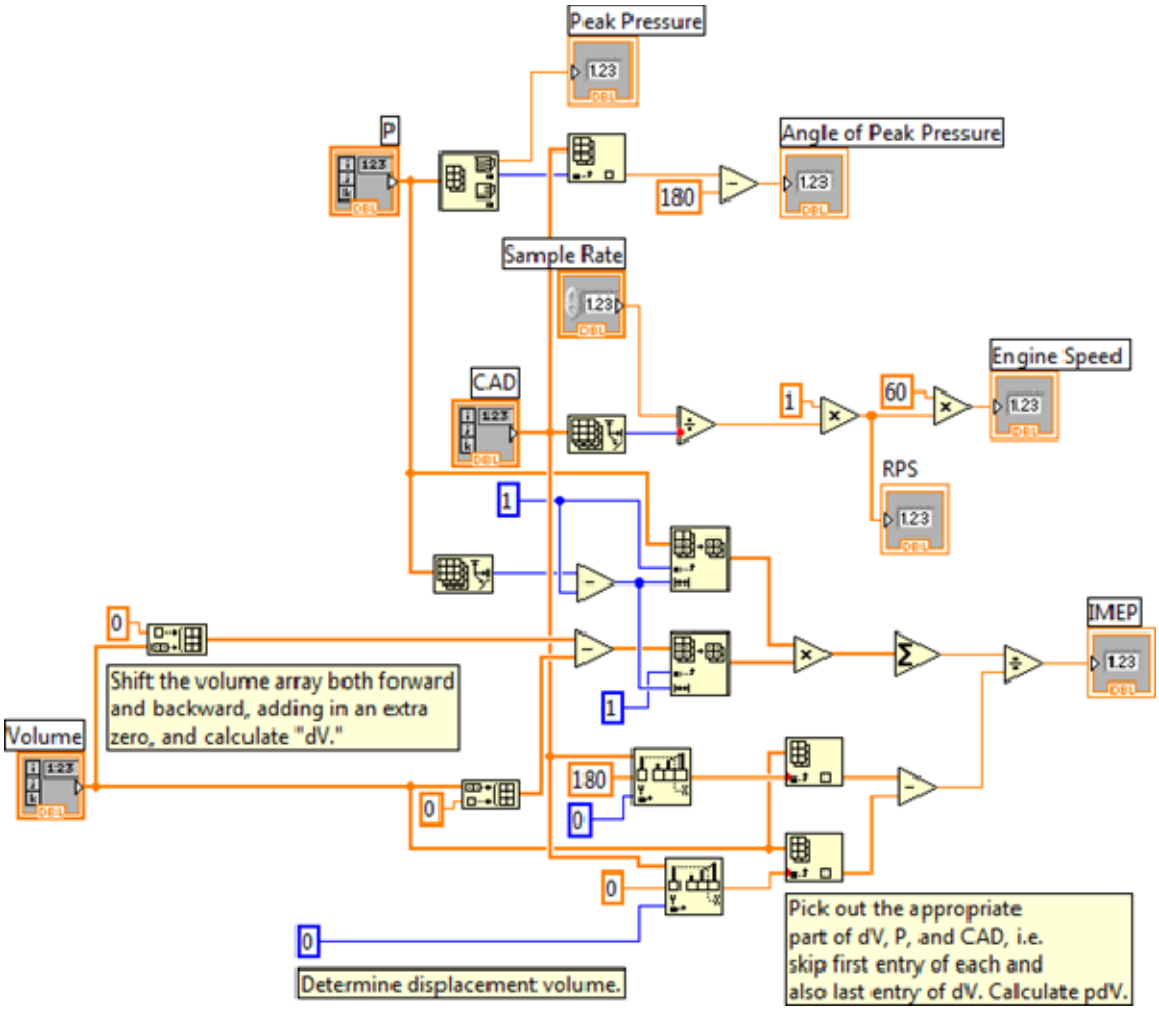

Figure 52. Cycle_Properties.vi

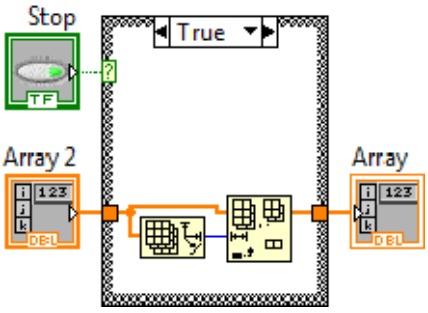

Figure 53. Clear_Array.vi

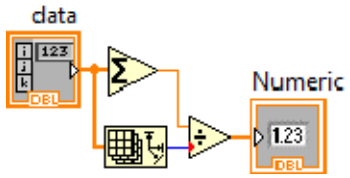

Figure 54. Array_Ave.vi

2. PHASE LOCK ENSEMBLE AVERAGING

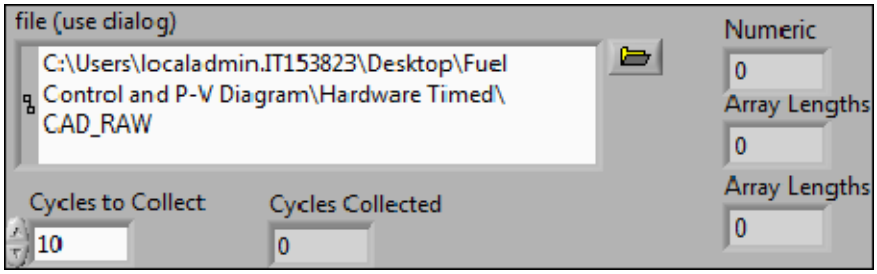

Figure 55. Front Panel of Phase Lock Ensemble (PLE.vi)

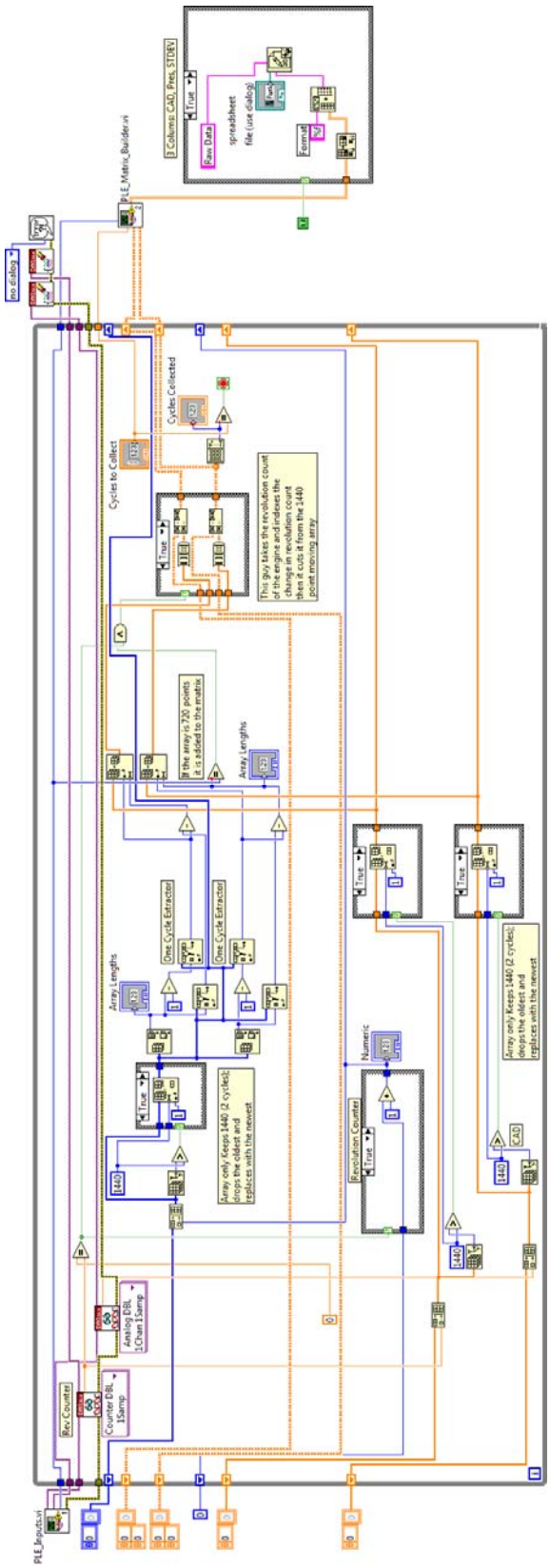

Figure 56. PLE.vi

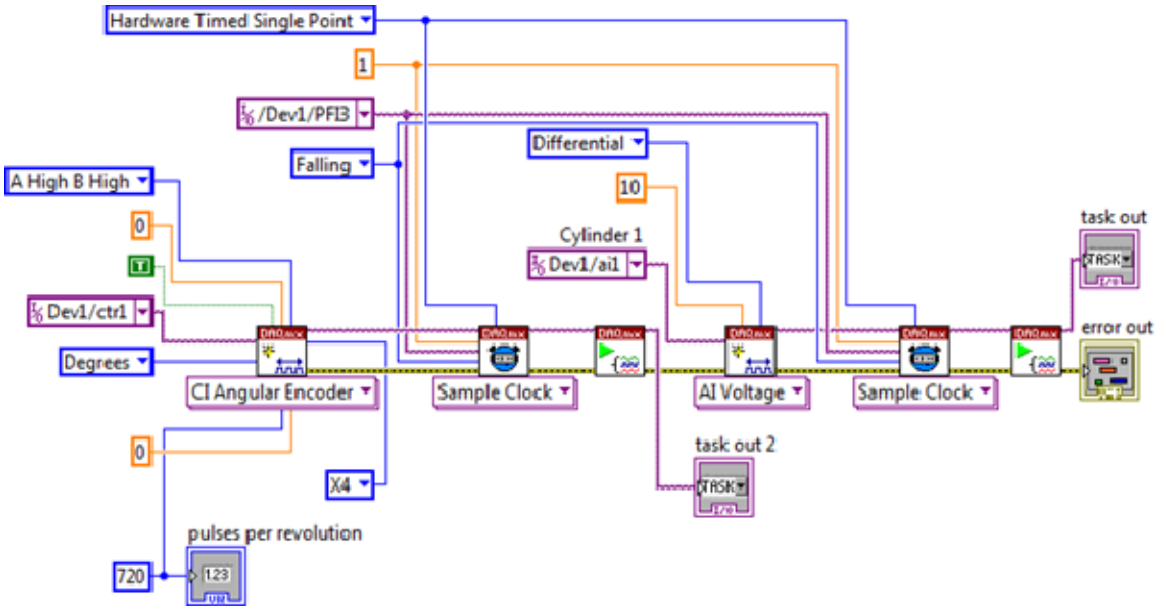

Figure 57. PLE_Inputs.vi

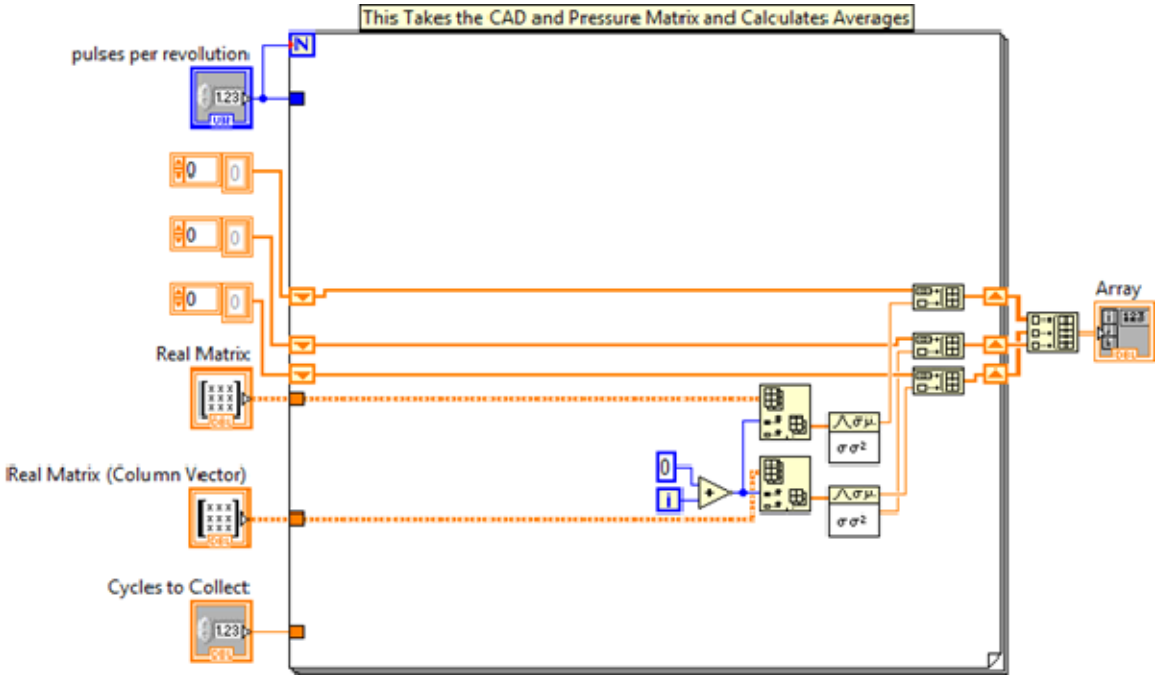

Figure 58. PLE_Matrix_Builder.vi

THIS PAGE INTENTIONALLY LEFT BLANK

APPENDIX D. OPTICAL ENCODER MOUNT DESIGN

The original optical encoder mount was a solid design that conducted heat too easily from the engine to the encoder. Inside the encoder is complex circuitry that produces many clean TTL signals in a very small volume. It is believed that previous encoder failure was due to the overheating of these circuits. Therefore, another mount was created that has a water passage to remove the heat from the engine as designed by Seivwright [24]. A centering pin was also created to reduce any misalignment stresses.

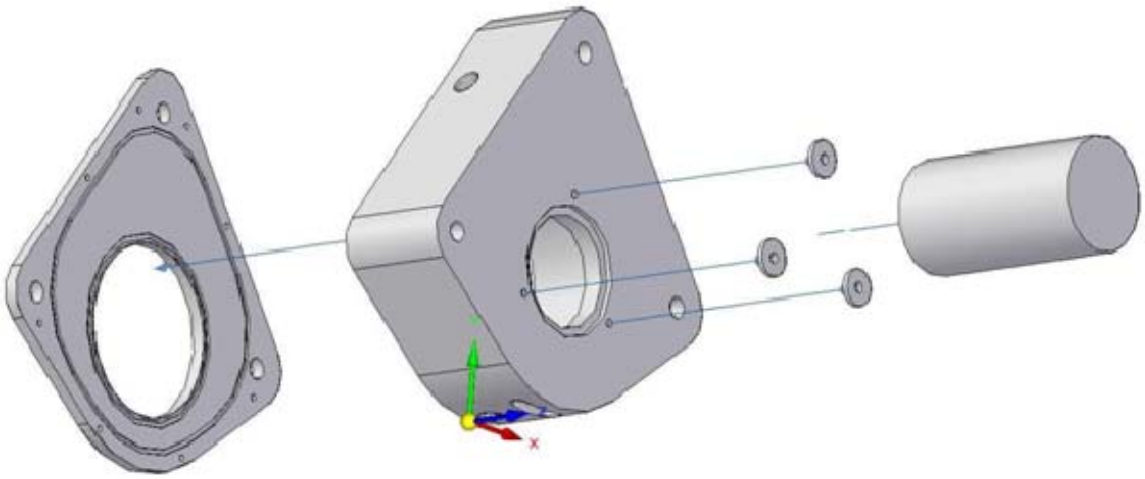

Figure 59. Optical Encoder Mount 2.0 Assembly

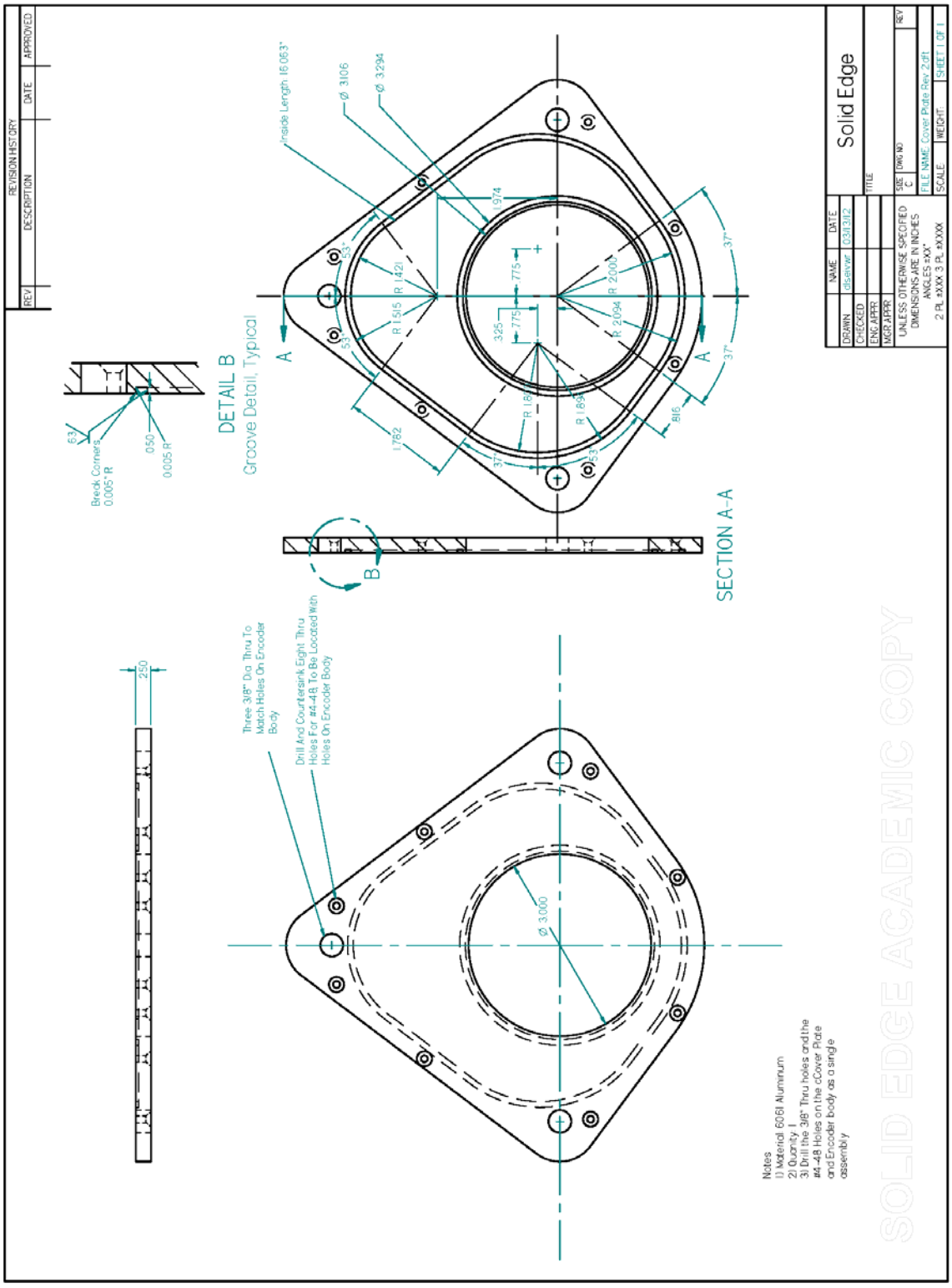

Figure 60. Engineering Drawing of Optical Encoder Mount Cover Plate

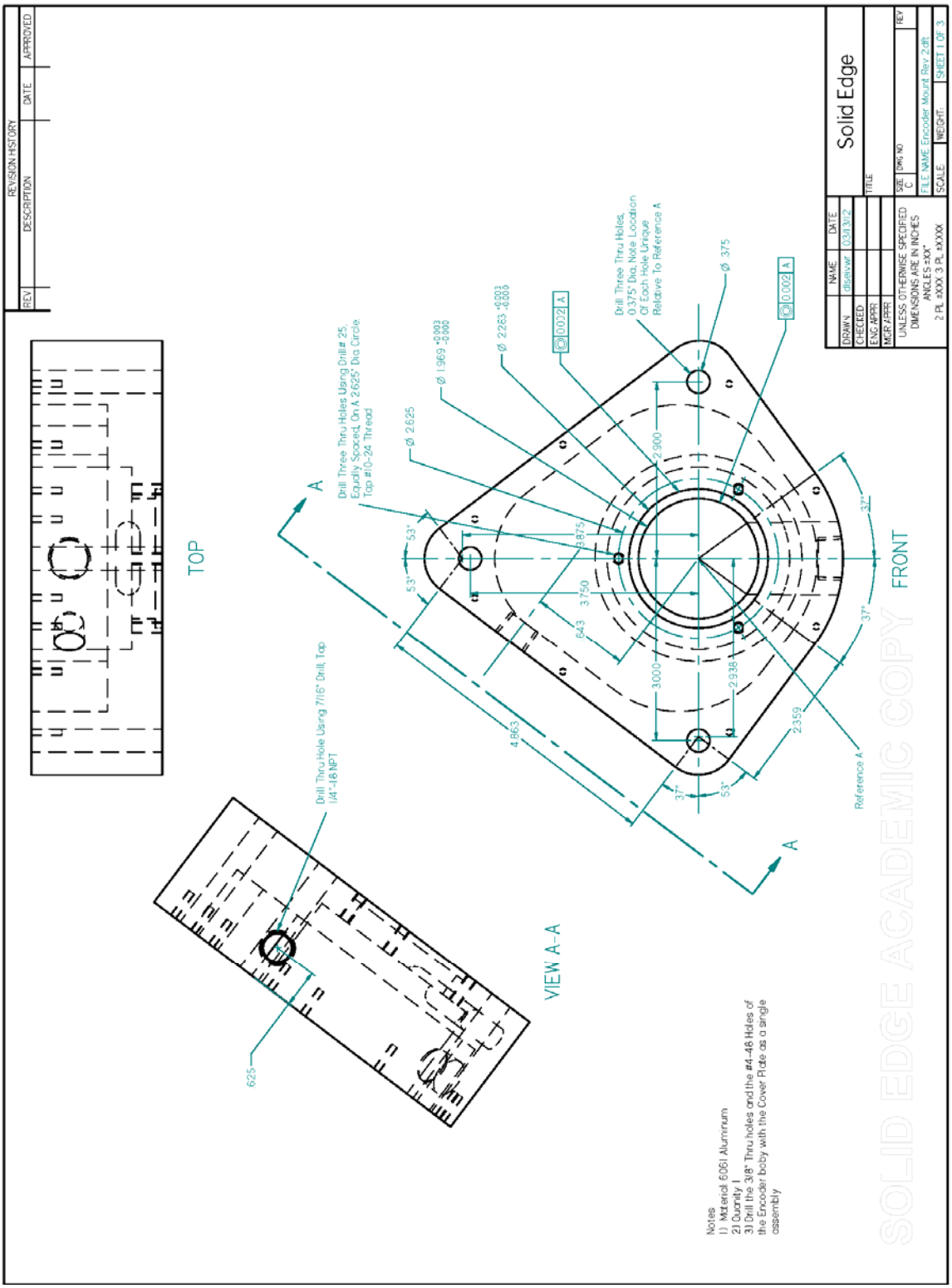

Figure 61. Engineering Drawing of Optical Encoder Mount Front

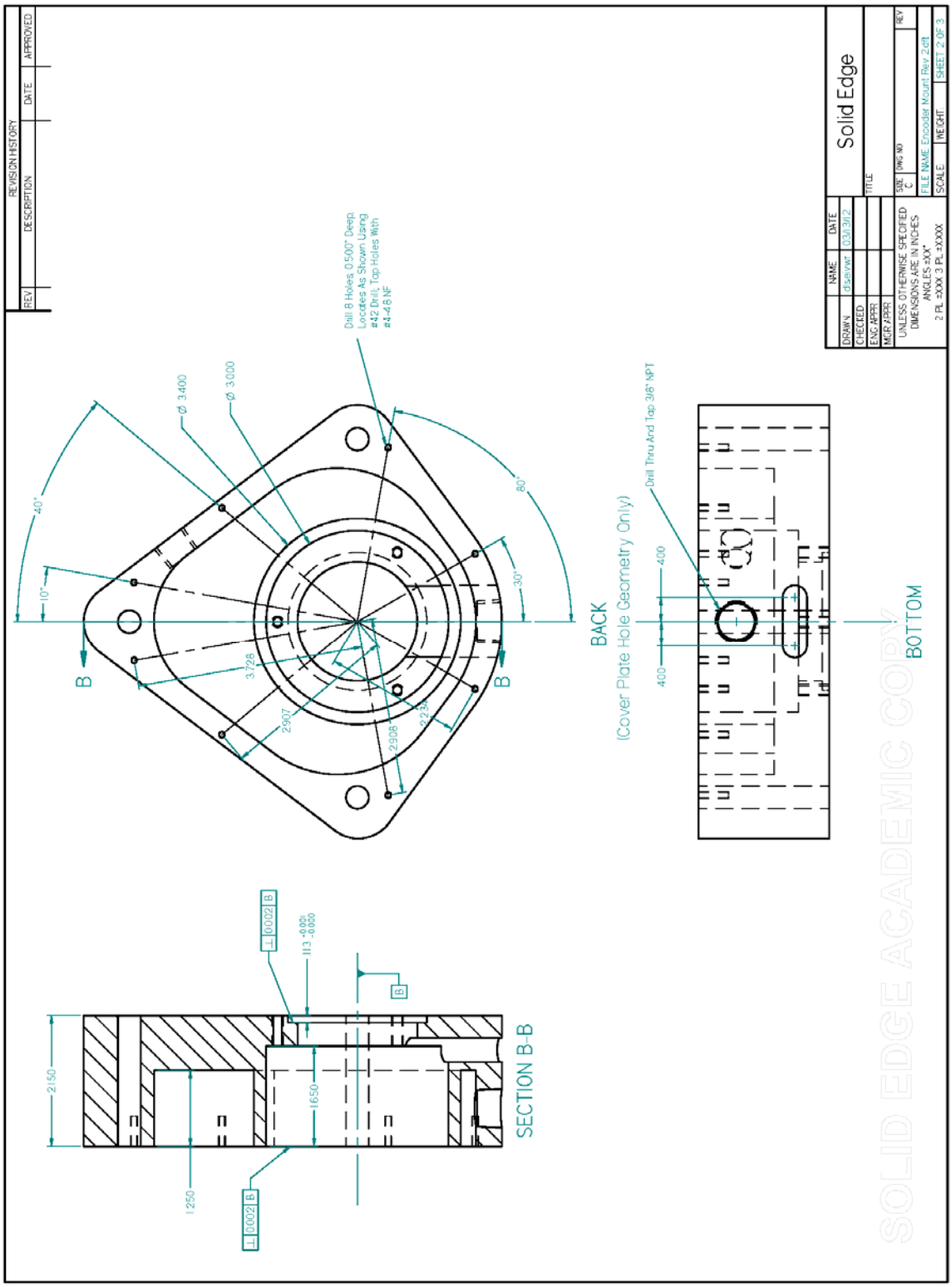

Figure 62. Engineering Drawing of Optical Encoder Mount Back

APPENDIX E. MATLAB SCRIPTS

1. FUEL DERIVATIVE SCRIPT

```
weight=xlsread('\weight\1.xlsx','A:A');
time=(((1:(length(weight)))*0.3)-.3)';
format longE
poly=polyfit(time,weight,1);
ANSWER=poly(1)
```

2. ANGLE OF PEAK, PEAK PRESSURE, INDICATED MEAN EFFECTIVE PRESSURE SCRIPT

```
clc
clear
%
%Data Import
Pres=xlsread('data_processing.xlsx','AN729:AN1448');
Vol=xlsread('data_processing.xlsx','B729:B1448');
CAD=0:.5:359.5;
%
%PP, AOP, IMEP
[PP,Index2]=max(Pres);
AOP=CAD(Index2);
IMEP=trapz(Vol,Pres)/(max(Vol)-min(Vol));
```

THIS PAGE INTENTIONALLY LEFT BLANK

APPENDIX F. DATA

All data in Appendix F was collected on 26 JULY 2012 including cycle diagrams:

1. DIESEL #2

Table 7. Diesel #2 Data Measurements

Fuel Type	**D2**					
RUN #	**25**	**26**	**27**	**28**	**29**	**30**
RPM	970	1290	1580	1300	1300	1280
Torque (ft*lbs)	60.3	58.9	60.1	59.1	89.1	119.9
dw/dt (lbs/s)	-0.00172	-0.00225	-0.00281	-0.00213	-0.00298	-0.00377
lambda	6.8	6.42	6.2	6.5	5.62	4.6
hp	11.14	14.47	18.08	14.63	22.05	29.22
BSFC (lbs/hp*hr)	0.557	0.560	0.559	0.525	0.487	0.464
Energy Fuel (J)	686.1938	674.064	686.5939	634.4401	886.738	1138.012
PP (Bar)	64.436	66.734	66.792	65.360	69.246	76.212
AOP (CAD)	182.0	182.5	185.0	184.5	184.0	184.0
IMEP (Bar)	2.462	2.616	2.695	2.544	3.186	4.140
BMEP (Bar)	1.945245	1.900081	1.938793	1.906533	2.874317	3.867907
FMEP (BAR)	0.516	0.715	0.756	0.638	0.311	0.272
SOI (CAD)	135.0	135.0	135.0	135.0	135.0	135.0
10%MB (CAD)	173.5	174.5	175.0	174.0	174.0	173.0
90%MB (CAD)	233.5	237.0	239.5	238.0	241.0	245.0
IGD (Deg)	38.5	39.5	40.0	39.0	39.0	38.0
BDR (Deg)	60.0	62.5	64.5	64.0	67.0	72.0

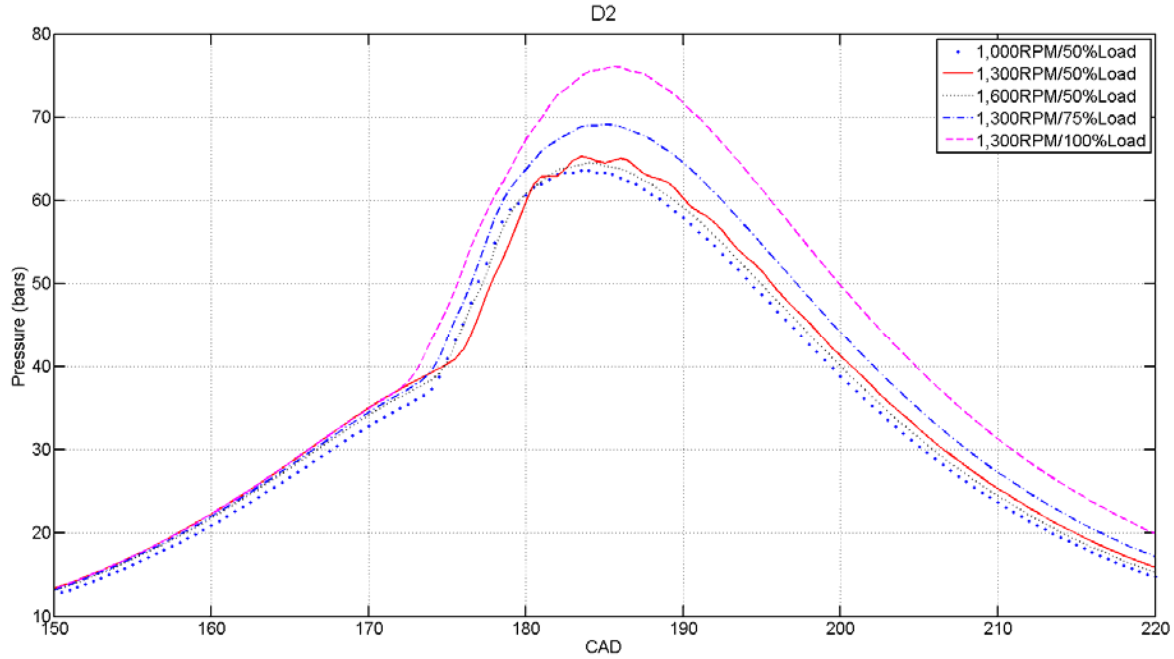

Figure 63. Pressure – CAD Plots of Diesel #2

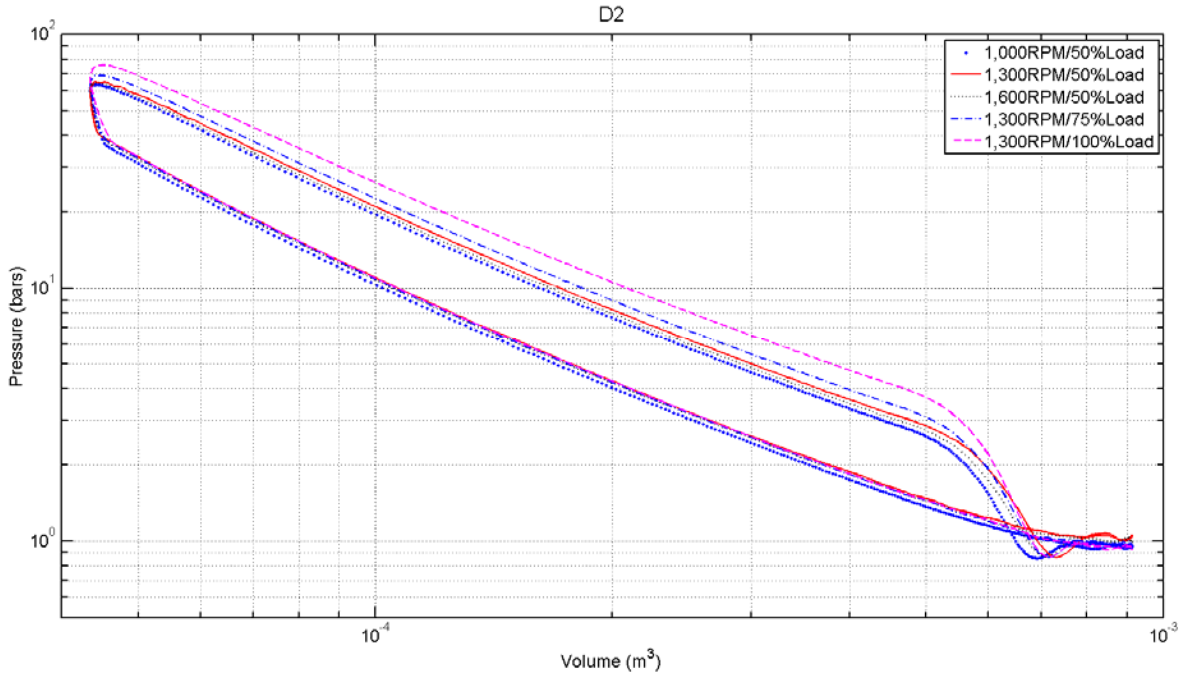

Figure 64. Pressure – Volume Plotes of Diesel #2

2. F-76

Table 8. F-76 Data Measurements

Fuel Type	F-76					
RUN #	**1**	**2**	**3**	**6**	**5**	**4**
RPM	1050	1300	1600	1290	1270	1300
Torque (ft*lbs)	60	59.8	60.8	58.9	88.6	119.8
dw/dt (lbs/s)	-	-0.00206	-0.00257	-0.00220	-0.00286	-0.00342
lambda	-	6.41	6.1	6.3	5.6	5.8
hp	12.00	14.80	18.52	14.47	21.42	29.65
BSFC (lbs/hp*hr)	-	0.501	0.499	0.547	0.480	0.415
Energy Fuel (J)	-	627.246	634.169	674.170	889.897	1040.584
PP (Bar)	-	67.066	67.557	67.708	70.087	76.781
AOP (CAD)	-	182.5	185.5	182.5	183.0	186.0
IMEP (Bar)	-	2.584	2.634	2.597	3.160	4.090
BMEP (Bar)	-	1.929	1.961	1.900	2.858	3.865
FMEP (BAR)	-	0.655	0.673	0.697	0.301	0.225
SOI (CAD)	-	135.0	135.0	135.0	135.0	135.0
10%MB (CAD)	-	174.5	175.5	174.5	174.0	173.0
90%MB (CAD)	-	237.5	241.0	236.5	242.0	245.0
IGD (Deg)	-	39.5	40.5	39.5	39.0	38.0
BDR (Deg)	-	63.0	65.5	62.0	68.0	72.0

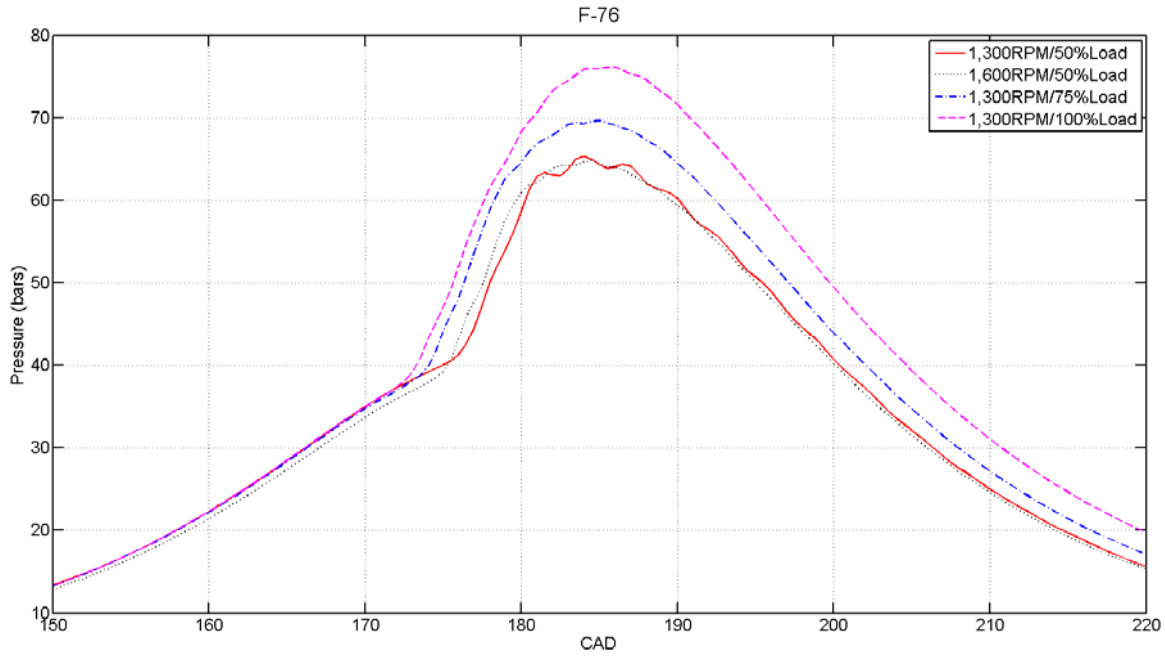

Figure 65. Pressure – CAD Plots of F-76

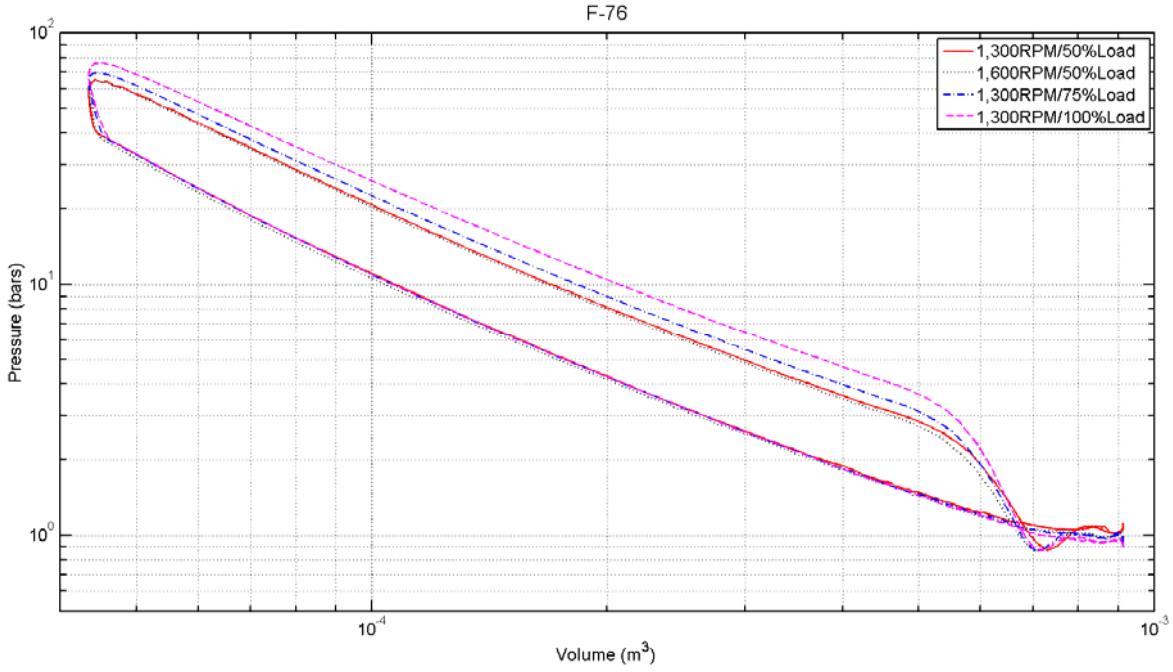

Figure 66. Pressure – Volume Plots of F-76

3. HRD ALGAE

Table 9. HRD Algae Data Measurements

Fuel Type	HRD Algae					
RUN #	**7**	**8**	**9**	**10**	**11**	**12**
RPM	1050	1280	1580	1300	1270	1290
Torque (ft*lbs)	56.7	59.3	59.3	59.3	92.3	118
dw/dt (lbs/s)	-0.00160	-0.00216	-0.00213	-0.00224	-0.00275	-0.00327
lambda	7.05	6.52	6.36	6.6	5.67	4.65
hp	11.34	14.45	17.84	14.68	22.32	28.98
BSFC (lbs/hp*hr)	0.509	0.539	0.430	0.549	0.444	0.406
Energy Fuel (J)	607.487	672.657	536.723	685.189	862.937	1008.616
PP (Bar)	63.909	64.436	64.328	63.006	68.987	76.147
AOP (CAD)	184.5	185.5	186.0	183.5	185.0	185.0
IMEP (Bar)	2.557	2.657	2.712	2.561	3.193	4.038
BMEP (Bar)	1.829	1.913	1.913	1.913	2.978	3.807
FMEP (BAR)	0.728	0.744	0.799	0.648	0.215	0.231
SOI (CAD)	135.0	135.0	135.0	135.0	135.0	135.0
10%MB (CAD)	172.0	173.0	174.0	173.0	172.5	172.0
90%MB (CAD)	233.5	237.5	241.0	238.0	241.5	245.5
IGD (Deg)	37.0	38.0	39.0	38.0	37.5	37.0
BDR (Deg)	61.5	64.5	67.0	65.0	69.0	73.5

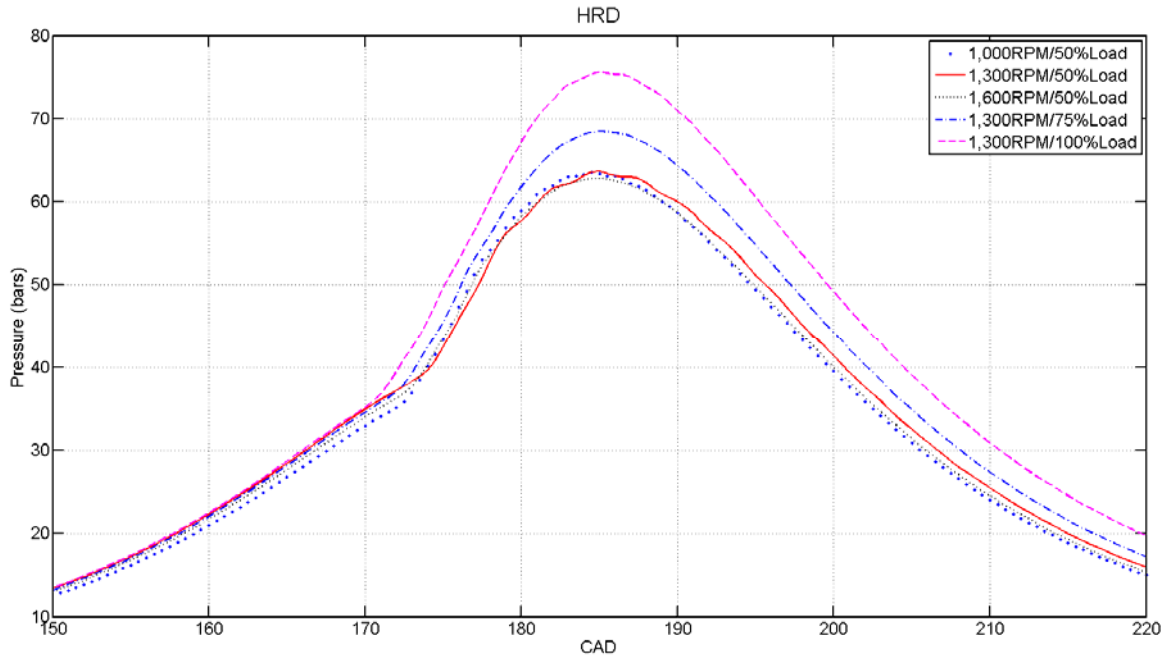

Figure 67. Pressure – CAD Plots of HRD Algae

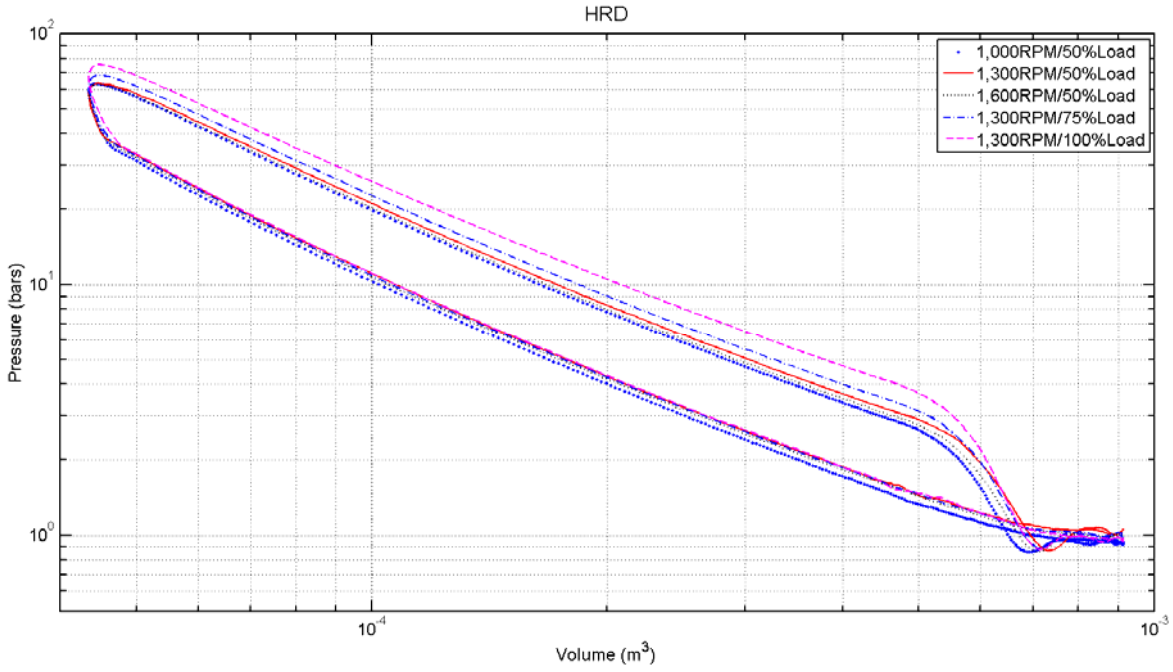

Figure 68. Pressure – Volume Plots of HRD Algae

4. JP-5

Table 10. JP-5 Data Measurements

Fuel Type	JP-5					
RUN #	**19**	**20**	**21**	**22**	**23**	**24**
RPM	1050	1280	1560	1310	1280	1270
Torque (ft*lbs)	56.7	58.9	59.6	59.6	85	121
dw/dt (lbs/s)	-0.00178	-0.00228	-0.00286	-0.00227	-0.00276	-0.00325
lambda	7	6.44	6.15	6.3	5.75	4.8
hp	11.34	14.35	17.70	14.87	20.72	29.26
BSFC (lbs/hp*hr)	0.565	0.571	0.581	0.550	0.480	0.400
Energy Fuel (J)	664.051	696.841	718.215	679.515	844.891	1002.170
PP (Bar)	66.455	68.416	-	67.440	70.933	77.594
AOP (CAD)	183.0	183.0	-	183.0	184.0	185.0
IMEP (Bar)	2.423	2.619	-	2.568	3.213	4.118
BMEP (Bar)	1.829	1.900	-	1.923	2.742	3.903
FMEP (BAR)	0.593	0.719	-	0.646	0.471	0.215
SOI (CAD)	135.0	135.0	-	135.0	135.0	135.0
10%MB (CAD)	174.0	175.0	-	175.0	174.5	173.5
90%MB (CAD)	233.0	236.5	-	237.5	241.5	244.0
IGD (Deg)	39.0	40.0	-	40.0	39.5	38.5
BDR (Deg)	59.0	61.5	-	62.5	67.0	70.5

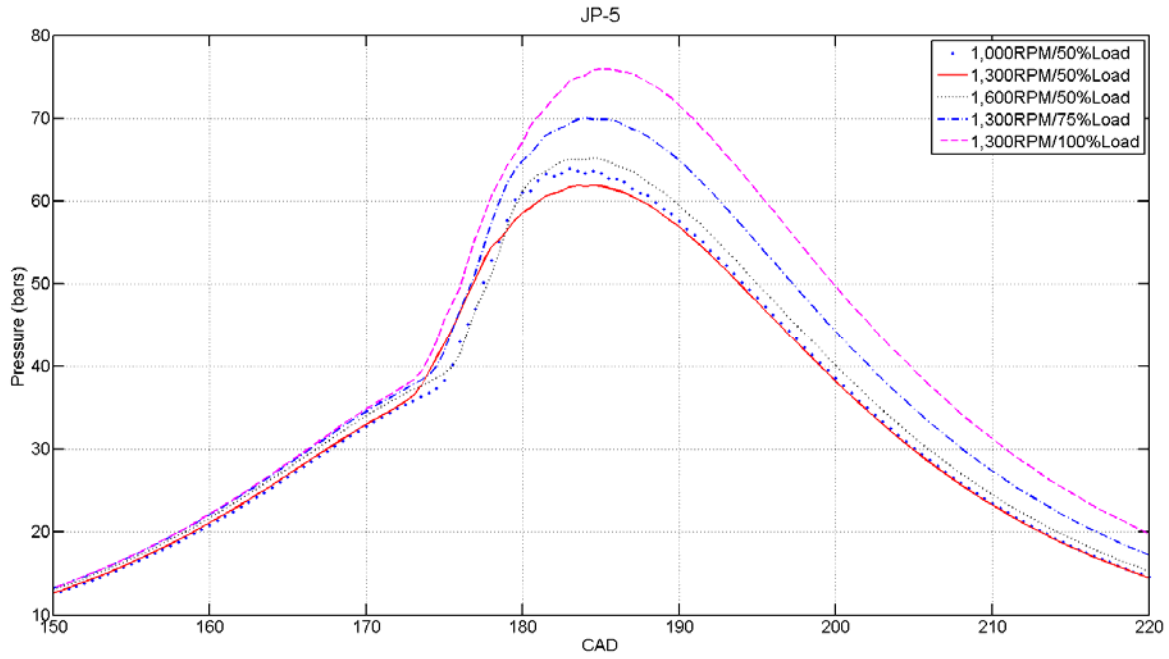

Figure 69. Pressure – CAD Plots of JP-5

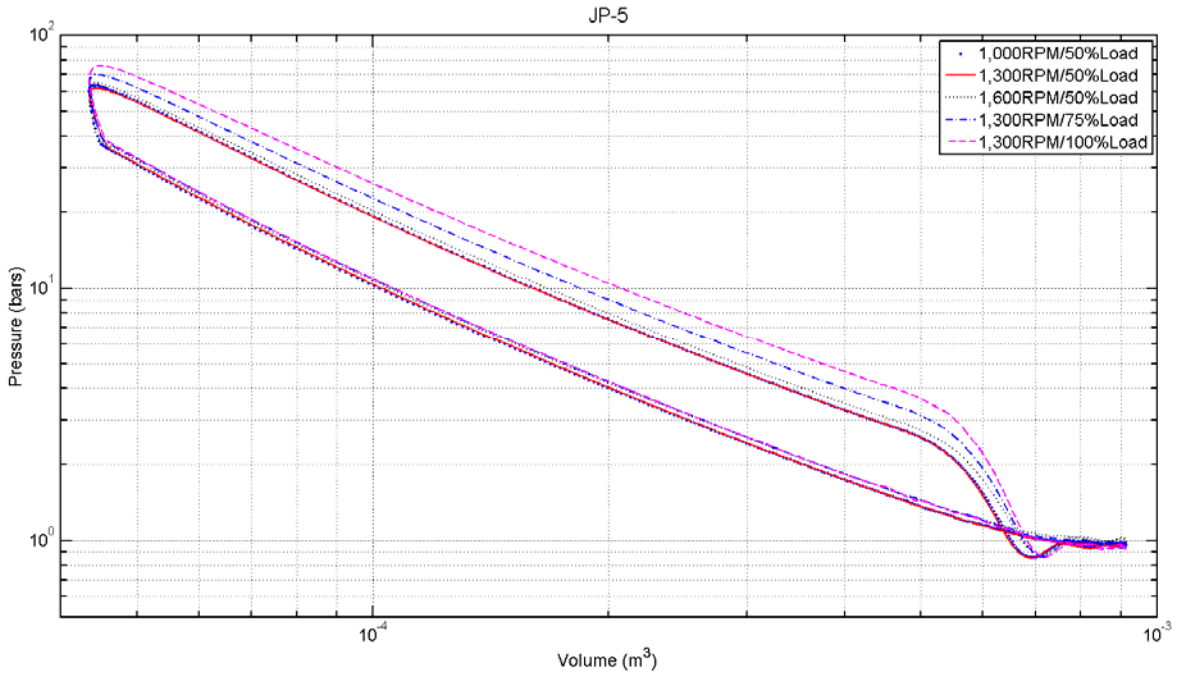

Figure 70. Pressure – Volume Plots of JP-5

5. HRJ CAMELINA

Table 11. HRJ Camelina Data Measurements

Fuel Type	HRJ Camelina					
RUN #	**13**	**14**	**15**	**16**	**17**	**18**
RPM	1030	1280	1600	1300	1280	1300
Torque (ft*lbs)	60	59.1	58.4	59.6	89.1	118
dw/dt (lbs/s)	-0.00145	-0.00249	-0.00239	-0.00208	-0.00240	-0.00353
lambda	6.66	6.45	6.2	6.43	5.78	4.6
hp	11.77	14.40	17.79	14.75	21.72	29.21
BSFC (lbs/hp*hr)	0.444	0.623	0.483	0.507	0.398	0.435
Energy Fuel (J)	561.152	774.957	593.866	636.762	747.498	1080.194
PP (Bar)	61.730	63.926	64.566	63.315	71.222	75.557
AOP (CAD)	185.0	184.0	184.0	186.0	184.0	186.5
IMEP (Bar)	2.352	2.514	2.611	2.480	3.349	4.117
BMEP (Bar)	1.936	1.907	1.884	1.923	2.874	3.807
FMEP (BAR)	0.416	0.607	0.727	0.558	0.474	0.311
SOI (CAD)	135.0	135.0	135.0	135.0	135.0	135.0
10%MB (CAD)	172.5	173.5	174.5	173.5	172.5	172.5
90%MB (CAD)	233.5	237.5	241.5	239.5	243.0	246.0
IGD (Deg)	37.5	38.5	39.5	38.5	37.5	37.5
BDR (Deg)	61.0	64.0	67.0	66.0	70.5	73.5

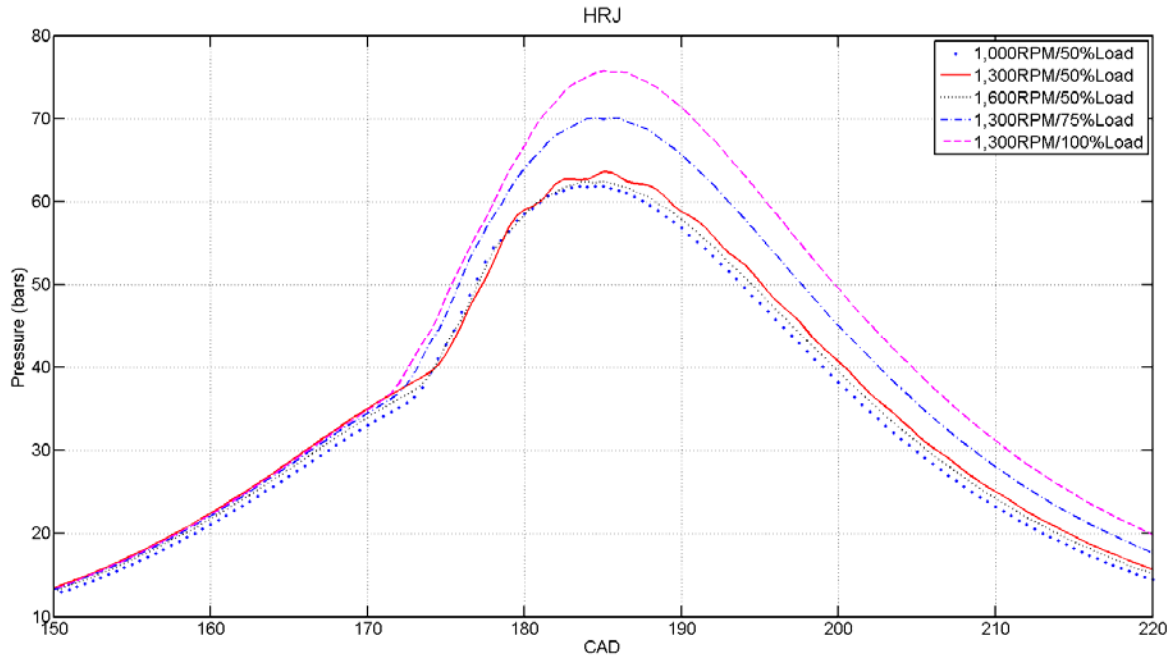

Figure 71. Pressure – CAD Plots of HRJ Camelina

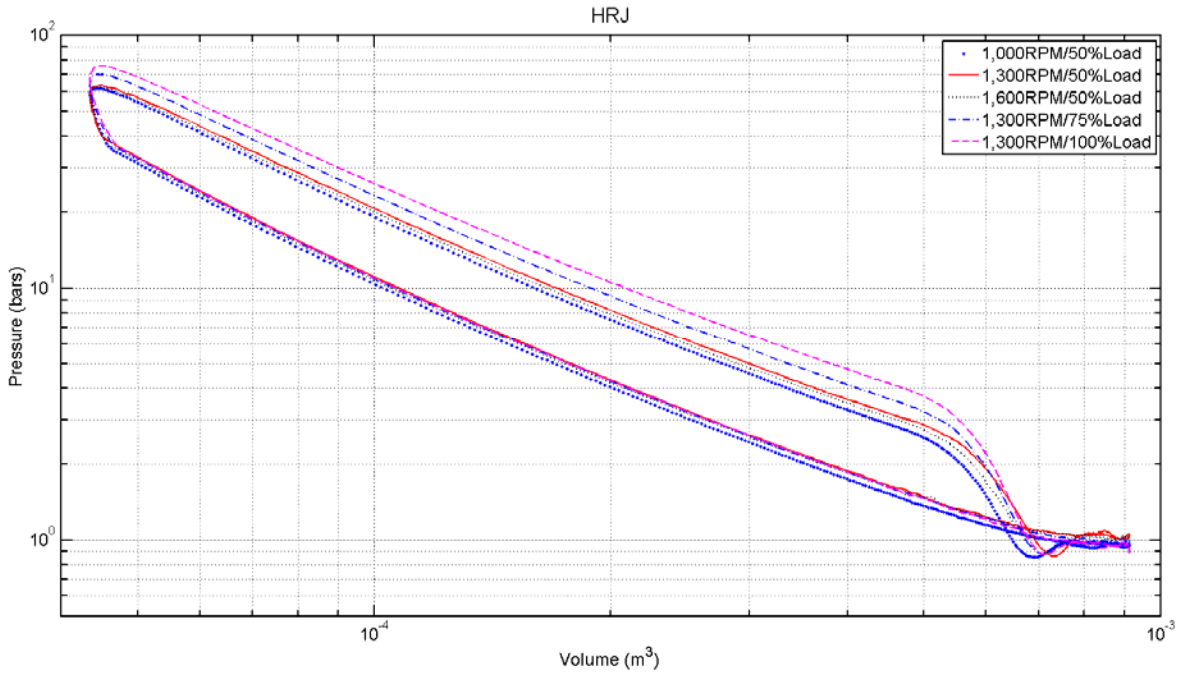

Figure 72. Pressure – Volume Plots of HRJ Camelina

6. 1,000 RPM AND 50 PERCENT LOAD

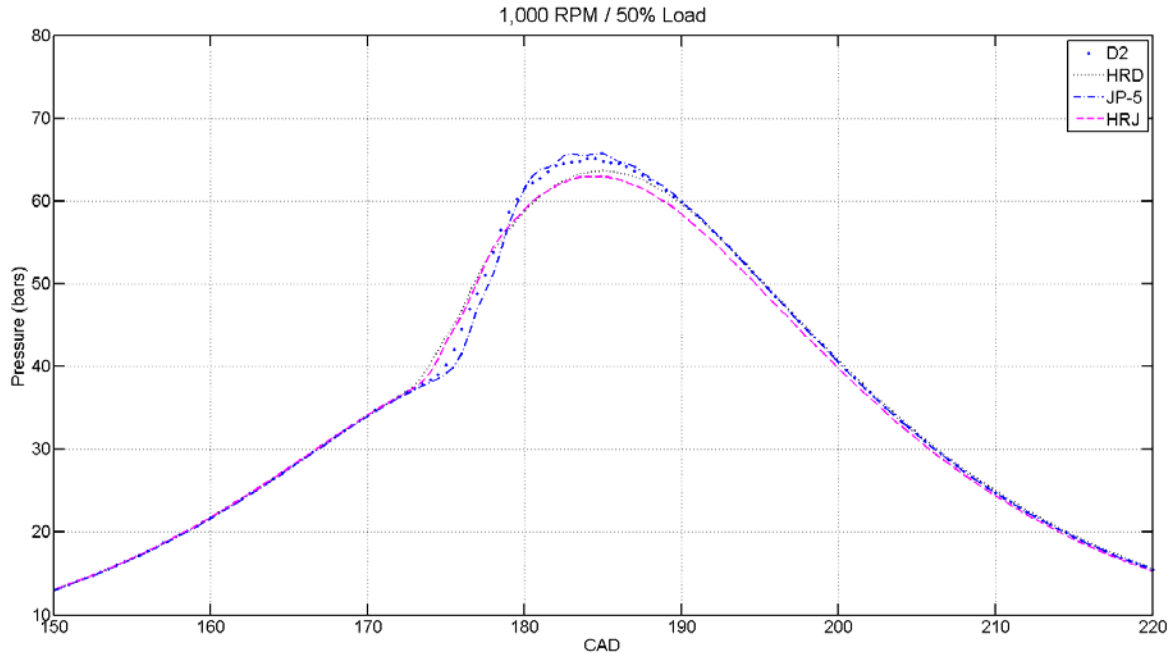

Figure 73. Pressure – CAD Plots of 1,000 RPM and 50% Load

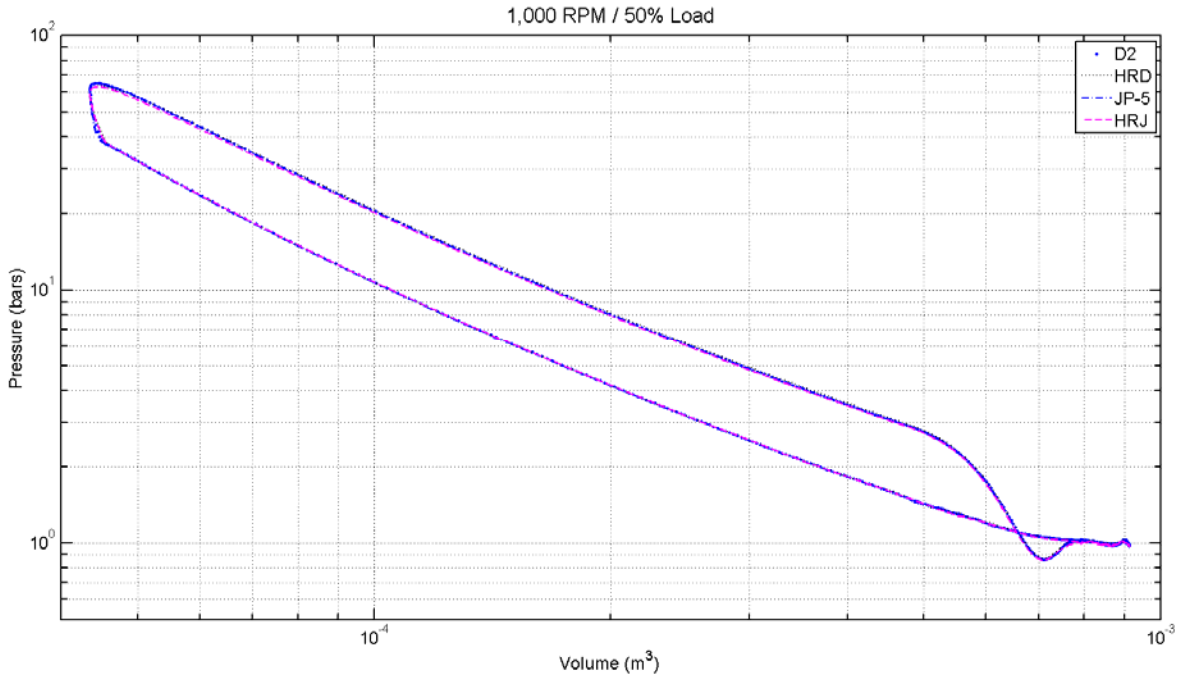

Figure 74. Pressure – Volume Plots of 1,000 RPM and 50% Load

7. 1,300 RPM AND 50 PERCENT LOAD

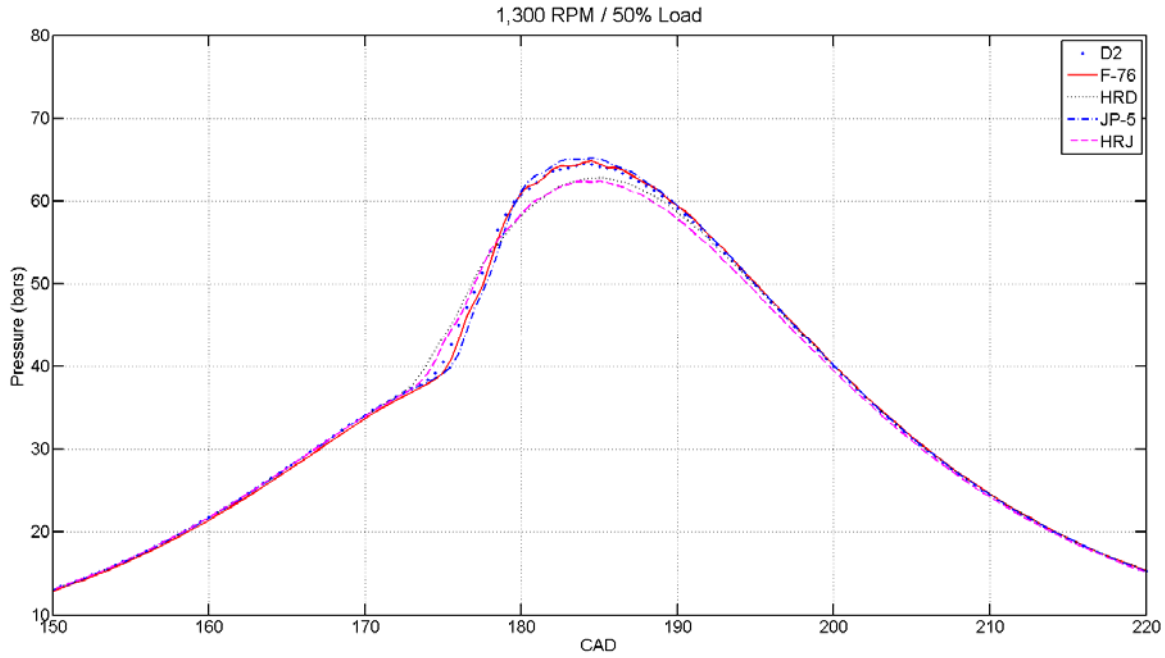

Figure 75. Pressure – CAD Plots of 1,300 RPM and 50% Load

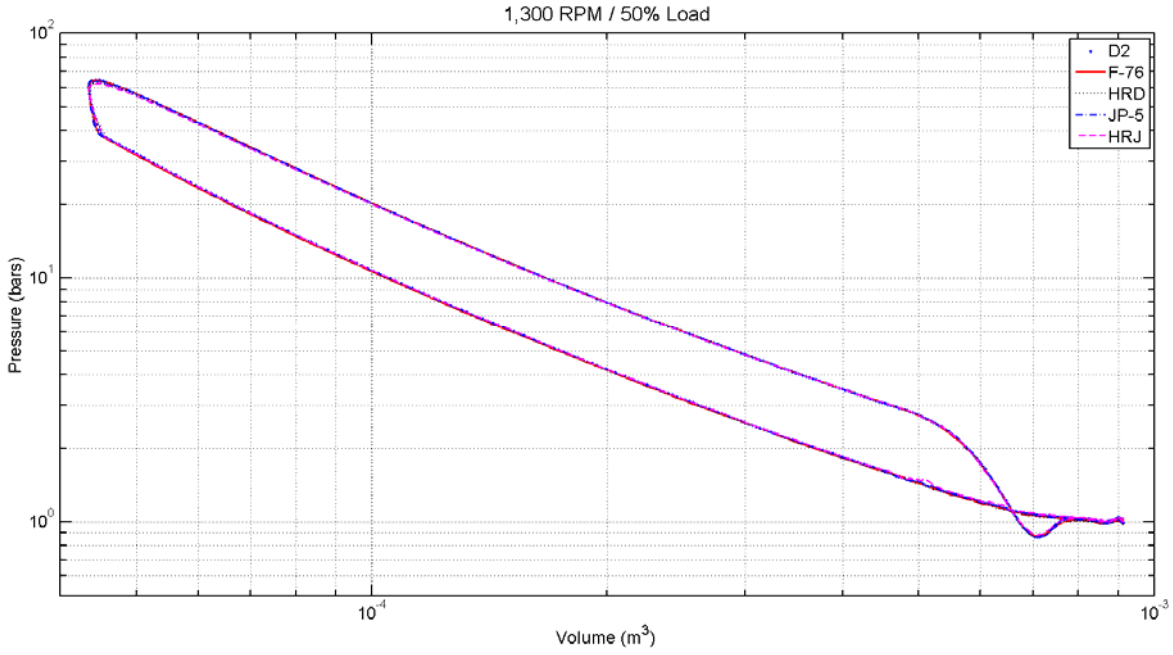

Figure 76. Pressure – Volume Plots of 1,300 RPM and 50% Load

8. 1,600 RPM AND 50 PERCENT LOAD

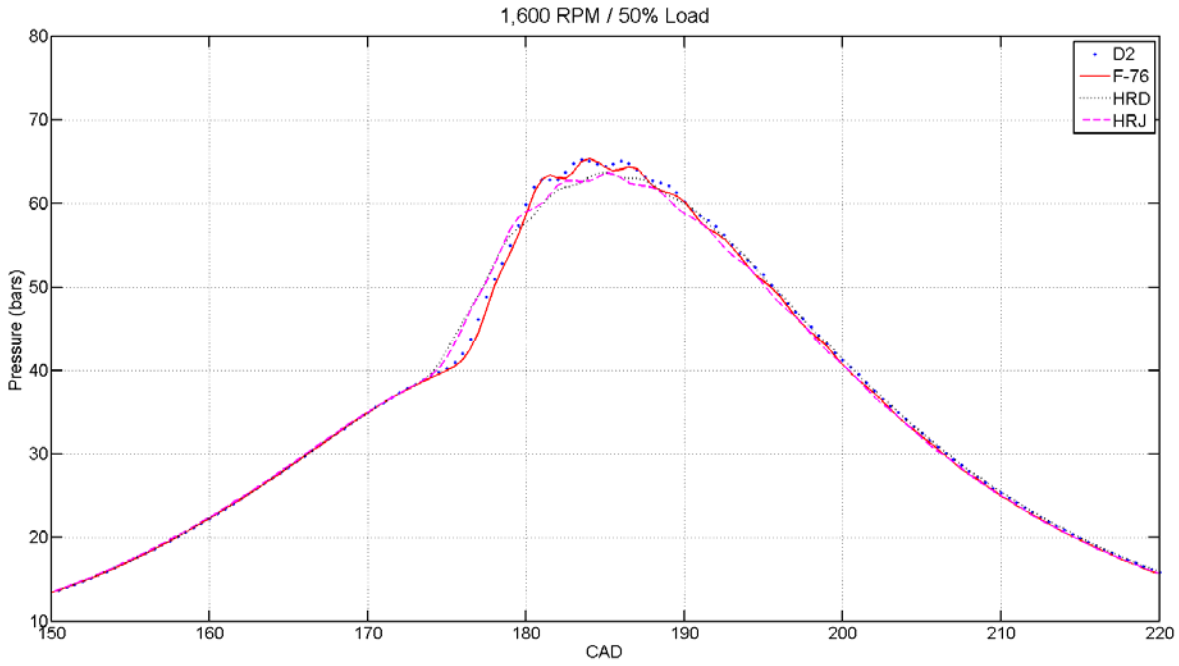

Figure 77. Pressure – CAD Plots of 1,600 RPM and 50% Load

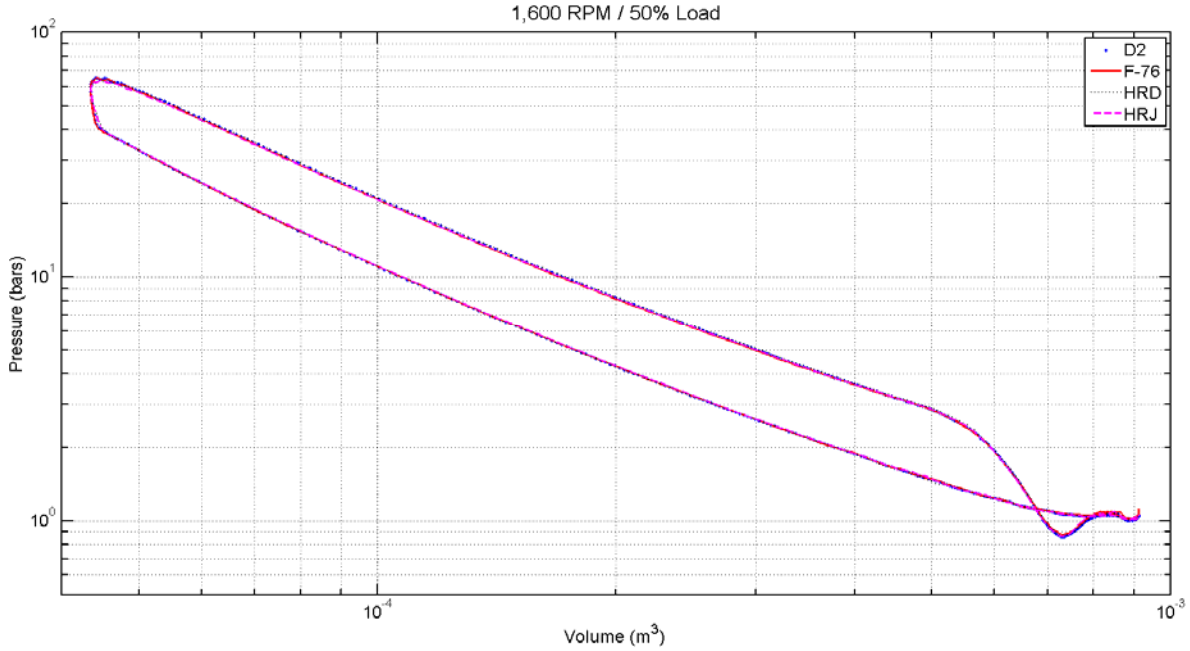

Figure 78. Pressure – Volume Plots of 1,600 RPM and 50% Load

9. 1,300 RPM AND 75 PERCENT LOAD

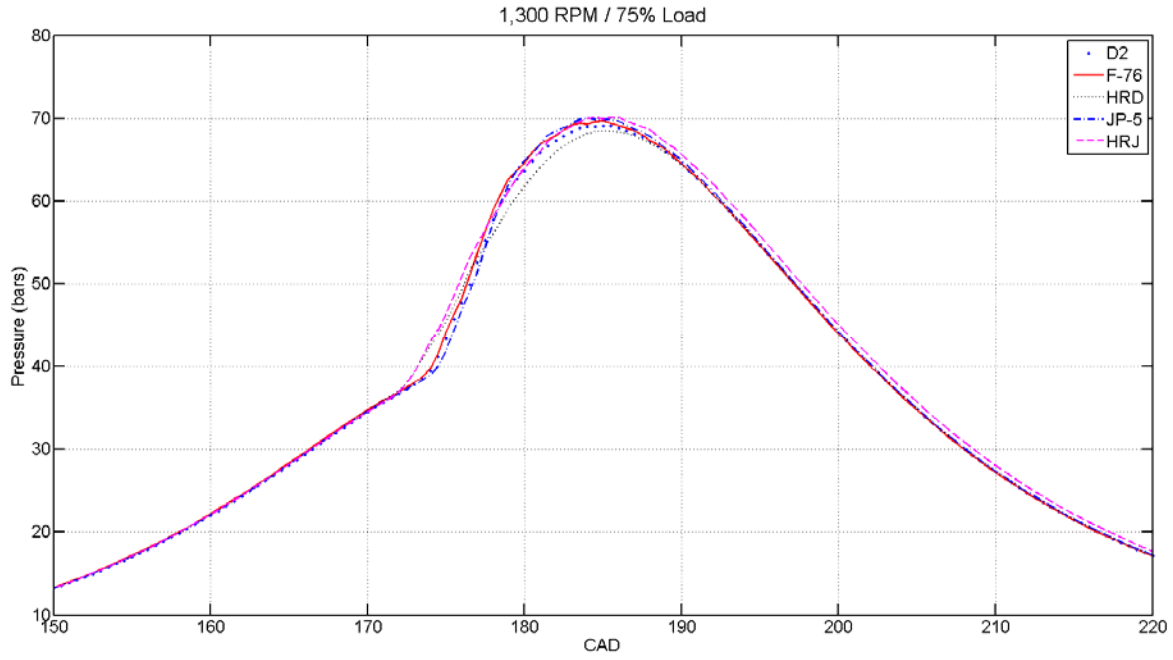

Figure 79. Pressure – CAD Plots of 1,300 RPM and 75% Load

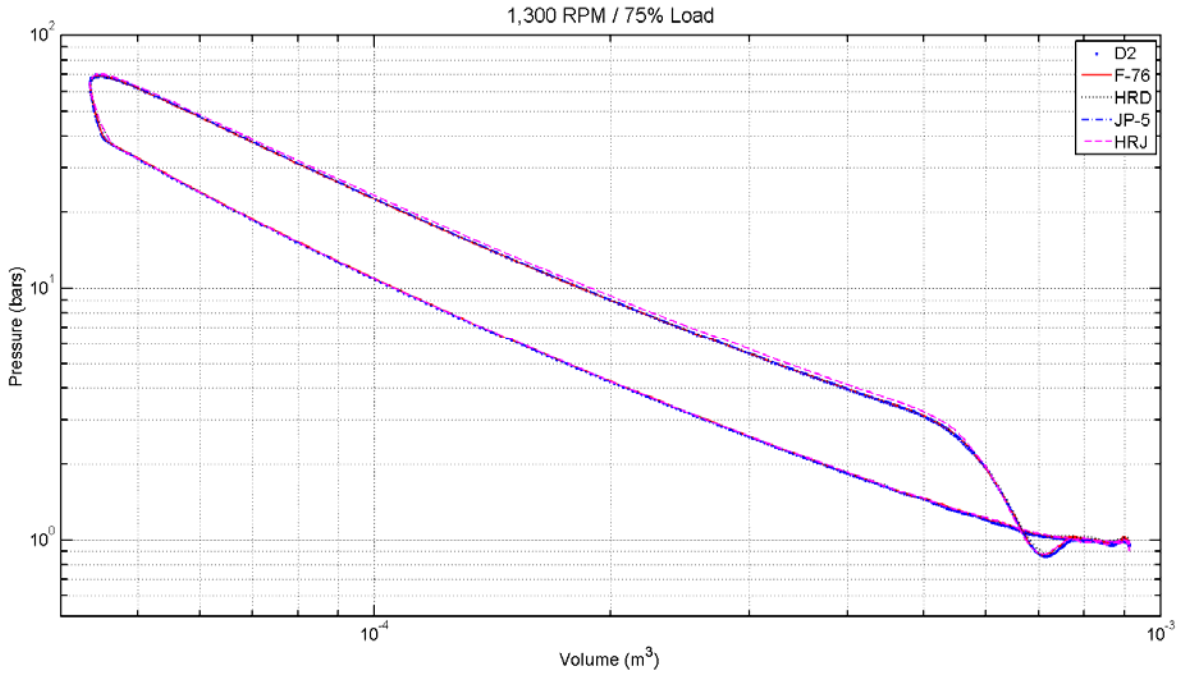

Figure 80. Pressure – Volume Plots of 1,300 RPM and 75% Load

10. 1,300 RPM AND 100 PERCENT LOAD

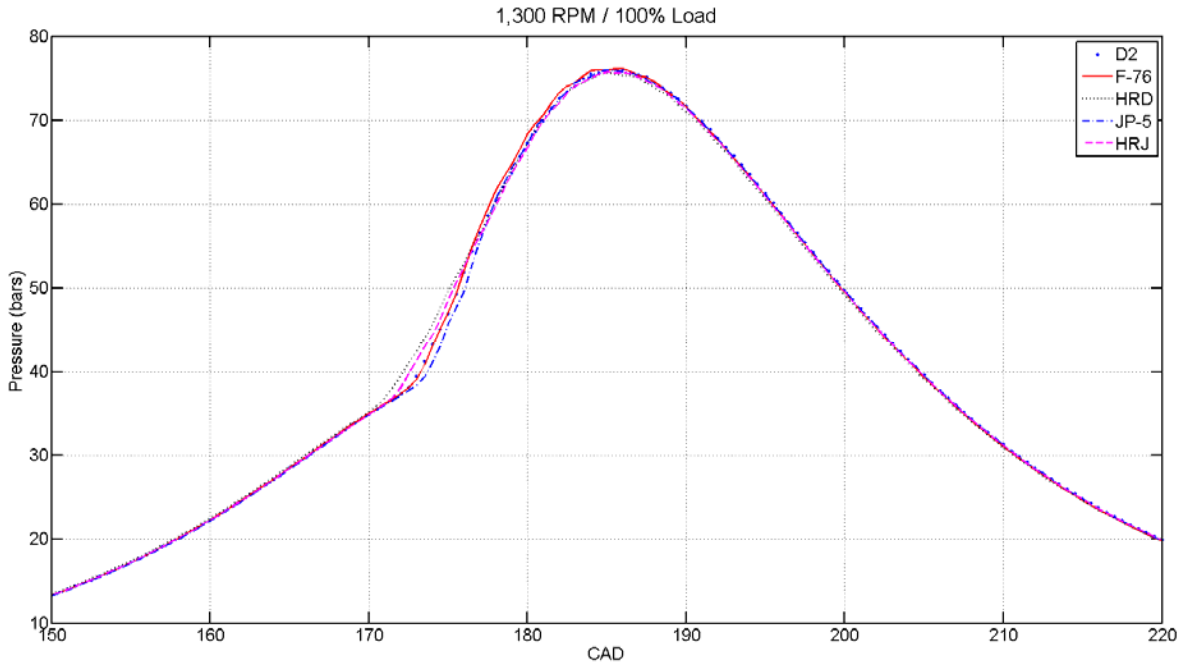

Figure 81. Pressure – CAD Plots of 1,300 RPM and 100% Load

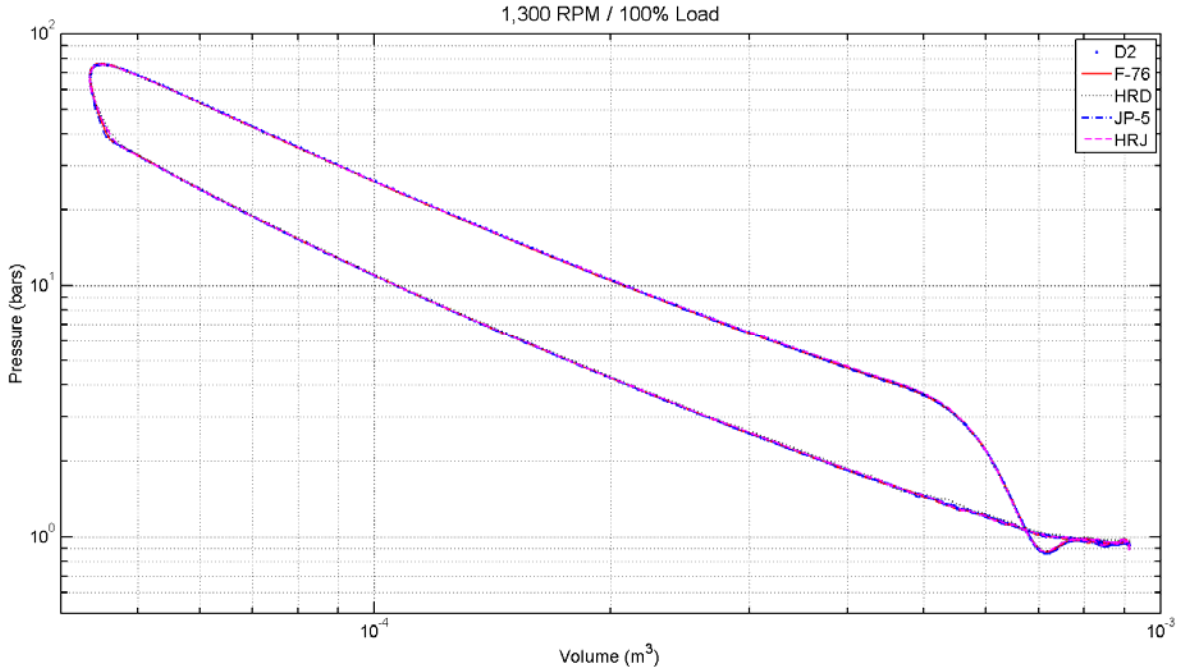

Figure 82. Pressure – Volume Plots of 1,300 RPM and 100% Load

THIS PAGE INTENTIONALLY LEFT BLANK

LIST OF REFERENCES

1. Fichman, B. T., "Annual Energy Review 2010." U.S. Energy Information Administration (EIA). http://www.eia.gov/totalenergy/data/annual/pdf/aer.pdf (accessed May 27, 2012).

2. Macapagal, P., USN, LT, "Energy." U.S. Department of the Navy Energy, Environment and Climate Change. http://greenfleet.dodlive.mil/energy/ (accessed May 24, 2012).

3. Bryan, G. T., USN, LT, Surface Warfare Officer. Interview by author. Naval Postgraduate School, May 24, 2012.

4. Beermann-Curtin, S., "Future Naval Fuels Program." Office of Naval Research. http://www.onr.navy.mil/Science-Technology/Departments/Code-33/All-Programs/332-naval-materials/Future-Naval-Fuels.aspx (accessed May 24, 2012).

5. Wright, L., "Navy Tests Biofuel-Powered 'Green Hornet'." The U.S. Navy. http://www.navy.mil/search/display.asp?story_id=52768 (accessed May 28, 2012).

6. Carr, M. A., Caton, P., Hamilton, L., Cowart, J., Pitz, W. and Mehl, M. "An Experimental and Modeling-Based Study into the Ignition Delay Characteristics of Diesel Surrogate Binary Blend Fuels." American Society of Mechanical Engineers ICEF2011-60027 (2011). http://asmedl.org/ (accessed May 24, 2012).

7. Bruno, T. J. and Baibourine, E. "Comparison of Biomass-Derived Turbine Fuels with the Composition-Explicit Distillation Curve Method." Energy and Fuels 25, no. 4 (2011): 184.

8. Challen, B. and Baranescu, R., Diesel Engine Reference Book, SAE Publishing, 1999.

9. Edward, T. “Kerosene Fuels for Aerospace Propulsion – Composition and Properties,” 38th AIAA/ASME/SAE/ASEE Joint Propulsion Conference and Exhibit, Indianapolis, IN, July, 2002.

10. Kuronen, M., Mikkonen, S., Aakko, P. And Murtonen, T. “Hydrotreated Vegetable Oil as Fuel for Heavy Duty Diesel Engines.” SAE Technical Paper #2007-01-4031, 2007.

11. Aatola, H., Larmi, M., Sarjovaara, T. and Mikkonen, S. “Hydrotreated Vegetable Oil (HVO) as a Renewable Diesel Fuel: Trade-off between Nox, Particulate Emission, and Fuel Consumption of a Heavy Duty Diesel Engine.” SAE Paper #2008-01-2500, 2008.

12. Kitano, K, Sakata, I. and Clark, R. ”Effects of GTL Fuel Properties on DI Diesel Combustion.” SAE Paper#2005-01-3763, 2005.

13. Moses, C.A. “Comparative Evaluation of Semi-Synthetic Jet Fuels.” CRC Report Project No. AV-2-04a, Sept., 2008.

14. Cathey, C., Tang, T., Shiraishi, T., Urushaihara, T., Kuthi, A. and Gundersen, M. "Nanosecond Plasma Ignition for Improved Performance of an Internal Combustion Engine." IEEE Transactions on Plasma Science 35, no. 6 (2007): 1664.

15. Shiraishi, T., Urushihara, T. and Gundersen, M. "A trial of ignition innovation of gasoline engine by nanosecond pulsed low temperature plasma ignition." Journal of Physics D: Applied Physics 42 (2009): 135208.

16. Armstrong, R. "Fault Assessment of a Diesel Engine using Vibration Measurements and Advanced Signal Processing." Naval Postgraduate School Thesis (1996).

17. Caton, P. A., Williams, S. A., Kamin, R. A., Luning-Prak, D., Hamilton, L. J., Cowart, J. S. “Hydrotreated Algae Renewable Fuel Performance in a Military Diesel Engine.” Internal Combustion Engine Division Spring Technical Conference. 2012, ICES 2012-81048.

18. Hamilton, L. J., Williams, S. A., Kamin, R. A., Carr, M. A., Caton, P. A., Cowart, J. S. “Renewable Fuel Performance in a Legacy Military Diesel Engine.” ASME Conf. Proc. 2011, 1095 (2011), DOI:10.1115/ES2011-54101.

19. Tunestal, P. “Model Baesd TDC Offset Estimation from Motored Cylinder Pressure Data.” Oil & Gas Science and Technology – Rev. IFP Energies nouvelles, Vol. 66, No. 4, (2011): 705-716.

20. Heywood, J. B. “Internal Combustion Engine Fundamentals.” Mc-Graw Hill, 1988.

21. Goering, C. E., “Engine Heat Release Via Spread Sheet.” Transactions of the ASAE 41, no.5 (1998): 1249-1253.

22. Hudson, J. W., “Development and Calibration of a Torsional Engine model for a Three-Cylinder, Two-Stroke Diesel Engine.” December 1997.

23. Cowart, J., Carr, M., Caton, P., Stoulig, L. et al., "High Cetane Fuel Combustion Performance in a Conventional Military Diesel Engine." SAE Int. J. Fuels Lubr. 4(1):34-47, 2011, doi:10.4271/2011-01-0334.

24. Seivwright, D. L. Optical Encoder Mount Design. March 13, 2012.

INITIAL DISTRIBUTION LIST

1. Defense Technical Information Center
   Ft. Belvoir, Virginia

2. Dudley Knox Library
   Naval Postgraduate School
   Monterey, California

3. Department Chairman, Code ME
   Naval Postgraduate School
   Monterey, California

4. Professor Knox T. Millsaps, Jr., Code ME/MI
   Naval Postgraduate School
   Monterey, California

5. Curricular Officer, Code 34
   Naval Postgraduate School
   Monterey, California

6. ENS Matthew Carr
   Turkey Point Road
   Edgewater, Maryland

7. Dr. Sharon Beermann-Curtin
   Office of Naval Research, Code 33, Division 332
   N. Randolph Street
   Arlington, Virginia

8. Professor Jim Cowart
   Engineering and Weapons Division
   United States Naval Academy
   Annapolis, Maryland